

Last edited August 28, 2006

Infrared Nebulae Around Young Stellar Objects

Michael S. Connelley¹Bo Reipurth²

and

Alan T. Tokunaga³

ABSTRACT

We present a K-band atlas of 106 reflection nebulae, 41 of which are new discoveries. We observed these nebulae with the UH 2.2 m telescope in the course of an imaging survey of 197 objects that were selected to be nearby young Class I sources. K-band images and flux calibrated surface brightness contour plots of each nebula are presented. We found that the near-IR luminosities and physical sizes of the nebulae increase with the bolometric luminosity of the illuminating sources. Only 22 nebulae, about 10% of these candidate Class I sources, have indications of shocked H₂ emission. The great variety of nebulae that we observed prevented us from classifying them based on morphology. However, we note that as the spectral index decreases, the central star is more frequently visible at K-band and the flux from the central star tends to be dominant over the flux from the nebula. For objects that have a higher spectral index, most of the K-band flux is from the reflection nebula, and the central star is less frequently visible. The nebula around IRAS 05450+0019 has a unique morphology, and we speculate that it may be an example of a disk shadow being projected into the surrounding cloud. We present J, H, and K-band images of this object with surface brightness contours, as well as its SED from 1.2 μm to 100 μm .

Subject headings: atlases — stars:formation — reflection nebulae — infrared:ISM

¹Institute for Astronomy, University of Hawai'i, 640 N. A'ohoku Pl., Hilo, HI 96720; msc@ifa.hawaii.edu

²Institute for Astronomy, University of Hawai'i, 640 N. A'ohoku Pl., Hilo, HI 96720; reipurth@ifa.hawaii.edu

³Institute for Astronomy, University of Hawai'i, 2680 Woodlawn Dr., Honolulu, HI 96822; tokunaga@ifa.hawaii.edu

1. Introduction

Reflection nebulae and star formation have been associated for a long time. Hind’s Variable Nebula (Hind 1864), near T Tauri, was the first reflection nebula associated with a young star, although T Tauri would not be identified as a young star for many more years. The variable nebulae around the stars R Monocerotis (Hubble 1916) and R Corona Australis (Knox-Shaw 1916) were discovered half of a century later. Cometary nebulae were subsequently associated with star formation (Ambartsumian 1954), but an extensive catalog of these nebulae (Gyulbudaghian & Magakian 1977) was not published until the completion of the Palomar Sky Survey. In 1979, Parsamian and Petrossian published a catalog of 106 cometary nebulae, classified into 4 groups, and a year later Cohen (1980) published a list of red and nebulous objects found on the Palomar plates. Most recently, Magakian (2003) merged several of these catalogs of reflection nebulae.

With the advent of large near-infrared arrays came the first major survey of infrared nebulae. Hodapp (1994) observed 164 CO outflow sources identified by Fukui (1989), and found many infrared reflection nebulae. More recently, infrared reflection nebulae have been studied with HST and NICMOS (e.g. Padgett et al. 1999; Reipurth et al. 2000). Technological developments lead to YSOs being studied from the ground out to 20 μm , as well as with the IRAS satellite. Based on these data, new star forming regions were, and continue to be, found and new classes of YSOs identified. Lada & Wilking (1984) identified three broad types of YSOs. Class I objects have an SED that is broader than a single temperature blackbody and rises beyond 2 μm , Class II objects have an SED that is broader than a single temperature blackbody and declines beyond 2 μm , and Class III objects have a stellar SED that is consistent with a single temperature blackbody. More recently, Class 0 sources have been identified which have the SED of a cold single temperature blackbody (André et al. 1993). Class 0 and many Class I objects are believed to be true protostars, and Class II objects are now identified with the T Tauri stars.

Many studies of young stellar objects focus on a few objects at a time, which may become well known, while numerous interesting objects languish in obscurity. We therefore developed our own sample of nearby Class I YSOs, that is not biased towards well known star forming regions or famous case objects, in the following manner. First, we defined criteria for selecting Class I sources (described in the next section) by combining data from the IRAS Point and Faint Source Catalogs, the Digitized Sky Survey, and 2MASS. Having selected our sample from these catalogs, we observed most of these objects at K-band with the University of Hawai’i 2.2 m telescope. We observed 197 of the 267 targets in our sample, omitting those sources that are too far south ($\delta < -40$) to be well observed from Mauna Kea, as well as very well known sources (e.g. R CrA). Among the 197 objects that were

observed, 106 were found to have an infrared reflection nebula. These objects are presented in this paper.

During the course of our observations, we found that a significant fraction of our candidate Class I sources are associated with reflection nebulae, many with interesting morphology. Judging by their citations in SIMBAD, we found that many of these candidate objects were not previously well known, including some of the largest and brightest nebulae in our survey. Among those sources we observed, about half showed some kind of nebula, and they are presented here.

2. Source Selection Criteria and Distances

Our goal was to compose a sample that contains only Class I YSOs within ~ 500 pc in order to be able to resolve close binary companions. We chose to define our own sample of Class I YSOs (versus drawing a sample from the literature) so that our sample would not be biased in favor of nor against the well known star forming regions, and so that we would have a clearly defined sample with well known properties.

We first selected all sources in the IRAS Point and Faint Source Catalogs that have increasing flux with wavelength from $12 \mu\text{m}$ through $100 \mu\text{m}$, and that were detected in the $25 \mu\text{m}$, $60 \mu\text{m}$, and $100 \mu\text{m}$ bands. These selection criteria were chosen to select sources with cool (~ 30 K) dust and have allowed some objects into our sample that are classified as Class 0 sources. We then visually inspected $15' \times 15'$ images from the Digitized Sky Survey (DSS) for each of the $\sim 12,000$ sources that satisfied the criteria described above, so that we could select sources that lie in the direction of nearby clouds with high optical extinction. Since we wanted our sample of Class I objects to be nearby, we were looking for fields with a well defined dark cloud and few stars (if any) that appear to be in front of the cloud. We also looked for light from gas emission or dust scattering since we sought to avoid more evolved objects in large HII regions or that have an optical reflection nebula. We eliminated from further consideration fields centered on a galaxy, planetary nebula, bright star, a distant bright or dark cloud, or an empty star field (i.e. a star field without a dark cloud, bright nebula, or any of the previously mentioned objects). This effectively eliminated galaxies, evolved stars, planetary nebulae, and other dusty objects from our sample. In our review of the DSS images, choosing which dark nebulae appear nearby and which do not was inevitably a subjective process. We have since found distance estimates to most of the objects in our sample. The distribution of distances to these YSOs, which has a median of 470 pc, is presented in Figure 1 (right), and confirms that our expectations of the appearance of nearby dark clouds were generally correct.

For all of the fields that satisfied the above criteria, 2MASS images in the J, H, and K-bands were then inspected to identify embedded sources. We selected sources that are clearly brighter from J to H to K-bands and set aside targets where the only stars that were seen by 2MASS are also visible on the DSS plates. Sources where no embedded stars were visible in 2MASS were not rejected because there are near-IR counterparts and nebulae that were undetected by 2MASS.

Our selection procedure yielded a sample of 267 objects that is almost entirely composed of Class I YSOs, as shown by the fact that the distribution of spectral indices (as defined by Lada 1990) for sources in this sample has a median value of +0.79 (Figure 1, left). To calculate the spectral indices, we used the IRAS 12 μm to 100 μm measurements (or from 25 μm if the source was undetected at 12 μm). We use the slope of the linear regression line through the data points as the spectral index. It must be noted that Lada (1990) defines the spectral index as $\alpha = -d\log\nu F_\nu/d\log\nu$, in which case a Class I protostar has a positive spectral index, Adams et al.(1987) define the spectral index without the minus sign, in which case a protostar would have a negative spectral index. Kenyon & Hartmann (1995) express the spectral index as $d\log\lambda F_\lambda/d\log\lambda$, in which case the spectral index of a protostar would be positive. We adopt the convention where the spectral index of a protostar is positive, and use the equation given by Lada (1990). There are a few targets that have a spectral index less than 0, which indicates that they may be Class II objects. There are also a few objects in the sample that have an increasing SED with wavelength and no near-IR counterpart. These are believed to be Class 0 sources. These spectral indices contain flux from all sources within the broad IRAS beam. Several sources have more than one YSO visible in the near-IR. Higher angular resolution mid- and far-IR observations of individual sources may yield different spectral indices.

3. Observations and Data Reduction

3.1. UH 2.2 m

Our K-band observations of the reflection nebulae were conducted with QUIRC, the 1024×1024 HgCdTe facility near-IR camera (Hodapp et al. 1996) on the University of Hawai'i 2.2 m telescope on Mauna Kea. All observations were made through the MKO (Tokunaga et al. 2002; Tokunaga & Vacca 2005) K-band filter (not K' or K_s). The camera's plate scale is 0".1886 per pixel, yielding a field of view of 193". Data were taken from January to September, 2003. Details of when each object was observed, as well as the integration times, are listed in Table 1. The mean image resolution (FWHM) for this data set is 0".87, with the best seeing being 0".58 and the worst 1".56. Each source was observed using either a

5 or a 9 point dither pattern, the telescope being offset $\sim 10''$ between exposures. Exposure times were usually 60 s, although shorter exposure times were used on some very bright sources (e.g. IRAS 21004+7811). In the case of IRAS 05450+0019, a very large nebula, separate sky frames were taken.

The data were subsequently reduced using IRAF. A dark image, itself the average of 10 individual darks and of the same exposure time as the target images, was subtracted from each on-source frame. To make a flat, each dark subtracted frame was scaled to have the same average value. These scaled images were then averaged together with a min-max rejection to make the flat, which was then normalized. Each dark subtracted (but not scaled) image was divided by this flat, then a constant was subtracted from each image to set the average sky counts to zero. Each processed frame was then registered and averaged together, using average sigma clipping rejection.

Selected UKIRT standard stars were observed and reduced in the same manner. Photometry was performed using the PHOT routine in IRAF, using an aperture 20 pixels in radius with a 20 pixel wide buffer between the aperture and the 20 pixel wide sky annulus. IDL was used to make the surface brightness contour plots. Boxcar smoothing of 3 pixels for the brighter parts of the image (since this is slightly less than the average FWHM in pixels) and 6 pixels for the fainter areas was used to reveal the faint nebulosity in the contours. The pixel counts in each reduced image was converted to a surface brightness through the relation:

$$\Sigma_K = K_{standard} - 2.5 \log \left(\frac{c_{nebula} - c_{sky}}{c_{standard}} \cdot \frac{t_{standard}}{t_{nebula}} \cdot A \right) - k(a_{standard} - a_{nebula}) \quad (1)$$

where Σ_K is the K-band surface brightness of the nebula in magnitudes per square arcsecond, $K_{standard}$ is the standard star's K-band magnitude, c_{nebula} is the number of counts for the pixel in question, c_{sky} is the average background sky counts in the nebula image, $c_{standard}$ is the number of counts measured through aperture photometry from the standard star, $a_{standard}$ is the airmass at which the standard star was observed, a_{nebula} is the airmass at which the nebula was observed, $k = 0.07$ is the coefficient for K-band atmospheric extinction per unit airmass (Krisciunas et al. 1987), t_{nebula} is the exposure time used for the nebula (usually 60 s), $t_{standard}$ is the exposure time used for the standard star, and A is the number of pixels that make a square arcsecond on the sky (in the case of QUIRC, $A = 28.114$).

The dithering and flat fielding processes eliminated a majority of potential image artifacts. The primary remaining artifact is a reduction of the background counts near a bright, spatially resolved object and in crowded fields. This occurs when there is an object in the field that is similar in size to the offsets of the dither pattern, and thus the resulting flat contains some contribution from the objects in the field of view. For most objects, this

is not an issue. Nevertheless, there are a number of nebulae where this continues to be a problem, such as for IRAS 16316–1540. This does affect the calculated surface brightness of the nebula, particularly near the faint extremities of the nebula. In such cases, we chose as our "sky" value the counts nearest the edge of the nebula to minimize this effect. Another kind of artifact are the diffraction spikes from the secondary mirror support. This is visible around very bright (usually saturated) stars, such as the near-IR counterpart to IRAS 20453+6746. Saturated sources can be identified by a large inner surface brightness contour, whereas the contours for unsaturated sources become progressively smaller towards the center of the PSF. Our images occasionally show elongated stellar PSFs caused by telescope wind shake. Triangular PSFs are due to print-through of the primary mirror support structure. One of the observing runs occurred immediately after the mirror was replaced in the telescope after recoating. During this run, the primary mirror cell had not yet been precisely adjusted, resulting in uneven mirror support.

3.2. IRTF

K-band and H₂ 2.122 μm narrow band observations of nebulae suspected of having shocked H₂ emission were conducted with the Spex 512×512 pixel guider array on the NASA IRTF. We selected nebulae that had not yet been imaged with the 2.122 μm H₂ narrow band filter before. The guider array has a plate scale of 0".12 per pixel, yielding a field of view of 61". All of the data were taken on the night of 23 Sep. 2005 under nonphotometric conditions. For each field, 7 K-band images were taken followed by (typically) 21 H₂ images. Although we had K-band images of each nebula taken with QUIRC, we took comparison K-band images with Spex in order to identify the field and to have images with the same plate scale and seeing as the H₂ data. Exposure times were typically 60 s, although some of the narrow band images were taken with a 120 s exposure time. A 7 point dither pattern was used with 10" offsets. The data reduction method was as described above. Due to the observing conditions and the fact that we already had flux calibrated K-band images, standard stars were not observed. The nebula associated with IRAS 05399–0121 is the only case where H₂ was not confirmed. For this object, there were no sources (either nebulous or stellar) in our H₂ images that we could use to register the images, so our data could not be reduced.

K-band, K-continuum, and H₂ images are shown in these figures as appropriate, as well as a 15" scale bar. The images labeled as "H₂ + K continuum" are broad K-band images. We first identified H₂ emission regions by subtracting a scaled K-band image from a narrow band H₂ image, determining the amount of scaling by the relative flux of field stars. The

K-continuum images were made by subtracting a scaled narrow band H₂ image from the K-band image. In this case, the scaling was determined by comparing the peak counts of H₂ features in the K-band and H₂ images in order to subtract out the H₂ features. The images labeled as "H₂ only" were made by subtracting a scaled K-continuum image from a narrowband H₂ image; the scaling again being determined by the relative flux of field stars.

4. The Atlas of Infrared Reflection Nebulae

4.1. Atlas of Nebulae

Figure 2 shows 60'' × 60'' K-band images of the majority of the nebulae in this paper. In some cases a larger field of view is necessary to show the whole nebula, and these nebulae are presented in Figures 3 through 9. Each image is centered on the K-band source, or occasionally offset to show two widely separated sources. The (0,0) coordinate in each image is the IRAS Point Source or Faint Source Catalog location. Tick marks designate a K-band source in each image (usually what we believe to be the near-IR counterpart to the IRAS source), and the 2MASS coordinate of that source is given in Table 2. Under the name of each IRAS source is a 5,000 AU scale bar for those objects where we found a distance estimate. The brightness and contrast of each image was chosen to most clearly show the morphological features of the nebulae. K-band surface brightness contours, calibrated in the MKO photometric system, are overlaid at 1 magnitude per square arcsecond intervals. The value of the first (outermost) K-band surface brightness contour is given in Table 1. The inner contours are white in order to show them against the black areas of each image. The J, H, and K_s magnitudes presented in Table 2 are from 2MASS and are in the internal 2MASS photometric system. When available, the magnitudes presented in Table 2 are from the 2MASS extended source catalog. If the object is not included in the extended source catalog, then the photometry from the point source catalog was used. Color conversion equations are presented in appendix A.

4.2. Notes on Sources

The following summarizes the results of a literature search on each source using the SIMBAD database. The information presented here is intended to be representative of what has been reported on each source and is not comprehensive. We hope that this information will be helpful in guiding the reader in future research. Objects described as spatially resolved or non-stellar have a FWHM significantly larger than field stars in the same image. Objects

described as unresolved point sources have a FWHM consistent with field stars in the same image. While the majority of sources have a near-IR counterpart at the IRAS coordinates, there are several cases where the suspected near-IR counterparts are up to tens of arcseconds away from the IRAS coordinates. We believe that these cases can have a variety of causes, all rooted in the large size of the IRAS beam. The hot near-IR counterpart may not be centered in the cooler region detected by IRAS at $60\ \mu\text{m}$ and $100\ \mu\text{m}$. The centroiding of a faint IRAS source may be affected by a much brighter nearby source. Finally, there are cases such as IRAS 16288–2450 where the IRAS position is right between two bright near-IR counterparts, both of which have reflection nebosity. In such a case IRAS detected both sources, and they are too close to be distinguished by IRAS.

We believe that a nebula is newly discovered if there are no citations in SIMBAD that include near-IR images. Among the 41 newly discovered nebulae, we noticed that there are two regions in the sky with a large number of previously unreported nebulae. One group with 10 nebulae is centered around $6^{\text{h}}0 - 10^{\circ}$, near the optical reflection nebula NGC 2149 in SW Monoceros. Being near Orion, it is likely to be associated with that star forming region. The other group is centered near $18^{\text{h}}5 - 1^{\circ}$ in Serpens and has 5 nebulae. These unexplored star forming clouds may harbor more young stars.

IRAS 00182+6223. This is a previously unreported nebula whose cloud has been detected in CO emission (Wouterloot & Brand 1989). This is the first near-IR image published of this source. We observed a $\sim 10''$ diffuse nebula extending to the north, as well as two stars near the nebula to the ESE.

IRAS 00465+5028. This nebula is associated with RNO 3, and the IRAS source has been extensively observed in the mm and radio. Yun & Clemens (1994a) were the first to publish near-IR images of this nebula. We observed a monopolar nebula extending to the north of an unresolved point source.

IRAS 01166+6635. This is a previously unreported nebula whose illuminating source has been associated with H₂O maser (Codella et al. 1995) and CO emission (Wouterloot & Brand 1989). This is the first near-IR image published on this object, showing a small diffuse nebula to the SE of an unresolved point source.

IRAS 02086+7600. This YSO in L1333 was first observed in the near-IR by Fujii et al. (2002), who conclude that this is likely to be a YSO rather than a post-ABG star. It has been detected in C¹⁸O, including a feature that may be an outflow (Obayashi et al. 1998). Our image shows what appears to be a small bipolar nebula. There is also a large, faint nebula to the west.

IRAS 03225+3034. This source is associated with the well known, highly embedded

protostellar binary star L1448N IRS 3. VLA observations have shown this source to be a 7".3 binary (Reipurth et al. 2002). Cardi et al. (2003) were only able to see one component of this binary at mid-IR wavelengths, concluding that the binary consists of a Class I source and a Class 0 source. This is the origin of HH 193A-C and HH 194A and B (Bally et al. 1997). We observed a $\sim 90''$ long jet-like nebula that may be mostly H₂ emission based on its morphology. Our image is presented in Figure 3.

IRAS 03245+3002. This nebula is associated with RNO 15 FIR in the L1455 cloud. This source is the origin of a CO outflow (Levreault 1988), water maser emission (Cesaroni et al. 1988), and the HH 318 flow (Bally et al. 1997). Davis et al. (1997) present H₂ S(1) imaging of the molecular jet that drives the CO outflow. There is no observed near-IR counterpart to this IRAS source, only a jet-like nebula $\sim 6''$ long to the SW ending in a small bow shock.

IRAS 03260+3111. A source in NGC 1333 that is well known for studies of silicate (Noguchi et al. 1993) and other molecular spectral features. It was first studied at near-IR wavelengths by Haisch et al. (2004). IRAS 8 in the study of NGC 1333 by Jennings et al. (1987) corresponds to this object. There is a large diffuse nebula around the bright stars to the east in Figure 4. To the west is a reflection nebula, with a fainter surrounding nebula elongated to the east and west.

IRAS 03271+3013. This object was first observed in the near-IR by Aspin (1992), who found shocked H₂ emission and estimated that there are about 50 magnitudes of extinction towards the H₂ line emission region. Our image shows a central nebula, with faint nebulosity arcing to the NE and to the SW.

IRAS 03301+3057. Also known as Barnard 1 IRS, this source is believed to be the origin of a CO outflow (Hirano et al. 1997). HH 431 was found near this source by Yan et al. (1998). This may be the first near-IR data published on this nebula. Our image shows a small nebula with a jet-like feature extending $\sim 5''.5$ to the WSW.

IRAS 03331+6256. This is a previously unreported near-IR nebula, and these are the first near-IR data published on this object. CO emission was detected by Wouterloot & Brand (1989). Our image shows a small faint nebula to the north of a point source that is likely the near-IR counterpart of the IRAS source. A faint companion $\sim 2''.5$ to the SSW of the source was observed to significantly brighten in the near-IR in mid-2004.

IRAS 03445+3242. Also known as Barnard 5 IRS 1, this object is the well known source of a CO outflow (Fuller et al. 1991; Yu et al., 1999) and the parsec scale jet HH 366 (Bally et al. 1996). Moore & Emerson (1994) found the nebula to show a steady decrease in luminosity of 0.27 magnitudes per year with constant near-IR color. The near-IR spectrum

shows H₂ and weak CO emission (Reipurth & Aspin 1997). In addition to a faint reflection nebula, our K-band image also shows what appear to be a few small knots of H₂ emission symmetrically placed to the ENE and WSW of the central star.

IRAS 03507+3801. This previously unreported near-IR reflection nebula is near HH 462, which was discovered by Aspin & Reipurth (2000). Our image shows a bright point source, a faint monopolar nebula to the SW, and what appears to be a faint loop to the NE.

IRAS 04016+2610. A well known YSO in L1489, this is the origin of a molecular outflow (Terebey et al. 1989; Hogerheijde et al. 1998) and several HH objects (Gómez et al. 1997b). The mass of the associated core has been estimated to be 2 M_⊙ based on NH₃ emission (Benson & Myers 1989). This Class I source has been detected as an unresolved 6 cm source by the VLA (Rodríguez et al. 1989), and was observed with HST by Padgett et al. (1999) who observed a 600 AU dust lane. Lucas et al. (2000) describe this system as having two perpendicular bipolar jets, based on VLA, MERLIN, and near-IR H₂ images. Our image shows a bipolar reflection nebula, brighter to the south, bisected by a dark lane.

IRAS 04067+3954. This is a previously unreported, large, and morphologically interesting reflection nebula. Although most of the K-band flux is scattered light from the bright spatially resolved nebula, there is a faint point source 5'' to the west of the brightest part of the nebula. The faint point source is the brightest object in the field at L', and probably represents the near-IR counterpart to the IRAS source.

IRAS 04073+3800. Also known as PP13S*, Sandell & Aspin (1998) found that this object is an FU Orionis pre-main sequence star and present near-IR imaging, spectroscopy, and sub-mm data. Aspin & Reipurth (2000) showed that this is the origin of the HH 463 outflow. Our image shows a bright point source with a bright loop of nebulosity to the SW.

IRAS 04169+2702. This well studied object is described in Park & Kenyon (2002) as a Class I object, and is the origin of HH 391 (Gómez et al. 1997b). Our image shows a bright point source with a faint monopolar nebula to the SW. There also appears to be a few small knots of H₂ emission to the SW.

IRAS 04189+2650. This is FS Tau, also known as Haro 6-5. FS Tau A (to the east) is a close binary and FS Tau B is the origin of the HH 157 outflow (Mundt & Raga 1991). FS Tau B is bisected by a dust lane ~600 AU wide (Padgett et al. 1999). Our image shows two bright unresolved point sources, with FS Tau B being surrounded by a faint reflection nebula.

IRAS 04191+1523. This nebula around a Class I source was imaged by Hodapp (1994), and is located 1' NE of the Class 0 source IRAM 04191+1522 (André et al. 1999).

The IRAM source shows evidence for outflow (Moriarty-Schieven et al. 1992), infall, and rotation in its 28,000 AU diameter envelope (Belloche et al. 2002). Our image shows a close pair of objects. The SW object is surrounded by an elongated nebula with a faint tail to the east.

IRAS 04223+3700. This source has a bright near-IR counterpart and is not visible optically. Wouterloot et al. (1993) were not able to detect CO emission from the associated cloud. We find that this object is an E-W oriented $1''0$ binary. There is also a faint reflection nebula $\sim 9''$ to the ENE.

IRAS 04239+2436. This is a well studied Class I protostar shown to be a $0''3$ binary by Reipurth et al. (2000) using NICMOS aboard HST. This is the origin of a CO outflow (Moriarty-Schieven et al. 1992) and the parsec scale HH 300 jet (Reipurth et al. 1997). Our image shows a bright central point source with a faint nebula to the north and east that may represent a wide cavity.

IRAS 04248+2612. Also known as HH 31 IRS 2, this is a well studied Class I source and jet, with near-IR extended emission described in Park & Kenyon (2002). Despite its impressive nebula, Kenyon & Hartmann (1995) estimated that the luminosity of this source is only $0.4 L_{\odot}$. HST imaging by Padgett et al. (1999) showed that this object is a $0''16$ binary. Our image shows a central point source with a large, bipolar-like reflection nebula.

IRAS 04275+3531. This is a previously unreported near-IR reflection nebula. CO emission has been detected from the associated cloud by Wouterloot & Brand (1989). Our image shows a spatially resolved central star with a faint monopolar nebula to the south.

IRAS 04287+1801. Well known as L1551 IRS 5, this is the origin of the HH 154 outflow. This is a binary radio source separated by 50 AU (Bieging & Cohen 1985), and is believed to have two aligned protoplanetary disks (Rodríguez et al. 1998). This FU Orionis type object shows deep CO bands in its near-IR spectrum that are characteristic of this kind of YSO (Reipurth & Aspin 1997). Our image shows a bright, large reflection nebula with a tail arcing to the SW.

IRAS 04302+2247. Known as the "Butterfly Star", this is a low luminosity source (estimated to have a bolometric luminosity of $0.34 L_{\odot}$ by Kenyon & Hartmann 1995) with a large, bright nebula. The associated cloud has been detected in CO emission (Bontemps et al. 1996) and this source is the origin of the HH 394 outflow (Gómez et al. 1997b). This nebula was observed with HST by Padgett et al. (1999), who describes a spectacular bipolar nebula bisected by a ~ 900 AU dust lane that completely obscures the central star. Wolf et al. (2003) present a model of this disk that calls for larger dust grains in the disk and smaller dust grains (similar to those in the ISM) in the envelope. Our image shows an

edge-on bipolar nebula with an obvious dark lane, as well as fainter absorption features on either side of the dark lane.

IRAS 04325+2402. Also known as L1535 IRS, this is a well known and complex object seen entirely in scattered light in the near-IR. Hartmann et al. (1999) used HST to image the complex morphology of this bipolar nebula. They comment on the low luminosity ($10^{-2} L_{\odot}$) companion to the north that could be a young brown dwarf. Both stars appear to be bisected by nearly edge-on disks. Wang et al. (2001) found this object to be the driving source of three Herbig-Haro objects (HH 434-6). Our image shows two spatially resolved objects, with the companion superimposed on the bipolar nebula of the primary source.

IRAS 04327+5432. This is a previously unreported near-IR nebula associated with HH 378 and L1400. Wouterloot et al. (1993) detected CO emission. Our image shows a point source with a faint nebula $\sim 4''$ to the SW. Faint nebulosity $\sim 1'$ to the NW was found to be H₂ emission.

IRAS 04365+2535. Also known as TMC-1A, this is a very well studied Class I source, with its near-IR extended emission described in Park & Kenyon (2002). Through CO observations, Brown & Chandler (1999) used the Keplerian rotation of the molecular envelope of this object to estimate a mass of 0.35 to 0.7 M_{\odot} . Terebey et al. (1989) observed high velocity CO indicative of an outflow. Windshake of the telescope has elongated our image in the east-west direction by about $0''.5$. We observed a bright point source with a faint bipolar nebula, slightly brighter to the south.

IRAS 04381+2540. Associated with TMC-1, this is a well studied Class I source. Its near-IR extended emission is described in Park & Kenyon (2002). Terebey et al. (1989) observed high velocity CO indicative of an outflow. Through CO observations, Brown & Chandler (1999) used the Keplerian rotation of the molecular envelope of this object to estimate a mass of 0.2 to 0.4 M_{\odot} . Our image shows a bright central source with a very faint bipolar reflection nebula. Windshake of the telescope has elongated our image in the east-west direction by about $0''.5$.

IRAS 04530+5126. This source illuminates a previously unreported near-IR reflection nebula associated with RNO 33. V347 Aurigae, the near-IR and optical counterpart of the IRAS source, is a flat-spectrum pre-main sequence H α emission line star (Weintraub 1990) associated with the L1438 dark cloud. We observed a very bright point source with a faint arc-shaped nebula to the south.

IRAS 04591–0856. This is a previously unreported near-IR reflection nebula. This source of a Herbig-Haro object was found by Persi et al. (1988) to possibly be in transition from Class I to Class II. Tapia et al. (1997) report that the colors are consistent with a Class

II source, and their nondetection of nebulosity prompts them to suggest it may be a Class III source. Our image shows a bright central star with a faint reflection nebula that may be bipolar. Windshake of the telescope has elongated our image in the east-west direction by about $0''.5$.

IRAS 05155+0707. This source is in the λ Ori molecular shell. It is between the parsec scale HH 114 and HH 115 flows, and there is a chain of faint HH knots that appear to emanate from this source (Reipurth et al. 1997). The cold Class 0 source HH 114 MMS is $1''.5$ to the NW (Chini et al. 1997), and may be the source of the HH 328/329 flows. Lee et al. (2002) find that the CO morphology and kinematics of the HH 114 and HH 115 outflows are consistent with a single driving source. Our image shows a spatially resolved central object in a bright, complex nebula with a possible companion $6''.5$ to the east. We also see H_2 emission extending $\sim 75''$ to the west, in the direction of HH 114.

IRAS 05302–0537. Also known as Haro 4-145 and associated with the Orion A-west molecular outflow, this object has been extensively studied at radio and mm wavelengths. CO emission from the bipolar outflow associated with this source was discovered by Fukui et al. (1986). Felli et al. (1992) found this object to be a source of H_2O maser emission. This object appears to be in the southern part of the Orion cloud, so we assume a distance of 470 pc. We observed a faint, diffuse nebula extending to the north from the bright star to the NW, as well as a small nebula to its SE.

IRAS 05311–0631. Also known as HH 83 VLA 1. The nebula associated with this source was imaged with HST by Reipurth et al. (2000). As in the HST image, we see a reflection nebula characteristic of a cavity. Optical spectroscopy shows that this is an emission line T Tauri star, and the infrared spectrum shows Br γ emission and no CO absorption or emission (Reipurth & Aspin 1997).

IRAS 05327–0457. This is a near-IR reflection nebula in NGC 1977 (just north of the Great Orion Nebula), associated with a maser observed by Henning et al. (1992). Mookerjee et al. (2000) present $143 \mu\text{m}$ and $185 \mu\text{m}$ observations, as well as HIRES processed IRAS maps of this source. Tsujimoto et al (2003) present near-IR colors and found that this X-ray source is a protostar. Our image shows a bright star, a diffuse nebula to the south, and three close pairs of stars nearby. Windshake of the telescope has elongated our image in the east-west direction by about $0''.5$.

IRAS 05378–0750. This object in the L1641 cloud is associated with object #146 in Chen & Tokunaga’s (1994) H and K imaging data. The nebulous object we observed is the faint source to the SSW of star #7 in their image of object #146. Morgan et al. (1991) did not detect a molecular outflow from this IRAS source. We observed a faint bipolar nebula

around an unresolved point source.

IRAS 05379–0758. This source is associated with object #163 in Chen & Tokunaga (1994). They note that star #7 (the star to the NE of the three in our image) is the brightest source at M band in object #163 and is thus likely to be the near-IR counterpart of the IRAS source. We observed faint diffuse nebulosity to the NE of this star and to the south of the southern star.

IRAS 05384–0808. Also known as L1641 S4. The cloud associated with this source was observed from 800 μm to 1.3 mm by Zavagno et al. (1997), who found a dust temperature of 32 K and mass of $0.4 M_{\odot}$. This nebula is #132 in the Magakian (2003) catalog of reflection nebulae. We observed diffuse nebulosity around the bright star to the south and west.

IRAS 05391–0841. This source is also in the L1641 cloud. Strom et al. (1989) and Chen & Tokunaga (1994) present near-IR images of this region. We observed three point sources, and a small nebula to the east that may be illuminated by a separate source.

IRAS 05399–0121. This source in the LBS 30 cloud core is a Class I YSO that is the origin of the large HH 92/93 outflow (Bally et al. 2002a). We observed knots of emission (possibly from H_2) extending $1'$ to the NW. There is no identifiable near-IR point source.

IRAS 05403–0818. Also known as L1641 S2, this source of a CO outflow (Chen et al. 1992) was studied by Chen & Tokunaga (1994) and was found to have an SED consistent with a Class I object. We observed a nebula extending to the east, towards knots of H_2 emission $\sim 30''$ away.

IRAS 05404–0948. This is a previously unreported near-IR reflection nebula. The cloud associated with this source has been mapped in ammonia (Jijina et al. 1999; Harju et al. 1993). We observed a bright point source with a diffuse nebula to the north and a companion to the SW. There is also a monopolar nebula, with no central point source visible in the near-IR, $28''$ to the SE.

IRAS 05405–0117. This is a previously unreported near-IR reflection nebula. The cloud associated with this source has been mapped in ammonia (Jijina et al. 1999; Harju et al. 1993). We observed a bright point source with a faint diffuse nebula to the NW.

IRAS 05413–0104. This source is the origin of the highly symmetrical HH 212 molecular outflow, discovered by Zinnecker et al. (1998). Water maser emission has been observed by the VLA (Furuya et al. 1999) from this Class 0 source. Wiseman et al. (2001) found that the $0.2 M_{\odot}$ core is elongated perpendicular to the jet axis, presumably due to rotational flattening. We observed several knots and bow shocks of what appears to be H_2 emission linearly and symmetrically arranged about a central source, which is not seen. The

nebula extends beyond the 3' field of view of our image. Our image is presented in Figure 3.

IRAS 05417+0907. This source is in the L1594 (λ Orionis) dark cloud, which has been the source of mm and sub-mm continuum and line studies. This object was found to be a source of water maser emission (Terebey et al. 1992) and is the origin of a CO outflow (Terebey et al. 1989). Hodapp (1994) was the first to present near-IR data on this nebula. Our image shows a diffuse nebula to the north of the central star, which is a 1''2 binary. There is also a faint nebula to the NE of a star to the south.

IRAS 05450+0019. The associated dense core has been extensively surveyed for ammonia emission (e.g., Jijina et al. 1999; Harju et al. 1993), and has been mapped at 450 μ m with SCUBA by Motte et al. (2001). This nebula is covered in more detail in section 6 of this paper. Images are presented in Figure 9, and the SED in Figure 10.

IRAS 05510–1018. This is a previously unreported nebula. We observed a point source to the NE and a spatially resolved object to the SW with a faint nebula to its east.

IRAS 05513–1024. A candidate Herbig Ae/Be star suspected to have a spectral type of B7 (Vieira et al. 2003). J through M band photometry was given by Fouqué et al. (1992). The nearby reflection nebula is the 158th entry in Magakian's Merged Catalogue of Reflection Nebulae (2003). In addition to a very bright star, we also observed an arc-shaped nebula $\sim 8''$ to the NE.

IRAS 05548–0935. This is a previously unreported nebula. Of the three stars in our image near the IRAS source, the middle one has a faint nebula to the east.

IRAS 05564–1329. This is a previously unreported nebula whose source has one prior citation (Codella et al. 1995, a non-detection of H₂O maser emission). Our image shows a 4''5 binary star, each with nebulosity to the SE.

IRAS 05581–1026. This is a previously unreported nebula associated with a source with no prior citations. We observed a faint monopolar nebula to the SW. The source appears to be bisected by an edge-on disk.

IRAS 05582–0950. This is a previously unreported infrared nebula that is associated with RNO 60 in Cohen's (1980) catalog of red nebulous objects. Our observation shows several stars and nebulae. There are two nebulae in our field, and the IRAS source position lies between them. To the east is a bipolar nebula, with a very bright half to the east and a much fainter half to the west. To the west of the IRAS source lies a faint nebula near a faint point source. Our image is presented in Figure 5.

IRAS 05596–0903. This is a previously unreported nebula associated with a source

with no prior citations. We observed a small clump of nebulosity with no source visible at K-band. There is another small patch of nebulosity, $88''$ to the SE, that may be related.

IRAS 05598–0906. This source has been found to be an H_2O maser source (Codella et al. 1995; Persi et al. 1994), and is near the X-ray source 1RXS J060216.7–090700. This object is $1'2$ north of the nebulous star GGD 10 (Gyulbudaghian et al. 1978). Follow up observations have shown that the bright star to the north, as well as the eastern and southern stars of the four to the south, are sub-arcsecond binaries. Our image shows diffuse nebulosity near each of the bright stars except for the one farthest west.

IRAS 06027–0714. This is a previously unreported reflection nebula, with no other publications with near-IR data. Similar in morphology to IRAS 05581–1026, we observe a monopolar nebula to the NNW of a spatially resolved source.

IRAS 06033–0710. This is a previously unreported reflection nebula, with no other publications with near-IR data. SIMBAD classifies this source as a galaxy. We observe an elongated nebula with a tail to the ENE.

IRAS 06047–1117. Yun et al. (2001) recently discovered this 0.4 pc jet originating from this candidate Class I source, and present continuum and narrow band H_2 images. Our observations through a narrow-band filter show shocked H_2 emission from a jet $2'9$ from end to end. Our image is presented in Figure 6.

IRAS 06057–0923. This is a previously unreported reflection nebula, with no publications with near-IR data. SIMBAD classifies this source as a galaxy although no galaxy is apparent in the DSS. Our image shows what could be a nebula with an edge-on disk or an embedded binary star.

IRAS 06249–0953. This is a previously unreported near-IR reflection nebula associated with a source with no prior citations. We observed a spatially resolved source surrounded by a triangular nebula. Our follow-up L' observations have found a companion star embedded in the nebula to the west.

IRAS 06368+0938. This is a previously unreported near-IR nebula in NGC 2264, associated with object #10 in Margulis et al. (1989) in the Monoceros OB1 cloud. They derive a luminosity of $5.7 L_\odot$ and a spectral index of $+0.8$ for this source via a different method. Our image shows several stars near the IRAS source. Two of the fainter ones to the west have faint nebulae, one of them bipolar.

IRAS 06381+1039. This object is near object #27 in Margulis et al. (1989) in the Monoceros OB1 cloud, and they derive a luminosity of $87 L_\odot$ and a spectral index of $+1.7$ via a different method. Based on near-IR imaging by Reipurth et al. (2004), this is the

source of the HH 576/7 outflow. This nebula in NGC 2264 has a spatially resolved central star and a curving nebula extending $20''$ to the east. The structure of the nebula suggests it is from H_2 emission.

IRAS 06382+1017. This nebula in the Monoceros OB1 star forming region is associated with HH 124 VLA and HH 571/2 (Reipurth et al. 2004). The VLA observations show a compact group of 6 sources near the IRAS source. This nebula was first imaged in the near-IR by Moneti & Reipurth (1995), and was identified as a Class I source by Margulis et al. (1989). Our K-band image shows a complex nebula extending to the NE of a spatially resolved source. Our follow up L' observations show that a tripple star (likely to be the near-IR counterpart to the IRAS source) lies in the resolved K-band peak $10/\text{arcsec}$ to the west of the IRAS position, and another fainter L' source lies at the tip of the nebulosity to the east. H_2 and [FeII] images by Reipurth et al. (2004) show several regions of shocked emission from multiple jets.

IRAS 06393+0913. This is a previously unreported near-IR nebula in the Monoceros OB1 star forming region. The H_2O maser source (Codella et al. 1995) was detected by IRAS, and the associated cloud has been detected in CO (Oliver et al. 1996; Wouterloot & Brand 1989). We observed a bright pair of stars at the location of the IRAS source. There is a fainter spatially resolved object, $23''$ to the WSW, with nebulosity on either side.

IRAS 07180–2356. This source is also known as HH 72 IRS, and is in the Bok globule L1660. Davis et al. (1997) presents $2.12 \mu\text{m}$ H_2 and narrow-band continuum images, showing a string of H_2 knots $4'$ long. This source was not detected as a water maser source by Furuya et al. (2003), but was detected by Felli et al. (1992). Reipurth & Aspin (1997) published a near-IR spectrum of this object, showing H_2 emission lines and CO bands in emission. They give the distance to this source as 1500 pc. Although the IRAS position is $\sim 23''$ west of a bright ($K = 11.6$) red ($H-K = 2.5$) star, MSX observed an $8.3 \mu\text{m}$ source at the location of this star. Thus, we believe that this star is the near-IR counterpart to the IRAS source. Our image shows a bright star surrounded by a small, faint nebula, with knots of H_2 emission to the east and west extending beyond our field of view.

IRAS 15398–3359. This is a previously unreported near-IR nebula associated with HH 185, in the Lupus 1 (Barnard 228) cloud. The envelope of this source was detected at 1.3 mm with a flux of 310 mJy (Reipurth et al. 1996). We observed a spatially resolved source with a broad, jet-like nebula extending $12''.5$ to the ENE.

IRAS 16288–2450. This source is better known as ρ Oph South. The IRAS source is between the binary T Tauri star to the west and a smaller nebula to the east (itself near the location of IRAS 16289-2450). Since the two near-IR counterparts are widely separated,

they are presented in two separate panels. L1689 IRS 5 is the wide T Tauri binary to the west. This is the origin of a high velocity molecular outflow (Wu et al. 2004). Our images show a faint, diffuse nebula around the binary T Tauri star. The nebula to the east has a higher surface brightness, is more elongated, and has a bright point source in the center.

IRAS 16295–4452. Moreira et al. (2000) were the first to publish near-IR data of this nebula in Norma, which they conclude is likely to be a Class I protostar. We observed a point source with faint, diffuse nebulosity in poor seeing (FWHM=1"2).

IRAS 16316–1540. Also known as L43 VLA 2 and RNO 91, this is a T Tauri star known to have a CO outflow (Mathieu et al. 1988), a bolometric luminosity of $4.3 L_{\odot}$ (Terebey et al. 1993), a mass of $0.5 M_{\odot}$ (Levreault 1988), and a disk 1700 AU in diameter (Weintraub et al. 1994). We observed a bright central star surrounded by a large, bright nebula. This in turn is surrounded by a large semi-circular nebula, roughly centered on the star, with a radius of $\sim 40''$.

IRAS 16442–0930. This is a previously unreported near-IR reflection nebula in L260. This object was detected at $850 \mu\text{m}$ by SCUBA (Visser, Richer, & Chandler 2002). Myers et al. (1987) present J through L' photometry, and derive a bolometric luminosity of $0.97 L_{\odot}$. We observed a point source in poor seeing (FWHM = 1"3) with faint, diffuse nebulosity to the south.

IRAS 17364–1946. This is a previously unreported near-IR nebula in L219 (Barnard 276) that is associated with an outflow (Wu et al. 2004). Our image shows a N-S elongated, spatially resolved near-IR source with faint nebulosity to the south.

IRAS 17441–0433. This is a previously unreported near-IR reflection nebula near L425. Although Carballo et al. (1992) could not determine if this is a galaxy or a YSO based on IRAS photometry and appearance on photographic plates, we are confident that this is a YSO due to its K-band morphology and its coincidence with a nearby dark cloud. We observed a spatially resolved near-IR source with a small nebula to the north with a smaller, faint nebula to the south.

IRAS 18148–0440. Also known as L483 FIR, this source was found to be in transition between Class 0 and Class I by Tafalla et al. (2000), whereas Pezzuto et al. (2002) classify this as a Class I object based on its ISO colors. Visser et al. (2002) find a total mass of $10 M_{\odot}$, extinction of $A_v \approx 182$, and detected the associated envelope at $450 \mu\text{m}$ and $850 \mu\text{m}$. This is also the origin of a CO outflow and a jet with shocked H_2 emission (Buckle et al. 1999), as well as water maser emission (Furuya et al. 2003). Although no near-IR point source was observed, we did notice that the morphology of the nebula has changed significantly compared to the images published by Fuller et al. (1995). We observed a faint

nebula divided into two main lobes. The western lobe has two K-band peaks. There is also a faint patch of nebula $55''$ west of the center of the western lobe.

IRAS 18264–0143. This is a previously unreported near-IR nebula, for which this is the first near-IR data published. We observed a spatially resolved source with a jet-like, but crooked, nebula extending $14''$ to the west.

IRAS 18270–0153. This is a previously unreported near-IR reflection nebula. The nebula is found $\sim 30''$ east of a star located at the IRAS coordinates, and engulfs a pair of point sources.

IRAS 18274–0212. This is a previously unreported near-IR nebula. Our image shows an unresolved near-IR point source with a small, faint nebula to the north. There is also a faint nebulous ribbon of emission $70''$ to the ESE that may be related to the IRAS source.

IRAS 18278–0212. This is a previously unreported near-IR nebula. MSX observed a mid-IR source at the location of the very red ($H-K \approx 3.2$) wide binary $\sim 10''$ south of the IRAS source location, and we believe this is the near-IR counterpart to the IRAS source. In addition to these stars, we observed a small but bright arc-shaped nebula $25''$ to the NW.

IRAS 18331–0035. This source is also known as HH 108 VLA 1. The associated HH flow was discovered by Reipurth & Eiroa (1992) with optical imaging. Siebenmorgen & Krügel (2000) found this to be a triple source, along with HH 108 MMS and a second core. Whereas the IRAS object is a source of emission at $14 \mu\text{m}$, the other two cores are seen in absorption against a diffuse background. Our image shows a spatially resolved nebula at the location of the IRAS source, with faint nebulosity extending to the south and north.

IRAS 18341–0113. This is a previously unreported near-IR reflection nebula, that 2MASS data shows is significantly redder than the bright star to the north. Our image also shows a small jet-like nebula, possibly associated with a faint nearby star, $27''$ to the NW of the bright star.

IRAS 18383+0059. This is a previously unreported near-IR reflection nebula. The PSF in this image is triangular because the primary mirror support was out of adjustment. Our image shows a wide binary star at the center of a faint monopolar nebula.

IRAS 18595–3712. This is a previously unreported near-IR reflection nebula in the VV CrA area. This source is also known as ISO-CrA 182 and MMS 23 in Chini et al. (2003). Olofsson et al. (1999) identify this object as a YSO candidate based on its mid-IR excess observed by ISO. To better show the bipolar morphology of this nebula, we employed additional smoothing over 12 pixels to show surface brightness contours down to $K = 21$.

IRAS 19266+0932. Also known as HBC 687 and Parsamian 21, and associated with HH 221, this is an FU Orionis type star (Staude et al. 1992). Polomski et al. (2005) found no mid-IR companions to this source, and present a detailed SED from 1 μm to 100 μm . Unique among the objects in this paper, the appearance of this nebula at K-band is very similar to its appearance in the optical.

IRAS 19411+2306. This is a previously unreported and complex reflection nebula and group of young stars. This object has not been detected as a source of methanol maser emission (Szymczak et al. 2000; Slysh et al. 1999), but it is the origin of a CO outflow (Beuther et al. 2002). The distance was estimated to be 4.3 kpc by Watson et al. (2003), whereas Guetter (1992) estimated a distance of 2.1 kpc to NGC 6823, which apparently hosts this source. Our image shows small patches of nebulosity near stars surrounded by a larger diffuse nebula.

IRAS 20353+6742. This nebula in L1152 was first observed in the infrared by Myers et al. (1987), who presents J through L-band photometry and calculate a bolometric luminosity of $3.3 L_{\odot}$ and a spectral slope of +2.06. This object may be the source of HH 376, and it is the origin of a bipolar high velocity CO outflow (Bontemps et al. 1996). We observed a spatially resolved near-IR source which appears to be bisected by a dust lane at the center of a faint bipolar nebula. It appears that the NE half is obscured just NE of the source.

IRAS 20361+5733. This is a previously unreported near-IR nebula that was observed to be a source of OH maser emission (Slysh et al. 1997). Our image shows three faint nebulae. The two to the west appear to be parts of a bipolar nebula.

IRAS 20377+5658. This faint reflection nebula in L1036 was first imaged in the near-IR by Hodapp (1994). This is the origin of a high velocity bipolar molecular outflow (Wu et al. 2004). We observed a bright point source with a faint loop of nebulosity to the NW.

IRAS 20386+6751. This source is also known as L1157 IRS and HH 375 VLA. This is the origin of a precessing bipolar molecular outflow (Gueth et al. 1996), an H₂O maser (Furuya et al. 2003), a CO outflow (Umemoto et al. 1992), shocked SiO emission (Zhang et al. 1995) and H₂ (Hodapp 1994), as well as emission from other molecules. Rodríguez & Reipurth (1998) observed this Class 0 source at the VLA to have a flux of 0.26 mJy at 3.6 mm. Molecular abundance gradients in the shocked gas show that this is a chemically active outflow (Bachiller et al. 2001). Our image shows two regions of shocked emission $\sim 1'$ to the north and south of an unseen source. Our image is presented in Figure 6.

IRAS 20453+6746. Better known as PV Cephei or RNO 125, this Herbig Ae/Be star is the origin of the parsec scale outflow HH 215. ISO spectra show no PAH emission, but

do show 10 μm silicate absorption (Acke & van den Ancker 2004). The star and associated nebula were brightest from 1977-79, having atomic emission lines with P Cygni profiles, but since then the emission lines have weakened (Magakian & Movsessian 2001). Optical [S II] images show knots in a precessing outflow, suggesting intermittent eruptions every ~ 2000 years (Gómez et al. 1997a). Our K-band image shows a very bright star, with an arc-like nebula to the east extending to the NE.

IRAS 20568+5217. This source is also known as HH 381 IRS. This is a previously unreported near-IR nebula. Near-IR spectroscopy shows a red continuum with deep CO absorption (Reipurth & Aspin 1997). Our image shows a bright central star at the center of a large bipolar nebula.

IRAS 20582+7724. This object in L1228 is the source of the HH 199 outflow. Reipurth et al. (2000) used HST/NICMOS and found a one armed spiral of circumstellar material similar to that seen around FU Ori stars. Bally et al. (1995) found that the axis of the CO outflow and HH knots differs from the axis of H₂ knots closer to the source by $\sim 40^\circ$. The narrow "jet" to the west in the contour plot is an electronic artifact from the detector array. In addition to a bright central star and monopolar nebula, we also observe faint knots of emission to the east and west that appear to be the above mentioned H₂ knots.

IRAS 21004+7811. This source is associated with the nebulae GY 21 and RNO 129. Persi et al. (1988) classified this object as a T Tauri star based on their J through L photometry. Our image shows a bright central binary with a nebulous loop to the NW. There is another larger and fainter loop-like nebula $\sim 50''$ to the west.

IRAS 21007+4951. This source in L988 has been observed in the near-IR by Hodapp (1994). It is the origin of a bipolar outflow (Clark 1986; Wu et al. 1996) as well as an H₂O maser (Brand et al. 1994). We observed a spatially resolved near-IR source with a faint, broad, jet-like nebula extending $\sim 25''$ to the WNW.

IRAS 21017+6742. This is a previously unreported near-IR reflection nebula associated with a YSO in the L1172D core that has been extensively studied at mm and radio wavelengths. It has been found to be the origin of a CO outflow (Myers et al. 1988). The envelope associated with this source has also been detected with SCUBA at 850 μm (Visser et al. 2002). Our image shows a bright star surrounded by a faint, diffuse nebula. An elongated K-band source is $18''$ to its NW. To the west, near the IRAS coordinates, is an unresolved star surrounded by a faint, diffuse nebula.

IRAS 21169+6804. Also known as CB 230, this object in L1177 was found by Yun (1996) to be a wide binary infrared source. N₂H⁺ maps show emission from both components, with the primary source having a thick disk with radius ~ 1600 AU. There are also two aligned

CO outflows, one for each component (Launhardt 2001). Only a single object is detected by SCUBA at 450 μm and 850 μm (Huard et al. 1999). Our image shows a large, bright monopolar nebula with a fainter spatially resolved companion $\sim 10''$ to the east.

IRAS 21352+4307. This is a previously unreported near-IR reflection nebula. Also known as CB 232, in the B 158 cloud, this is the origin of a CO outflow (Yun & Clemens 1994b). Yun & Clemens (1995) classify this source as a Class I object and present near-IR photometry and colors. A strong 850 μm source was detected near CB232:SMM2, $\sim 6''$ to the west of the IRAS source (Huard et al. 1999). Our image shows an unresolved point source with a small, faint nebula to the north.

IRAS 21388+5622. This is the source of HH 588 in a bright rimmed cloud in IC 1396, which has been detected in CS emission (Bronfman et al. 1996) and H₂O maser emission (Brand et al. 1994). Our image shows a bright near-IR source in a monopolar nebula extending $\sim 10''$ to the ENE. There is also a spatially resolved object at the SW end of a line of stars to the north of the monopolar nebula.

IRAS 21391+5802. This source is in L1121, in the IC 1396N core. Beltrán et al. (2002, 2004) used CS and methanol emission to probe the outflow, and estimate that there is about 5 M_{\odot} of circumstellar material. They conclude that the source and outflow properties are consistent with this being a low mass Class 0 source. This object is also a source of H₂O maser emission (Furuya et al. 2003). Our image shows a bright, jet-like nebula near the IRAS coordinate as well as several large patches of nebulosity around the field.

IRAS 21445+5712. This is a previously unreported near-IR reflection nebula in IC 1396. It has been detected in CO emission (Wouterloot & Brand 1989). Our image shows an E-W elongated nebula, as well as several stars embedded in a nebula $\sim 85''$ to the NW.

IRAS 21454+4718. Better known as V1735 Cygni, this is in L1031 in the IC 5146 star cluster, itself the subject of a study by Herbig & Dahm (2002). Although this is a well known FU Orionis star, Pezzuto et al. (2002) classified this as a T Tauri star based on its ISO colors. Ábraham et al. (2004) found this star faded by $\sim 40\%$ in the near-IR from about 1975 to 2000. This source was observed to be the origin of a CO outflow by Levreault (1983). The reflection nebula to the ENE is at the location of the submillimeter source V1735 Cyg SM1.

IRAS 21569+5842. This source in L1143 is likely to be a YSO in transition between Class I and II based on its IRAS SED and optical/near-IR imaging (Magnier et al. 1999). Our image shows a bright non-stellar object with a faint nebula to the north.

IRAS 22051+5848. Also known as HH 354 IRS, this object is in L1165 (Reipurth et al. 1997). Near-IR spectra show a red continuum with deep CO absorption that is very similar to the spectrum of L1551 IRS 5 (Reipurth & Aspin 1997). The cold envelope associated with this IRAS source was detected at $850 \mu\text{m}$ by Visser et al. (2002), who derive a total mass of $29.4 M_{\odot}$, and whose ^{12}CO maps show a bipolar outflow. Persi et al. (1988) reported near-IR photometry of this nebula and found it to be blueward of the main sequence reddening vector in a J-H vs. H-K color-color diagram, suggesting that scattered light dominates the near-IR flux from this nebula. Our image shows a spatially resolved near-IR source with a nebula extending to the SSW. The bright E-W elongated bar of nebulosity $\sim 13''$ to the SSW of the source, as well as a faint streak of nebulosity extending farther to the SSW, are optically visible in the DSS plates.

IRAS 22176+6303. This is the well known source Sharpless 140 IRS 1, also known as RAFGL 2884, in the L1240 dark cloud. This is the origin of a high velocity CO outflow (Bally & Lada 1983), HH 615-8 (Bally et al. 2002b), as well as methanol and H_2O masers. Beichman et al. (1979) found three $20 \mu\text{m}$ sources associated with this nebula. Radio observations have shown that IRS 2 and IRS 3 are both binary (Schwartz 1989). Megeath et al. (2004) analyses color-color data from the Spitzer Space Telescope to classify cluster members in the field around S140 IRS 1. At K-band we observed IRS 1 as the bright central star in a large, complex nebula. IRS 2 is a fainter object embedded in the nebula to the east. IRS 3, to the north, was not detected. Our image is presented in Figure 7.

IRAS 22266+6845. Umemoto et al. (1991) found this source in L1221 to drive an unusual U-shaped CO outflow. Lee et al. (2002) report that the CO emission is complicated by multiple outflows with multiple driving sources, and state that there may be another outflow source $25''$ to the east of the IRAS source. This object is likely to be the origin of the HH 363 flow, and it has been detected as a source of water maser emission by Furuya et al. (2003). Our image shows a wide binary star with nebulosity to the north and east.

IRAS 22267+6244. This nebula in L1203 was first observed in the near-IR by Hodapp (1994), and was found to be the origin of a CO outflow (Wouterloot & Brand 1989). MSX shows a double source separated by $39''$ at $8.28 \mu\text{m}$ that is too embedded to be seen in our K-band data. We observed a large, faint nebula with a broad, dark band across the center. There is a star, with a bright nebula to its west, on the southern edge of the large nebula. Our image is presented in Figure 8.

IRAS 22272+6358. This source is in L1206. Our image shows a bright point source to the east (IRAS 22272+6358B) surrounded by a diffuse nebula to the NE. IRAS 22272+6358A, about $45''$ to the west, is seen only as an elongated nebula. Ressler & Shure (1991) found that IRAS 22272+6358A is a Class I object with a nearly edge on disk, based

on their J through M photometry as well as IRAS and radio data. It is seen only in scattered light in the near-IR and is the origin of a CO outflow (Sugitani et al. 1989). IRAS 22272+6358B is seen directly in the near-IR and is either a late Class I or an early Class II object. Pezzuto et al. (2002) classify IRAS 22272+6358B as a Class I source, although it nearly has the ISO colors of a Class II source.

IRAS 22376+7455. These are previously unreported near-IR reflection nebulae in L1251B. An optically visible nebula and HH outflows were discovered by Eiroa et al. (1994), although this IRAS source does not seem to be the origin of the HH 189 outflow. Sato & Fukui (1989) observed two CO outflows in L1251, one from IRAS 22343+7501, and another from this source. Nikolic et al. (2003) found this source, which they identify with core #4 (H2b) in their paper, to be coincident with emission from H^{13}CN , HN^{13}C , ^{13}CO , C^{18}O , C^{34}S , H^{13}CO^+ , and SO. This was also observed to be the source of water maser emission by Furuya et al. (2003). Our image shows several stars in a small group. At the SE end is a large bipolar nebula. In the middle of the group is a small nebula arcing north of a faint, spatially resolved source. To the west is a faint star with an elongated nebula to its south. Faint nebulosity engulfs the whole group.

IRAS 23037+6213. This source, situated in the Cepheus C cloud, has been observed in the near-IR by Hodapp (1994). It has been found to be the origin of H_2O maser emission (Wouterloot & Walmsley 1986) and CO emission (Wouterloot & Brand 1989). Megeath et al. (2004) uses color-color data from the Spitzer Space Telescope to classify cluster members over a 3 pc wide region.

5. General Properties of Sources

5.1. Luminosity Distribution

In order to calculate the bolometric luminosity of our sources from the IRAS fluxes, we used the following relation:

$$L_{bol}(L_{\odot}) = [4.16 \times 10^{-6} \cdot F_{12} + 3.54 \times 10^{-6} \cdot F_{25} + 9.59 \times 10^{-7} \cdot F_{60} + 6.57 \times 10^{-7} \cdot F_{100}] \cdot D^2 \quad (2)$$

where F is the IRAS flux density in Jy at the wavelength (in microns) indicated by the subscript, and D is the distance to the source in parsecs. This formula, described by Reipurth et al. (1993), includes an estimate of flux emitted at sub-millimeter wavelengths based on their finding that the material responsible for the flux beyond 100 μm tends to have a characteristic temperature of 36 K. The IRAS 100 μm flux has been used to roughly estimate the submillimeter contribution to the bolometric luminosity by fitting a 36 K blackbody to

the IRAS 100 μm data point. The luminosity distribution presented in Figure 11 has a median value of $L_{bol} = 5.8 L_{\odot}$, with most of the sources having a luminosity between $0.5 L_{\odot}$ and $30 L_{\odot}$.

5.2. Nebula Evolution and Morphology

As a star begins to form, an outflow from the young star starts to carve a bipolar cavity out of the surrounding material. The cavity gets larger and wider as the star evolves and the outflow disperses the surrounding cloud (Arce & Sargent (2006) and citations therein). Once enough of the cloud has been dispersed, the young star becomes optically visible in the T Tauri phase. Having produced this atlas of near-IR reflection nebulae, we sought to classify them into morphological groups in an attempt to derive an evolutionary sequence and test this model.

We sought to do this through a comparison of the average spectral index for various morphological groups, under the assumption that a higher spectral index indicates a younger object. After careful inspection of all of the nebulae, it became apparent that a clear, one dimensional classification scheme was not practical because we were unable to unambiguously place each nebula in a morphological group. Although there are a number of cases where it is easy to classify the morphology of an individual nebula, there is also a large number of nebulae that defy simple morphological classification. If an evolutionary trend were to be found, another method was required. Assuming that the spectral index decreases with time, we examined the nebulae in this atlas in the order of their spectral indices. After doing this, we noticed the following trends.

The clearest trend, and the most quantifiable, is that the central star of the nebula tends to become more visible as the spectral index decreases. Among the one-third of the nebulae with the highest spectral index, there are 4 cases where a star, believed to be the central source, is visible as an unresolved point source. For these objects, most of the flux is scattered light from the nebula or what appears to be shocked emission. Among the one-third of the nebulae with the lowest spectral index, there are 5 cases where we cannot see a central unresolved point source. Light from the central star dominates the K-band flux for these objects.

Other trends we noticed are less obvious and less quantifiable. In order to understand if younger sources are more likely to have shocked H_2 emission, we considered the one-third of these 106 nebulae with the highest spectral index versus the one-third of sources with the lowest spectral index. Among the one-third of the nebulae with the highest spectral

index, 25% (9/35) show what appears to be shocked H_2 emission. Among the one-third of the nebulae with the lowest spectral index, we found that 9% (3/35) of cases appear to have shocked H_2 emission. In these cases, the apparent H_2 emission is confined to a few isolated knots, as opposed to the long chains of emission often found around the younger sources. This is consistent with the expectation that young stars experience accretion events, leading to bursts of outflow activity.

We also noticed that the nebulae around the older objects tend to be round and less elongated, diffuse and closer to the central star. For the younger objects, structured nebulosity could more often be found farther from the IRAS source, often as part of shocked emission or as a bipolar nebula. Comparatively less of the scattered light is very close to the central source. Finally, we noticed that we tend to find diffuse, arc shaped reflection nebulae (e.g. IRAS 03445+3242) only around sources with a low spectral index.

Overall, these general trends that we noticed are consistent with the concept of nebula evolution described above. Younger objects are surrounded by more dust, and thus are rarely seen directly at K-band. Shocked H_2 more likely to be found around younger objects, especially as large jets. As the cloud is dissipated, the star becomes directly visible and dominates the near-IR flux. We interpret nebulae such as those around IRAS 03445+3242 and HH 83 VLA 1 as light scattering off of the walls of a cavity that has been almost completely dispersed.

5.3. Nebula Brightness and Size

The nebulae in this paper range in size from being just larger than a stellar point to over $3'$ long, and display a similarly broad range of morphologies. The amount, distribution, and structure of the surrounding dust, as well as our point of view, can lead to nebulae appearing very different although they are at the same evolutionary stage. This limits the accuracy of our comparison of the sizes and near-IR brightness of the nebulae to the bolometric luminosities of these objects. Also, in cases where the central star is very bright at K-band, such as IRAS 21004+7811, the extent of the surface brightness contour may be dominated by the scattered light from the telescope rather than from the nebula. Cases where the flux is clearly dominated by light from the star rather than the nebula or where scattered light from the star dominates the apparent size of the nebula were not considered in the following analysis. Since our goal was to determine if there is a correlation between the nebula brightness and size with the source bolometric luminosity, we only considered the part of the nebula believed to be illuminated by the IRAS source. For example, we found two small nebulae near IRAS 06368+0938, but they are far enough from the IRAS source

position that it is unclear which nebula, if any, is associated with the IRAS source. Such cases were not considered in this analysis.

The K-band magnitudes for the nebulae are from the 2MASS extended source catalog for the cases where the nebula is included in this catalog. If not, the magnitude from the point source catalog was used. These magnitudes were converted to absolute magnitudes for the sources whose distances are known. This was then divided by 2.5 to directly compare the log of the bolometric luminosity to the log of the K-band flux. Figure 12 includes the 73 sources that have both 2MASS fluxes and distance estimates. The bolometric luminosities are as described above. Although we excluded objects where flux from the central star dominated over the flux from the nebula, in most cases there is still some near-IR flux from associated stars. The extent of this contamination varies from case to case.

We found a correlation between the near-IR brightness of the nebulae and the bolometric luminosity of the IRAS source as shown in Figure 12. The best fit power law relation has an index of 0.75 ± 0.09 , as this is the slope of the linear regression line on the log-log plot. The standard deviation from the regression line is 1.63 magnitudes. Since this analysis did not include nebulae where the near-IR luminosity is dominated by the central star, and since the central star tends to be visible on older objects, this correlation is biased against older stars. A significant amount of scatter is expected due to the diversity of objects in this sample, i.e. some sources are clearly seen through little extinction while others are nearly completely obscured at $2.2 \mu\text{m}$.

A mathematical model developed by Pendleton et al. (1990) shows that, for the case of a star illuminating a homogeneous medium, the luminosity of a reflection nebula should be proportional to the luminosity of the illuminating star. The nebulae illuminated by high bolometric luminosity sources appear to be underluminous in the near-IR because, as we have found, sources with higher bolometric luminosity tend to have a higher spectral index. Objects with a higher spectral index tend to be younger and cooler, and thus emit less near-IR flux than sources with a lower index. Furthermore, we expect that younger sources will tend to be surrounded by more dust, increasing the amount of extinction. Thus a nebula around such a source would appear to be underluminous in the near-IR given its bolometric luminosity.

To estimate the size of a nebula, we determined the total area contained within the $K = 19$ magnitudes per square arcsecond surface brightness contour. This contour was chosen as it is the faintest contour in nearly all of the figures. We took the square root of the area within the contour to determine the size of a box that would contain the same area, and this is the value we used as the apparent size of the nebula. We find a correlation between the bolometric luminosity of the IRAS source and the nebula’s linear size for those

nebulae where we have a distance estimate, and this is presented in Figure 13. Those cases where the measured size of the nebula is dominated by scattered light from a bright central star are noted by an asterisk in the last column of Table 2. On a log-log plot, the slope of the regression line is 0.41 ± 0.04 , with the data points having a standard deviation from the regression line of 0.25 (a factor of 1.76). The sizes d of the nebulae tend to follow the power law relation over several decades of luminosity. We find it interesting that the two sources with the lowest luminosity (IRAS 04302+2247, $L_{bol} = 0.28 L_{\odot}$, and IRAS 04248+2612, $L_{bol} = 0.33 L_{\odot}$) are both associated with bright and well known reflection nebula. In the case of IRAS 04302+2247, the central star cannot be seen at near-IR wavelengths because the circumstellar disk is seen edge on, whereas the central source of IRAS 04248+2612 has been resolved as a $0''.3$ binary by HST (Reipurth et al. 2000).

We believe that the scatter in the plot is due to the various ages, the various morphologies, the amount of extinction and the uncertainties in the distance to the nebula. We do not believe that uncertainties in the distance to these sources is the origin of these correlations between bolometric luminosity, near-IR luminosity, and size. Distance uncertainties are typically no greater than a factor of 2, whereas these relationships of near-IR brightness and size vs. bolometric luminosity cover several orders of magnitude in scale.

5.4. Shocked H₂ Emission

Having observed 197 sources at K-band, we found 22 nebulae that appear to be the source of shocked H₂ emission. We suspected a nebula to be a source of shocked H₂ emission if we found multiple distinct clumps of emission, linearly or symmetrically arranged about the central star. In comparison, reflection nebulae due to dust scattered light tend to be smooth, with diffuse edges. We performed follow-up observations using a $2.122 \mu\text{m}$ H₂ filter for 9 nebulae suspected of having shocked H₂ emission but not yet observed through a H₂ filter. We confirmed the presence of H₂ emission for all of them, thus we are confident that what we believe looks like H₂ emission actually is. These nebulae are listed in Table 3, which also includes the coordinates of a marked star or clump in each field.

Although 61% of the objects presented in this paper are known sources of molecular outflows (either through millimeter line emission, or they are the source of an HH object), relatively few show shocked H₂ emission. For example, IRAS 05311–0631 is the source of a well known Herbig-Haro outflow (HH 83), yet shows no signs of shocked emission within $1''.5$. It is possible that there is shocked emission that we did not see, either because it is too faint or outside of our $3'$ field of view with QUIRC. At any given time, it appears that $\sim 10\%$ (22/197) of Class I objects are sources of shocked H₂ emission.

Figures 14 through 22 show, as necessary, broad K-band, K-band – H₂, H₂ – K-band, and H₂ emission of the nebulae we observed in H₂. A 15'' scale bar is under the label in each figure. The morphology of this emission varies from a few knots, such as to the east of IRAS 03445+3242, to a series of bow shocks such as to the west of IRAS 05155+0707. In several cases, the morphology of the emission is in the form of a few small bow shocks. IRAS 21391+5802 has a series of shocks to the NE and a few knots to the NW of the source, which itself is only seen in scattered continuum light. There are many cases where reflection nebulae and H₂ emission are coincident. In such cases, narrow band imaging is very useful to confidently identify the nature of the observed nebulae. Aside from a small knot near IRAS 05403-0818, the H₂ emission we observed tends to be found quite far from the YSO. It is not uncommon for shocked emission to be found 80'' away. In the case of IRAS 00182+6223, the H₂ emission 53'' away has a projected separation of 1.2 pc.

5.5. Binary Frequency

The observations presented in this paper were made to explore the circumstellar environment around our sample of candidate Class I sources. As such, these data have limited use for constraining the binary frequency of these sources. An exposure time of 60 s was used for all observations to obtain a homogeneous data set, which resulted in many of the central stars being saturated. A program is underway to determine the binary frequency of a large number of Class I YSOs. We have tailored an observing program for this purpose, being careful not to saturate and observing through H, K, and L' filters. A forthcoming publication will present the results of this program.

6. IRAS 05450+0019

Although it does not have an unusually high bolometric luminosity, IRAS 05450+0019 is the source of one of the brightest reflection nebulae in this sample. This nebula is also one of the largest, being over 2' (0.3 pc) in extent. Only large collimated outflows such as HH 212 and IRAS 06047–1117, and nebulae around very luminous sources such as IRAS 22176+6303, are larger. This suggests that a special set of criteria must be met (e.g. a luminous source, enough dust distributed over a large area to scatter light but not enough to obscure the nebula) for such a bright and large nebula to be visible.

Although it is not well known as a bright nebula, IRAS 05450+0019 has been observed several times in the radio and mm. It has been observed in the course of surveys for emission

from H₂O (Wouterloot & Walmsley 1986) and methanol (Slysh et al. 1999) masers, CO (Likkell et al. 1991), ammonia (e.g., Jijina et al. 1999), H¹³CO, and CO¹⁸O (Aoyama et al. 2001). This object is 7'.6 ESE of NGC 2071, a center of high mass star formation (e.g., Aspin et al. 1992), in the Orion B molecular cloud. It is associated with NGC 2071e and is at a distance of ~500 pc (Clark 1991). Harju et al. (1993) estimated the bolometric luminosity to be 47 L_⊙, which is considerably greater than our estimate of 27.6 L_⊙. Having measured the ammonia mass, they infer a total mass of 86 M_⊙ for a clump 40'' E of the IRAS source (near the K-band peak), plus 12 M_⊙ for a clump 2' WNW of the IRAS source. They found that this pair of clumps has about 20 times as much potential energy as kinetic energy, and thus it is possible that they are coalescing. Launhardt et al. (1996) observed dust emission from the associated dust envelope at 1.3 mm but found no compact source, suggesting this object has an optically thin dust envelope. They estimate this object has about 10 M_⊙ in gas with 2 M_⊙ in the dust envelope, and is internally heated. The 1.3 mm peak corresponds to the bright component of the nebula to the east of the IRAS source. They also observed this nebula at K-band using the La Silla 2.2 m telescope, and present a small near-IR image overlaid with the millimeter map.

J, H, and K-band images with surface brightness contours are presented in Figure 9. In addition to IRAS observations at 12, 25, 60, and 100 μm, IRAS 05450+0019 was observed by ISO at 6.7 μm and 14.3 μm. Figure 10 shows the SED of this source, combining these data with data from IRTF at L'-band and the 2MASS extended source catalog for the J, H, and K_s data points. The nebula appears to be bipolar, with a broad dark band across the center. The eastern side is much brighter than the western, suggesting that the eastern side is tilted towards our line of sight. If the central dark band is from a disk seen nearly edge on, then it would be much larger (~15,000 AU or 0.07 pc in diameter) than would be expected (~100 AU for a protoplanetary or debris disk, ~1000 AU for a CTTS disk). Finally, this dark band appears tilted relative to the axis of the reflection nebula by ~ 20°, which is unique among the nebulae in this paper.

It is possible that the dark band is the shadow of a much smaller disk being projected into the surrounding dust cloud. This concept is proposed and examined by Hodapp et al. (2004) to explain the unusually large apparent size (~ 3000AU) of the disk around ASR41 in NGC 1333. They argue that if what they see is caused by an obscuring band in front of a nebula, then the band should be more prominent at shorter wavelengths, which is contrary to their observations. We note that in the case of our observations, the dark band does not seem more apparent at shorter wavelengths. The nebula seen by Hodapp et al. (2004) is almost equally bright on both sides of the dark band and thus is seen nearly edge-on, which helps to make the disk shadow easy to see. The nebula around IRAS 05450+0019 does not seem to be seen edge-on from our point of view, rather the eastern side is tilted towards

us. Pontoppidan & Dullemond (2005), who present more detailed modeling of disk shadows, show that a dark band can be visible for inclinations as low as 60° (90° being edge-on). Thus, even for cases where we do not see the disk edge-on, as it seems for the case of IRAS 05450+0019, a disk shadow may still be visible.

7. Conclusions

We have conducted a K-band imaging survey of 197 nearby candidate Class I sources. Most of our sources are between 150 pc and 500 pc away, and have a spectral index from 0 to 2. We found 106 near-IR counterparts that are associated with nebulae, 41 of which have not been previously reported. Among these are two areas, one in Orion and another in Serpens, that have a significant number of new nebulae. Based on our observations and archival data, we have come to the following conclusions:

1) Sources with higher bolometric luminosities tend to have larger, brighter nebulae. However, the near-IR brightness of the nebulae do not scale directly with the bolometric luminosity of the source. We believe this is because the more luminous sources have a tendency to be younger.

2) We found that the near-IR flux from younger objects tends to be mostly from the nebula, and the central star is rarely visible at K-band. For older YSOs, the central star is almost always visible at K-band. Most of the near-IR flux comes from the central star, and the much fainter nebula does not tend to be visible as far from the star.

3) Although many Class I sources are known to have molecular outflows, only $\sim 10\%$ show what appears to be shocked H_2 emission. This suggests that, at any given time, shocked H_2 emission is rare within ~ 0.15 pc the central star. Also, Class I YSOs that appear to be less evolved are more likely to be the source of H_2 emission than ones that appear more evolved.

4) Among all of the nebulae observed in this sample, IRAS 05450+0019 deserves special attention. Although it is relatively unknown, it is among the largest and brightest nebulae in this sample. It appears to be a nearly edge-on bipolar reflection nebula with a very large dark band that may be the shadow of a smaller disk projected into the surrounding envelope.

Acknowledgments We would like to thank our referee for a thorough review and constructive comments, which significantly improved this paper. This research has made use of the SIMBAD database, operated at CDS, Strasbourg, France. This research has made use of NASA’s Astrophysics Data System. The Digitized Sky Surveys were produced at the

Space Telescope Science Institute under U.S. Government grant NAG W-2166. The images of these surveys are based on photographic data obtained using the Oschin Schmidt Telescope on Palomar Mountain and the UK Schmidt Telescope. The plates were processed into the present compressed digital form with the permission of these institutions. The National Geographic Society - Palomar Observatory Sky Atlas (POSS-I) was made by the California Institute of Technology with grants from the National Geographic Society. The Second Palomar Observatory Sky Survey (POSS-II) was made by the California Institute of Technology with funds from the National Science Foundation, the National Geographic Society, the Sloan Foundation, the Samuel Oschin Foundation, and the Eastman Kodak Corporation. The Oschin Schmidt Telescope is operated by the California Institute of Technology and Palomar Observatory. The UK Schmidt Telescope was operated by the Royal Observatory Edinburgh, with funding from the UK Science and Engineering Research Council (later the UK Particle Physics and Astronomy Research Council), until 1988 June, and thereafter by the Anglo-Australian Observatory. The blue plates of the southern Sky Atlas and its Equatorial Extension (together known as the SERC-J), as well as the Equatorial Red (ER), and the Second Epoch [red] Survey (SES) were all taken with the UK Schmidt. Supplemental funding for sky-survey work at the ST ScI is provided by the European Southern Observatory. This research has made use of the NASA/ IPAC Infrared Science Archive, which is operated by the Jet Propulsion Laboratory, California Institute of Technology, under contract with the National Aeronautics and Space Administration. This publication makes use of data products from the Two Micron All Sky Survey, which is a joint project of the University of Massachusetts and the Infrared Processing and Analysis Center/California Institute of Technology, funded by the National Aeronautics and Space Administration and the National Science Foundation.

A. 2MASS to MKO Color Transformations

In this paper, we use both the Mauna Kea Observatories (MKO) and 2MASS photometric systems. The surface brightness contours in Figure 2 through 9 are in the MKO system whereas the photometry in Table 2 is in the 2MASS system. We have derived the following equations to convert between these two systems. These equations were derived by comparing the UKIRT faint standard stars, observed by UKIRT in the MKO system, to the 2MASS magnitudes of the same stars. The values and one sigma uncertainties given are based on linear fits to the data. These relations are limited by the fact that there are few red UKIRT standard stars. Also, using the (J–H) and (H–K) colors to derive an H magnitude (eqs. 3 - 6) may not yield the same result. To do so would require that (J–H)/(H–K) is a constant, which is generally not true. However, in the case of the UKIRT standard stars,

this is approximately true.

$$J_{2MASS} = (0.015 \pm 0.005) + (0.050 \pm 0.010)(J - H)_{MKO} + J_{MKO} \quad (\text{A1})$$

$$J_{MKO} = (-0.012 \pm 0.005) + (-0.055 \pm 0.008)(J - H)_{2MASS} + J_{2MASS} \quad (\text{A2})$$

$$H_{2MASS} = (0.025 \pm 0.004) + (-0.028 \pm 0.007)(J - H)_{MKO} + H_{MKO} \quad (\text{A3})$$

$$H_{2MASS} = (0.021 \pm 0.003) + (-0.044 \pm 0.010)(H - K)_{MKO} + H_{MKO} \quad (\text{A4})$$

$$H_{MKO} = (-0.026 \pm 0.003) + (0.029 \pm 0.006)(J - H)_{2MASS} + H_{2MASS} \quad (\text{A5})$$

$$H_{MKO} = (-0.021 \pm 0.003) + (0.041 \pm 0.011)(H - K_s)_{2MASS} + H_{2MASS} \quad (\text{A6})$$

$$K_{s,2MASS} = (0.014 \pm 0.004) + (0.042 \pm 0.013)(H - K)_{MKO} + K_{MKO} \quad (\text{A7})$$

$$K_{MKO} = (-0.016 \pm 0.004) + (-0.030 \pm 0.015)(H - K_s)_{2MASS} + K_{s,2MASS} \quad (\text{A8})$$

$$(J - H)_{2MASS} = (-0.010 \pm 0.006) + (1.078 \pm 0.011)(J - H)_{MKO} \quad (\text{A9})$$

$$(J - K_s)_{2MASS} = (0.004 \pm 0.006) + (1.018 \pm 0.008)(J - K)_{MKO} \quad (\text{A10})$$

$$(H - K_s)_{2MASS} = (0.007 \pm 0.004) + (0.914 \pm 0.013)(H - K)_{MKO} \quad (\text{A11})$$

REFERENCES

- Ábrahám, P., Kóspál, Á., Csizmadia, Sz., Kun, M., Moór, A., & Prusti, T., 2004, *A&A*, 428, 89
- Acke, B., & van den Ancker, M., 2004, *A&A*, 426, 151
- Adams, F., Lada, C., & Shu, F., 1987, *ApJ*, 312, 788
- Ambartsumian, V., 1954, *Soobshch. Byurakan. Astrofiz. Obs.*, 13, 3
- André, P., Motte, F., & Bacmann, A., 1999, *ApJ*, 513, L57
- André, P., Ward-Thompson, D., & Barsony, M., 1993, *ApJ*, 406, 122
- Aoyama, H., Mizuno, N., Yamamoto, H., Onishi, T., Mizuno, A., & Fukui, Y., 2001, *PASJ*, 53, 1053
- Arce, H., & Sargent, A., 2006, *astro-ph/0605139*
- Aspin, C., 1992, *A&A*, 266, 416
- Aspin, C., & Reipurth, B., 2000, *MNRAS*, 311, 522
- Aspin, C., Sandell, G., & Walther, D., 1992, *MNRAS*, 258, 684
- Bachiller, R., Perez Gutiérrez, M., Kumar, M., & Tafalla, M., 2001, *A&A*, 372, 899
- Bally, J., Devine, D., & Alten, V., 1996, *ApJ*, 473, 921
- Bally, J., Devine, D., Alten, V., & Sutherland, R., 1997, *ApJ*, 478, 603
- Bally, J., Devine, D., Fesen, R., & Lane, A., 1995, *ApJ*, 454, 345
- Bally, J., & Lada, C., 1983, *ApJ*, 265, 824
- Bally, J., Reipurth, B., & Aspin, C., 2002a, *ApJ*, 574, L79
- Bally, J., Reipurth, B., Walawender, J., & Armond, T., 2002b, *AJ*, 124, 2152
- Battinelli, P., & Capuzzo-Dolcetta, R., 1991, *MNRAS*, 249, 76
- Beichman, C., Becklin, E., & Wynn-Williams, C.G., 1979, *ApJ*, 232, L47
- Belloche, A., André, P., Despois, D., & Blinder, S., 2002, *A&A*, 393, 927

- Beltrán, M., Girart, J., Estalella, R., & Ho, P., 2004, *A&A*, 426, 941
- Beltrán, M., Girart, J., Estalella, R., Ho, P., & Palau, A., 2002, *ApJ*, 573, 246
- Benson, P., & Myers, P., 1989, *ApJS*, 71, 89
- Beuther, H., Schilke, P., Sirdharan, T., Menten, K., Walmsley, C., & Wyrowski, F., 2002, *A&A*, 383, 892
- Bieging, J., & Cohen, M., 1985, *ApJ*, 289, L5
- Bontemps, S., André, P., Terebey, S., & Cabrit, S., 1996, *A&A*, 311, 858
- Brand, J., et al., 1994, *A&AS*, 103, 541
- Bronfman, L., Nyman, L., & May, J., 1996, *A&AS*, 115, 81
- Brown, D., & Chandler, C., 1999, *MNRAS*, 303, 855
- Buckle, J., Hatchell, J., & Fuller, G., 1999, *A&A*, 348, 584
- Carballo, R., Wesselius, P., & Whittet, D., 1992, *A&A*, 262, 106
- Cardi, D. R., Telesco, C. M., Williams, J. P., Fisher, R. S., Packham, C., Pina, R., & Radomski, J., 2003, *ApJ*, 585, 392
- Cesaroni, R., Palagi, F., Felli, M., Catarzi, M., Comoretto, G., Di Franco, S., Giovanardi, C., & Palla, F., 1988, *A&AS*, 76, 445
- Chen, H., Fukui, Y., & Yang, J., 1992, *ApJ*, 398, 544
- Chen, H., & Tokunaga, A., 1994, *ApJS*, 90, 149
- Chini, R., Reipurth, B., Sievers, A., Ward-Thompson, D., Haslam, C., Kreysa, E., & Lemke, R., 1997, *A&A*, 325, 542
- Chini, R., Kämpgen, K., Reipurth, B., Albrecht, M., Kreysa, E., Lemke, R., Nielbock, M., et al., 2003, *A&A*, 409, 235
- Clark, F., 1986, *A&A*, 164, L19
- Clark, F., 1991, *ApJS*, 75, 611
- Codella, C., Palumbo, G. G. C., Pareschi, G., Scappini, F., Caselli, P., & Attolini, M. R., 1995, *MNRAS*, 276, 57

- Cohen, M., 1980, *AJ*, 85, 29
- Davis, C., Ray, T., Eisloffel, J., & Corcoran, D, 1997, *A&A*, 324, 263
- Eiroa, C., Torrelles, J., Miranda, L., Anglada, G., & Estalella, R., 1994, *A&AS*, 108, 73
- Felli, M., Palagi, & Tofani, G., 1992, *A&A*, 255, 293
- Fouqué, P., Le Bertre, T., Epchtein, N., Guglielmo, F., & Kerschbaum, F., 1992, *A&A*, 93, 151
- Fujii, T., Nakada, Y., & Parthasarathy, M., 2002, *A&A*, 385, 884
- Fukui, Y., 1989, in *Workshop on Low-Mass Star Formation and Pre-Main-Sequence Objects (ESO Conf. and Workshop Proc. 33)*, ed. B. Reipurth (Garching: ESO), 2
- Fukui, Y., Sugitani, K., Takaba, H., Iwata, T., Mizuno, A., Ogawa, H., & Kawabata, K., 1986, *ApJ*, 311, L85
- Fuller, G., Lada, E., Masson, C., & Myers, P., 1995, *ApJ*, 453, 754
- Fuller, G., Myers, P., Welch, W., Goldsmith, P., Langer, W., Campbell, B., Guilloteau, S., & Wilson, R., 1991, *ApJ*, 376, 135
- Furuya, R., Kitamura, Y., Saito, M., Kawabe, R., & Wootten, H. A., 1999, *ApJ*, 525, 821
- Furuya, R., Kitamura, Y., Wootten, A., Claussen, M., & Kawabe, R., 2003, *ApJS*, 144, 71
- Gómez, M., Kenyon, S. & Whitney, B., 1997a, *AJ*, 114, 265
- Gómez, M., Whitney, B., & Kenyon, S., 1997b, *AJ*, 114, 1138
- Gueth, F., Guilloteau, S., & Bachiller, R., 1996, *A&A*, 307, 891
- Guetter, H., 1992, *AJ*, 103, 197
- Gyulbudaghian, A., Glushkov, Y., & Denisyuk, E., 1978, *ApJ*, 224, L137
- Gyulbudaghian, A., & Magakian, T., 1977, *SvAL*, 3, 58
- Haisch, K., Greene, T., Barsony, M., & Stahler, S., 2004, *AJ*, 127, 174
- Harju, J., Walmsley, C., & Wouterloot, J., 1993, *A&AS*, 98, 51
- Hartmann, L., Calvet, N., Allen, L., Chen, H., & Jayawardhana, R., 1999, *AJ*, 118, 1784

- Henning, T., Cesaroni, R., Walmsley, & Pfau, W., 1992, *A&AS*, 93, 525
- Herbig, G., & Dahm, S., 2002, *AJ*, 123, 304
- Hilton, J., & Lahulla, J., 1995, *A&AS*, 113, 325
- Hind, J., 1864, *MNRAS*, 24, 65
- Hirano, N., Kameya, O., Mikami, H., Saito, S., Umemoto, T., & Yamamoto, S., 1997, *ApJ*, 478, 631
- Hodapp, K., 1994, *ApJS*, 94, 615
- Hodapp, K., Hora, J., Hall, D., Cowie, L., Metzger, M., Irwin, E., Vural, K., et al., 1996, *New Astronomy*, 1, 177
- Hodapp, K., Walker, C., Reipurth, B., Wood, K., Bally, J., Whitney, B., & Connelley, M., 2004, *ApJ*, 601, L79
- Hogerheijde, M., van Dishoeck, E., Blake, G., & van Langevelde, H. J., 1998, *ApJ*, 502, 315
- Huard, T., Sandell, G., & Weintraub, D., 1999, *ApJ*, 526, 833
- Hubble, E., 1916, *ApJ*, 44, 190
- Jennings, R., Cameron, D., Cudlip, & Hirst, C., 1987, *MNRAS*, 226, 461
- Jijina, J., Myers, P., & Adams, F., 1999, *ApJS*, 125, 161
- Kenyon, S., & Hartmann, L., 1995, *ApJS*, 101, 117
- Knox Shaw, H., 1916, *MNRAS*, 76, 646
- Krisciunas, K., Sinton, W., Tholen, K., Tokunaga, A., Golisch, W., Griep, D., Kaminski, C, et al., 1987, *PSAP*, 99, 887
- Kun, M., Aoyama, H., Yoshikawa, N., Kawamura, A., Yonekura, Y., Onishi, T., & Fukui, Y., 2001, *PASJ*, 53, 1063
- Lada, C., & Wilking, B., 1984, *ApJ*, 287, 610
- Lada, C., 1990, in "The Physics of Star Formation and Early Stellar Evolution", eds. Lada, C., & Kylafis, N., Kluwer Academic Publishers, p. 343

- Launhardt, R., 2001, *The Formation of Binary Stars*, Proceedings of IAU Symp. 200, ed. Zinnecker, H., & Mathieu, R. (San Francisco: Astronomical Society of the Pacific), 117
- Launhardt, R., & Henning, T., 1997, *A&A*, 326, 329
- Lee, C., Mundy, L., Stone, J., & Ostriker, E., 2002, *ApJ*, 576, 294
- Levreault, R., 1983, *ApJ*, 265, 855
- Levreault, R., 1988, *ApJ*, 330, 897
- Likkell, L., Forveille, T., Omont, A., & Morris, M., 1991, *ApJS*, 75, 611
- Lucas, P., Blundell, K., & Roche, P., 2000, *MNRAS*, 318, 526
- Magakian, T., 2003, *A&A*, 399, 141
- Magakian, T., & Movsessian, T., 2001, *Ap*, 44, 419
- Magnier, E., Volp, A., Laan, K., Van den Ancker, M., & Waters, L., 1999, *A&A*, 352, 228
- Margulis, M., Lada, C., & Young, E., 1989, *ApJ*, 345, 906
- Marraco, R., & Rydgren, A., 1981, *AJ*, 86, 62
- Mathieu, R., Benson, P., Fuller, G., Myers, P., & Schild, R., 1988, *ApJ*, 330, 385
- Megeath, S., Allen, L., Gutermuth, R., Pipher, J., Myers, P., Calvet, N., Hartmann, L., et al., 2004, *ApJS*, 154, 363
- Moneti, A., & Reipurth, B., 1995, *A&A*, 301, 721
- Mookerjee, B., Ghosh, S., Rengarajan, T., Tandon, S., & Verma, R., 2000, *AJ*, 120, 1954
- Moore, T., & Emerson, J., 1994, *MNRAS*, 271, 243
- Moreira, M., Jessop, N., Santos, C., & Yun, J., 2000, *AJ*, 119, 2960
- Morgan, J., Schloerb, F., Snell, R., & Bally, J., 1991, *ApJ*, 376, 618
- Moriarty-Schieven, G., Wannier, P., Tamura, M., & Keene, J., 1992, *AJ*, 400, 260
- Motte, F., André, P., Ward-Thompson, D., & Bontemps, S., 2001, *A&A*, 372, L41
- Mundt, R., & Raga, A., 1991, *A&A*, 252, 740

- Myers, P., Fuller, G., Mathieu, R., Beichman, C., Benson, P., Schild, R., & Emerson, J., 1987, *ApJ*, 319, 340
- Myers, P., Heyer, M., Snell, R., & Goldsmith, P., 1988, *ApJ*, 324, 907
- Nikolic, S., Johansson, L., & Harju, J., 2003, *A&A*, 409, 941
- Noguchi, K., Qian, Z., Wang, G., & Wang, J., 1993, *PASJ*, 45, 65
- Obayashi, A., Kun, M., Sato, F., Yonekura, Y., & Fukui, Y., 1998, *AJ*, 115, 274
- Oliver, R., Mashedier M., & Thaddeus, P., 1996, *A&A*, 315, 578
- Olofsson, G., Hultgren, M., Kaas, A. A., Bontemps, S., Nordh, L., Abergel, A., André, P., et al., 1999, *A&A*, 350, 883
- Padgett, D., Brandner, W., Stapelfeldt, K., Strom, S., Terebey, S., & Koerner, D., 1999, *ApJ*, 117, 1490
- Park, S., & Kenyon, S., 2002, *AJ*, 123, 3370
- Parsamian, E., & Petrosian, V., 1979, *SoByu*, 51, 12
- Pendleton, Y., Tielens, A., & Werner, M., 1990, *ApJ*, 349, 107
- Persi, P., Ferrari-Toniolo, M., Busso, M., Robberto, M., Scaltriti, F., & Silvestro, G., 1988, *AJ*, 95, 1167
- Persi, P., Palagi, F., & Felli, M., 1994, *A&A*, 291, 577
- Pezzuto, S., Grillo, F., Benedettini, M., Caux, E., Di Giorgio, A., Giannini, T., Leeks, S., et al., 2002, *MNRAS*, 330, 1034
- Polomski, E., Woodward, C., Holmes, E., Butner, H., Lynch, D., Russell, R., Sitko, M., et al., 2005, *AJ*, 129, 1035
- Pontoppidan, K. M., Dullemond, C. P., 2005, *A&A*, 435, 595
- Reipurth, B., & Aspin, C., 1997, *AJ*, 114, 2700
- Reipurth, B., Bally, J., & Devine, D., 1997, *AJ*, 114, 2708
- Reipurth, B., Chini, R., Krügel, E., Kreysa, E., & Sievers, A., 1993, *A&A*, 273, 221
- Reipurth, B., & Eiroa, C., 1992, *A&A*, 256, L1

- Reipurth, B., Nyman, L., & Chini, R., 1996, *A&A*, 314, 258
- Reipurth, B., Rodríguez, L., Anglada, G., & Bally, J., 2002, *AJ*, 124, 1045
- Reipurth, B., Yu, K., Moriarty-Schieven, G., Bally, J., Aspin, C., & Heathcote, S., 2004, *AJ*, 127, 1069
- Reipurth, B., Yu, K. C., Heathcote, S., Bally, J., & Rodríguez, L., 2000, *AJ*, 120, 1449
- Ressler, M., & Shure, M., 1991, *AJ*, 102, 1398
- Rodríguez, L., Myers, P., Cruz-González, I., & Terebey, S., 1989, *ApJ*, 347, 461
- Rodríguez, L., & Reipurth, B., 1998, *RevMexAA*, 34, 13
- Sagar, R., & Joshi, U., 1983, *MNRAS*, 205, 747
- Sandell, G., & Aspin, C., 1998, *A&A*, 333, 1016
- Sato, F., & Fukui, Y., 1989, *ApJ*, 343, 773
- Schwartz, P.R., 1989, *ApJ*, 338, L25
- Siebenmorgen, R., & Krügel, E., 2000, *A&A*, 364, 625
- Slysh, V., Dzura, A., Val'tts, I., & Gerard, E., 1994, *A&AS*, 106, 87
- Slysh, V., Dzura, A., Val'tts, I., & Gerard, E., 1997, *A&AS*, 124, 85
- Slysh, V., Val'tts, I., Kalenskii, S., Voronkov, M., Palagi, F., Tofani, G., & Catarzi, M., 1999, *A&AS*, 134, 115
- Staude, H., & Neckel, T., 1992, *ApJ*, 400, 556
- Straizys, V., Cernis, K., Kazlauskas, A., & Meistas, E., 1992, *BaltA*, 1, 149
- Strom, K., Newton, G., Strom, S., Searman, R., Carrasco, L., Cruz-González, I., Serrano, A., & Grasdalen, G., 1989, *ApJS*, 71, 183
- Sugitani, K., Fukui, Y., Mizuno, A., & Ohashi, N., 1989, *ApJ*, 342, 87
- Szymczak, M., Hrynek, G., & Kus, A., 2000, *A&AS*, 143, 269
- Tafalla, M., Myers, P., Mardones, D., & Bachiller, R., 2000, *A&A*, 359, 967
- Tapia, M., Persi, P., Bohigas, J., & Ferrari-Toniolo, M., 1997, *AJ*, 113, 1769

- Terebey, S., Chandler, C. J., & André, P., 1993, *ApJ*, 414, 759
- Terebey, S., Vogel, S., & Myers, P., 1989, *ApJ*, 340, 472
- Terebey, S., Vogel, S., & Myers, P., 1992, *ApJ*, 390, 181
- Tokunaga, A., & Vacca, W., 2005, *PASP*, 117, 421
- Tokunaga, A., Simons, D., & Vacca, W., 2002, *PASP*, 114, 180
- Tsujimoto, M., Koyama, K., Kobayashi, N., Goto, M., Tsuboi, Y & Tokunaga, A., 2003, *AJ*, 125, 1537
- Umemoto, T., Hirano, N., Kameya, O., Fukui, Y., Kuno, N., & Takubo, K., 1991, *ApJ*, 377, 510
- Umemoto, T., Iwata, T., Fukui, Y., Mikami, H., Yamamoto, S., & Kameya, O., 1992, *ApJ*, 392, L83
- Vieira, S., Corradi, W., Alencar, S., Mendes, L., Torres, C., Quast, G., Guimarães, M., & Da Silva, L., 2003, *AJ*, 126, 2971
- Visser, A., Richer, J., & Chandler, C., 2002, *AJ*, 124, 2756
- Wang, H, Yang, J, Wang, M., Deng, L., Yan, J., & Chen, J., 2001, *AJ*, 121, 1551
- Watson, C., Araya, E., Sewilo, M., Churchwell, E., Hofner, P., & Kurtz, S., 2003, *ApJ*, 587, 714
- Weintraub, D., 1990, *ApJS*, 74, 575
- Weintraub, D., Tegler, S., Kastner, J, & Rettig, T., 1994, *ApJ*, 423, 674
- Wiseman, J., Wootten, A., Zinnecker, H., & McCaughrean, M., 2001, *ApJ*, 550, L87
- Wolf, S., Padgett, D., & Stapelfeldt, K., 2003, *ApJ*, 588, 373
- Wouterloot, J., & Brand, J., 1989, *A&AS*, 80, 149
- Wouterloot, J., Brand, J., & Fiegle, K., 1993, *A&AS*, 98, 589
- Wouterloot, J., & Walmsley, C., 1986, *A&A*, 168, 237
- Wu, Y., Huang, M., & He, J., 1996, *A&AS*, 115, 283
- Wu, Y., Wei, Y., Zhao, M., Shi, Y., Yu, W., Qin, S., & Huang, M., 2004, *A&A*, 426, 503

- Yan, J., Wang, H., Wang, M., Deng, L., Yang, J., & Chen, J., 1998, *AJ*, 116, 2438
- Yu, K., Billawala, Y., & Bally, J., 1999, *AJ*, 118, 2940
- Yun, J., Santos, C., Clemens, D., Afonso, J., McCaughrean, M., Preibisch, T., Stanke, T., & Zinnecker, H., 2001, *A&A*, 372, L33
- Yun, J., 1996, *AJ*, 111, 930
- Yun, J., & Clemens, D., 1995, *AJ*, 109, 742
- Yun, J., & Clemens, D., 1994a, *AJ*, 108, 612
- Yun, J., & Clemens, D., 1994b, *ApJS*, 92, 145
- Zavagno, A., Molinari, S., Tommasi, E., Saraceno, P., & Griffin, M., 1997, *A&A*, 325, 685
- Zinnecker, H., McCaughrean, M., & Rayner, J., 1998, *Nature*, 394, 862
- Zhang, Q., Ho, P., Wright, M., & Wilner, D., 1995, *ApJ*, 451, L71

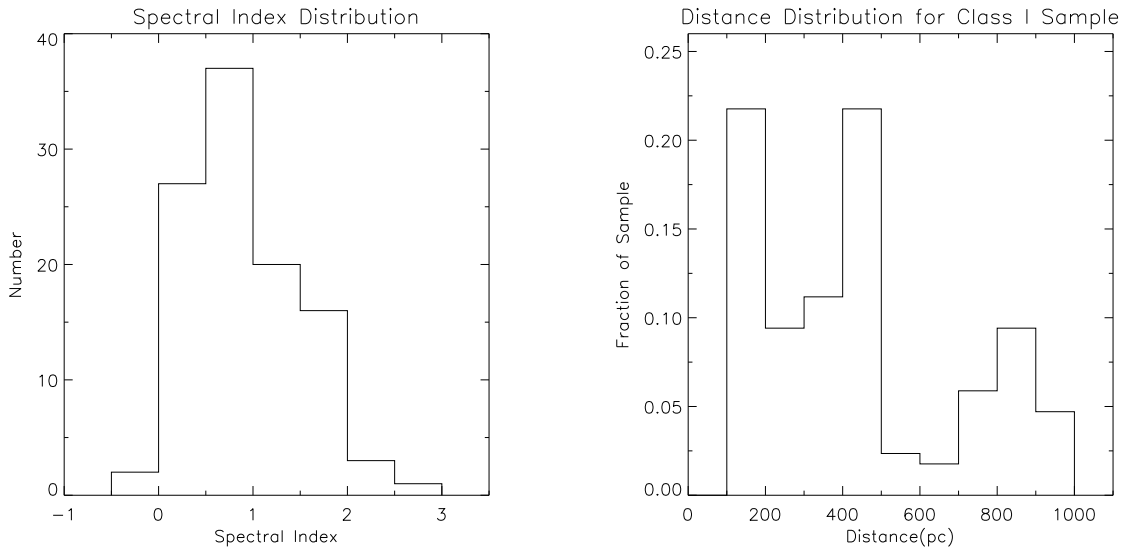


Fig. 1.— Left: Our sample’s spectral index distribution, with a median value of $+0.79$. This plot shows that only a few of our sources are T Tauri stars (index < 0), and the majority are transitional (i.e. between Class II and I) or Class I YSOs. Right: Distribution of distances to our sample objects, which has a median value of 470 pc.

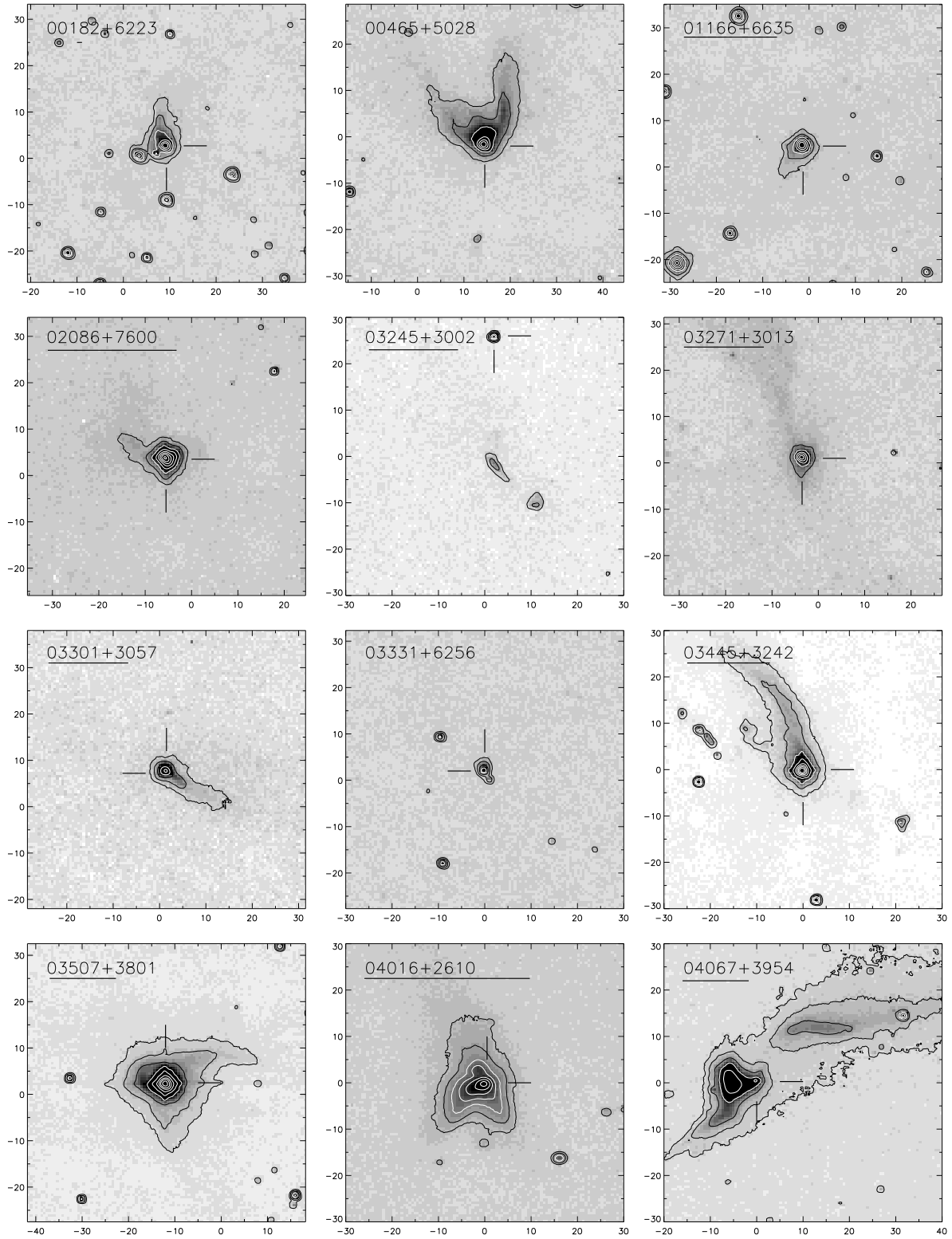


Fig. 2.— $60'' \times 60''$ images of each source, with the IRAS position at (0,0). The 2MASS coordinates for the star indicated with tick marks is given in Table 2. A 5,000 AU scale bar is under the name of each object for which we have a distance estimate.

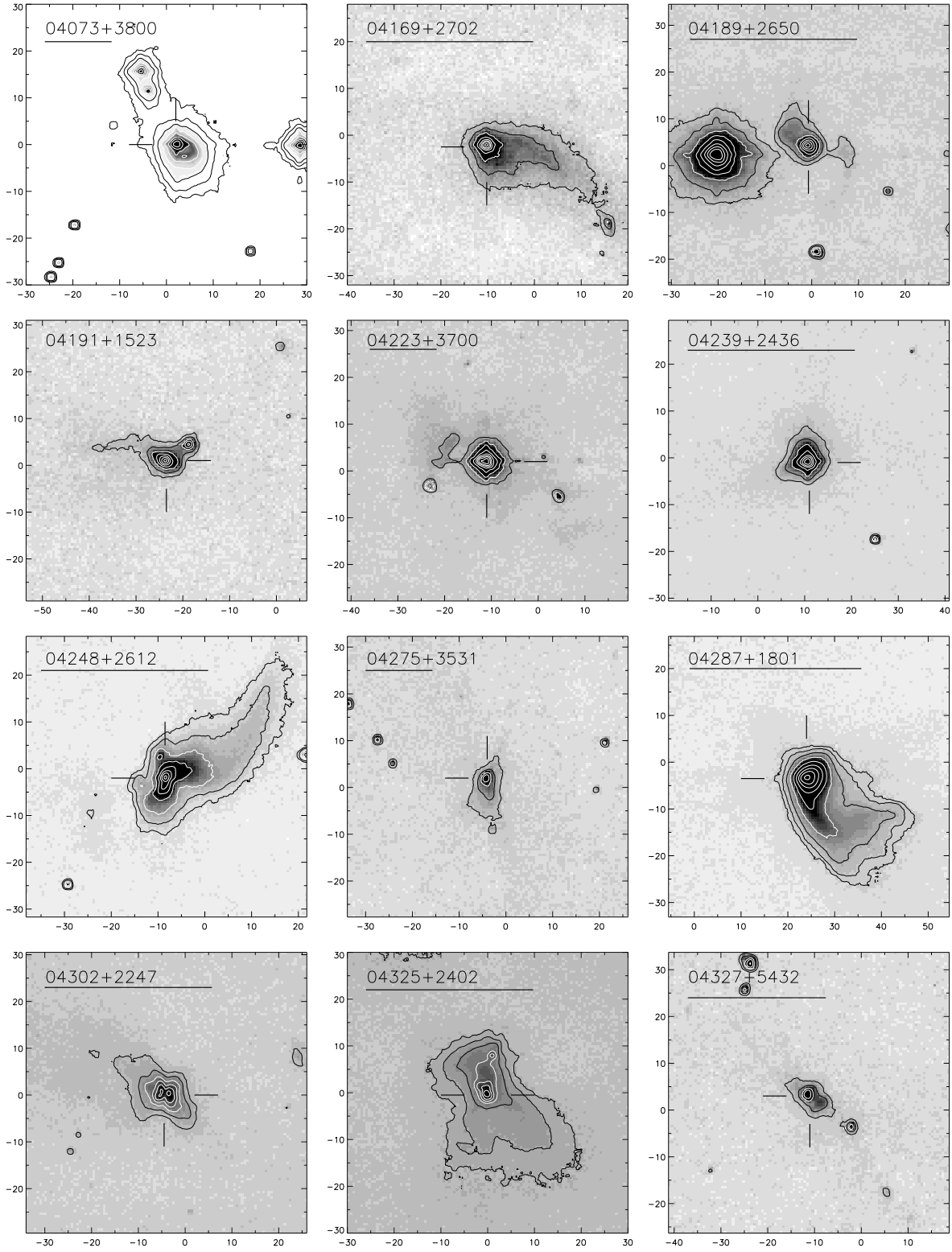


Fig. 2.—

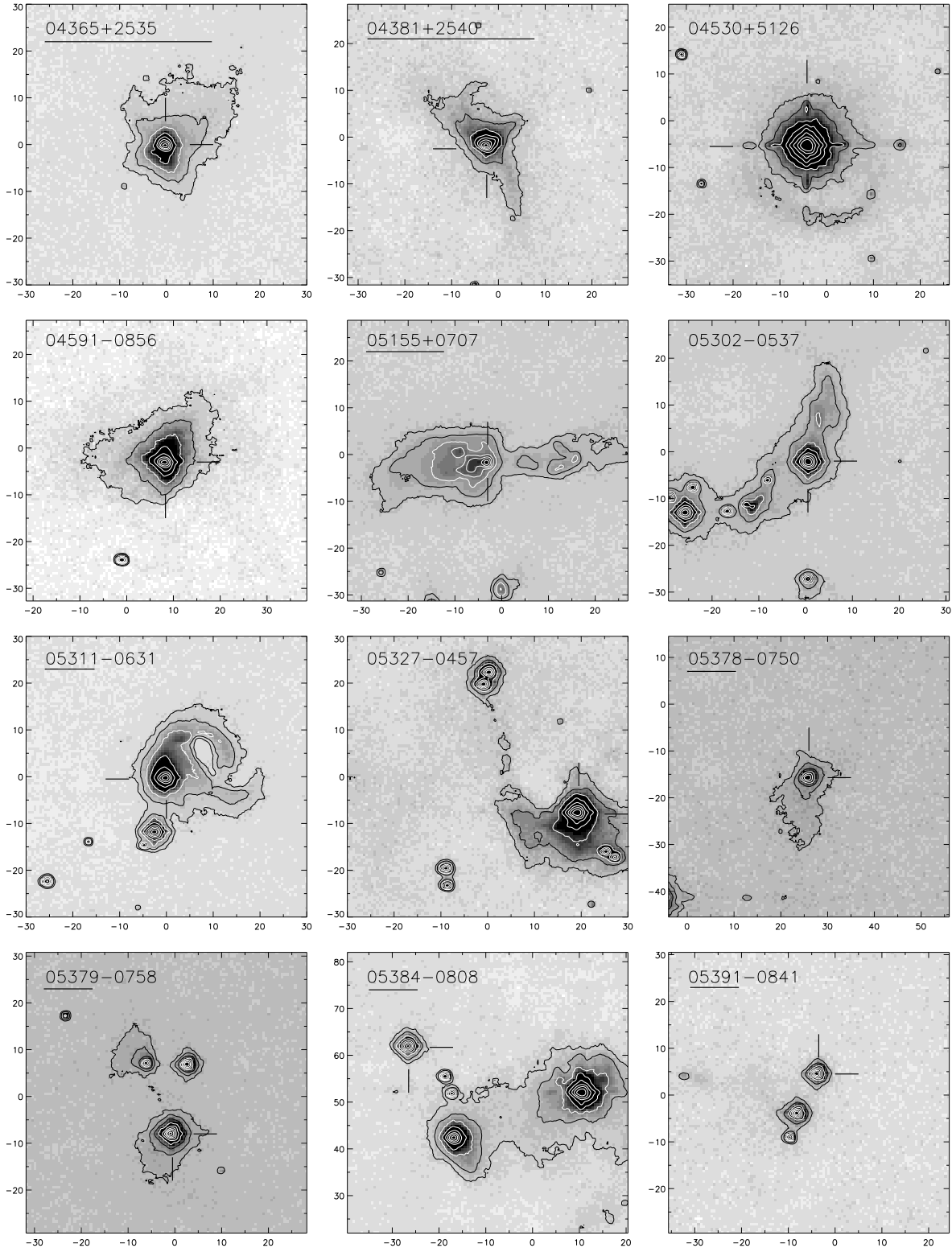


Fig. 2.—

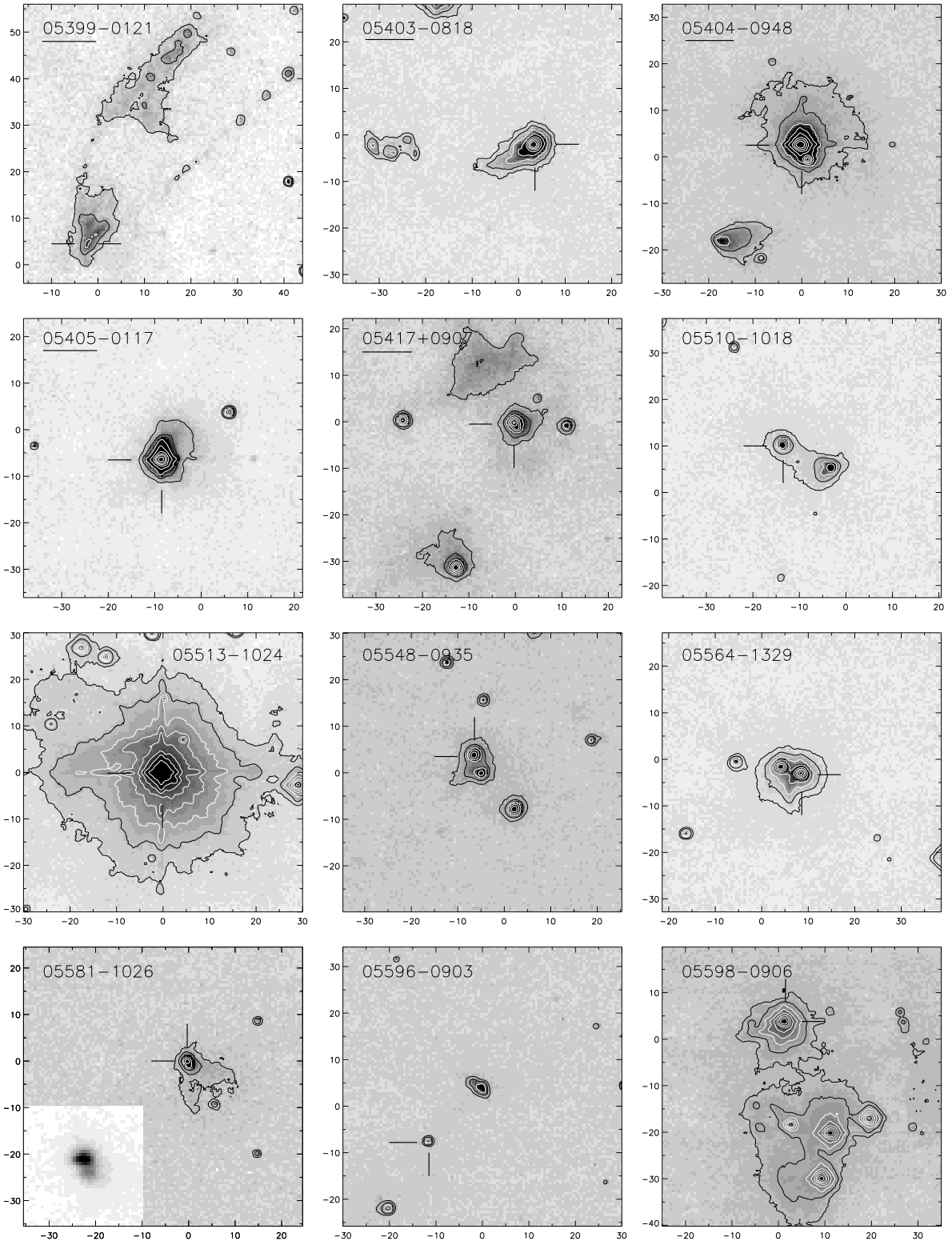


Fig. 2.—

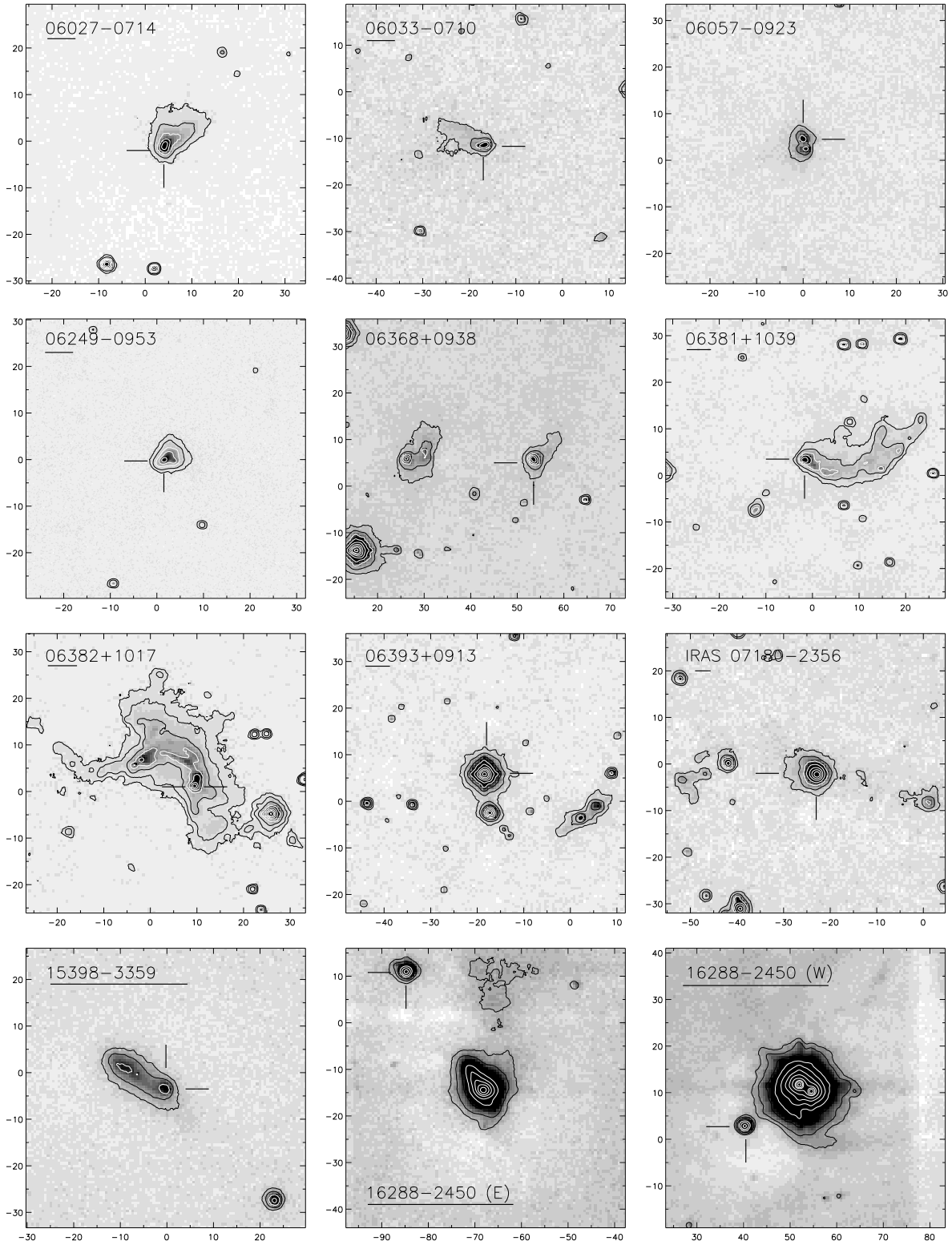


Fig. 2.—

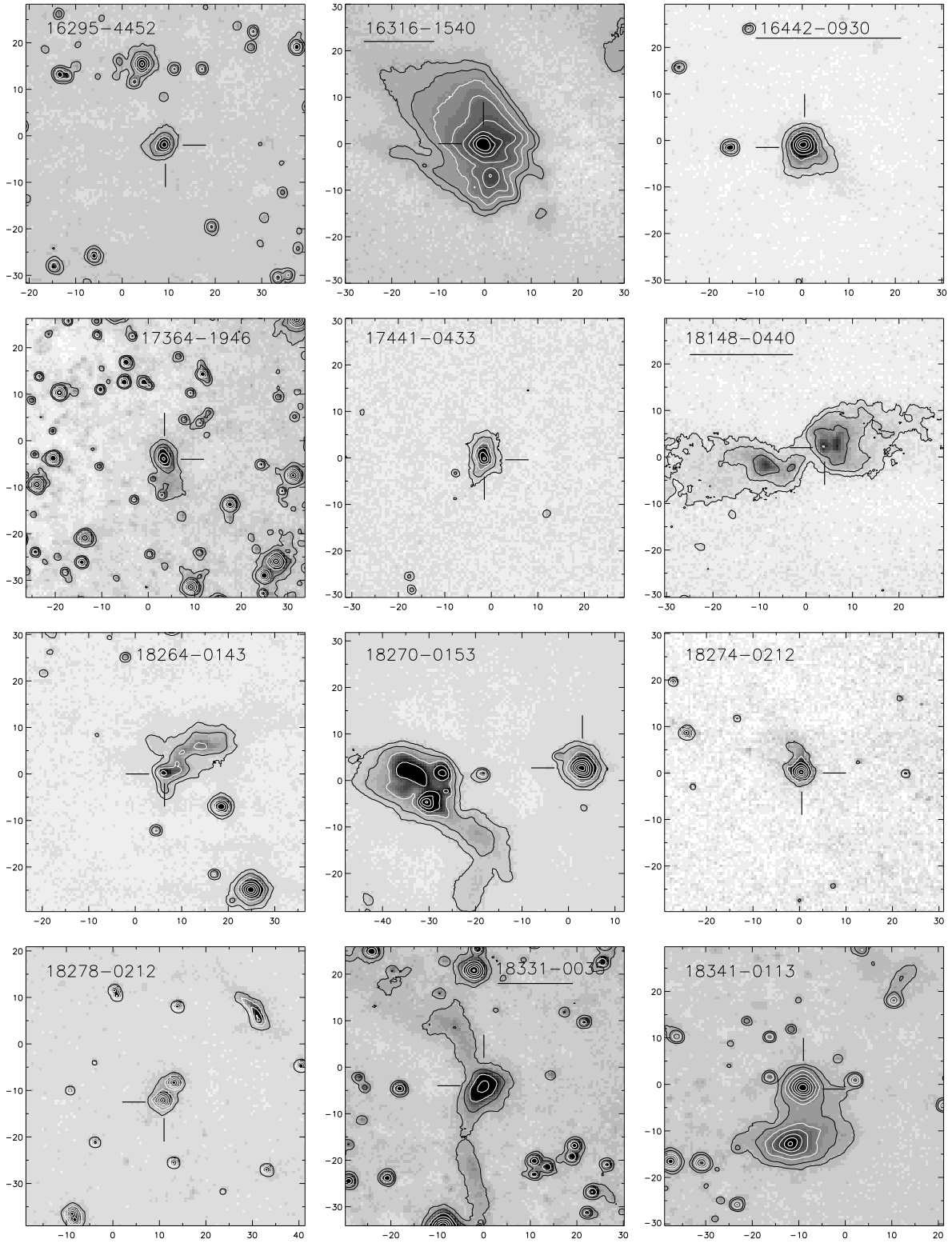


Fig. 2.—

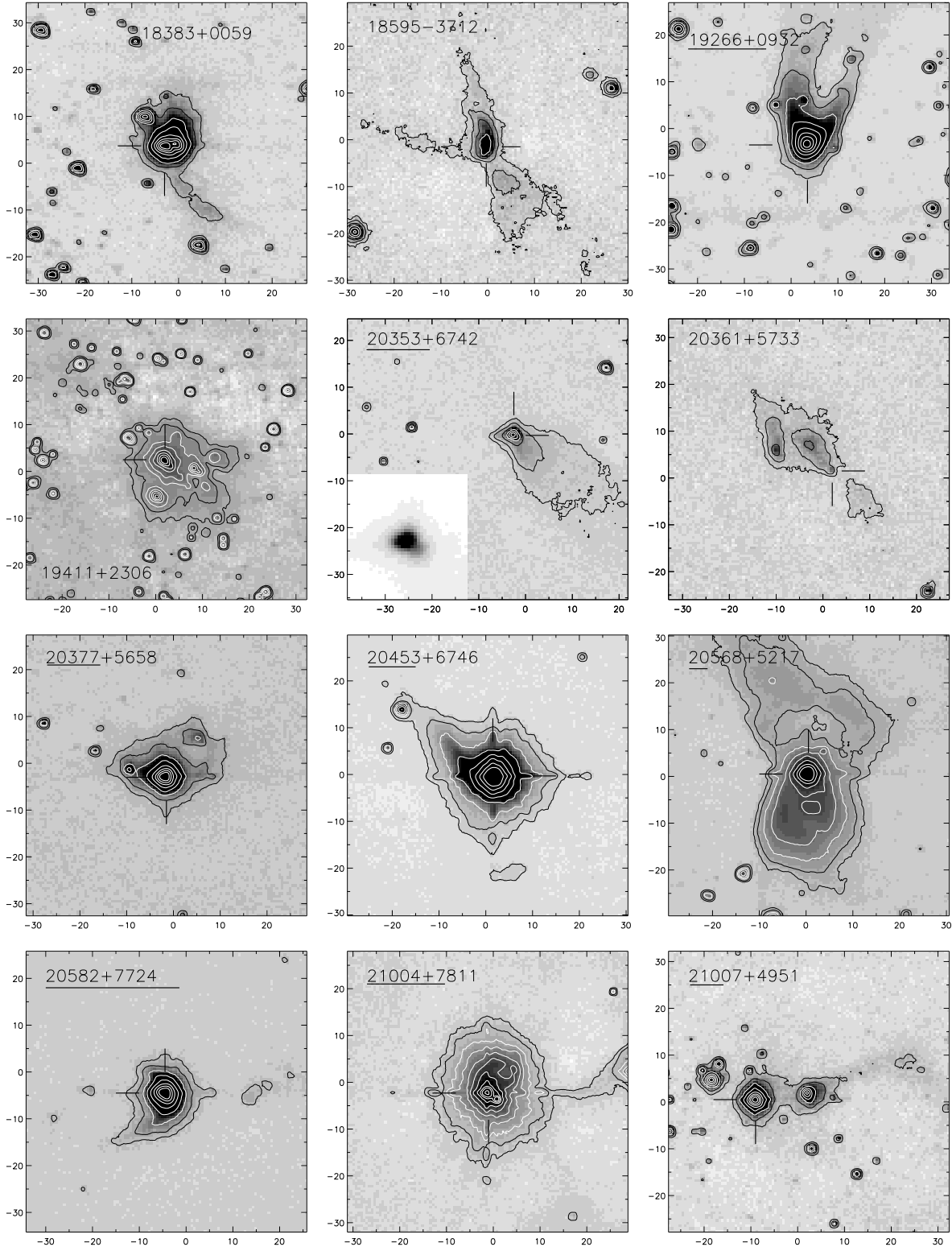


Fig. 2.—

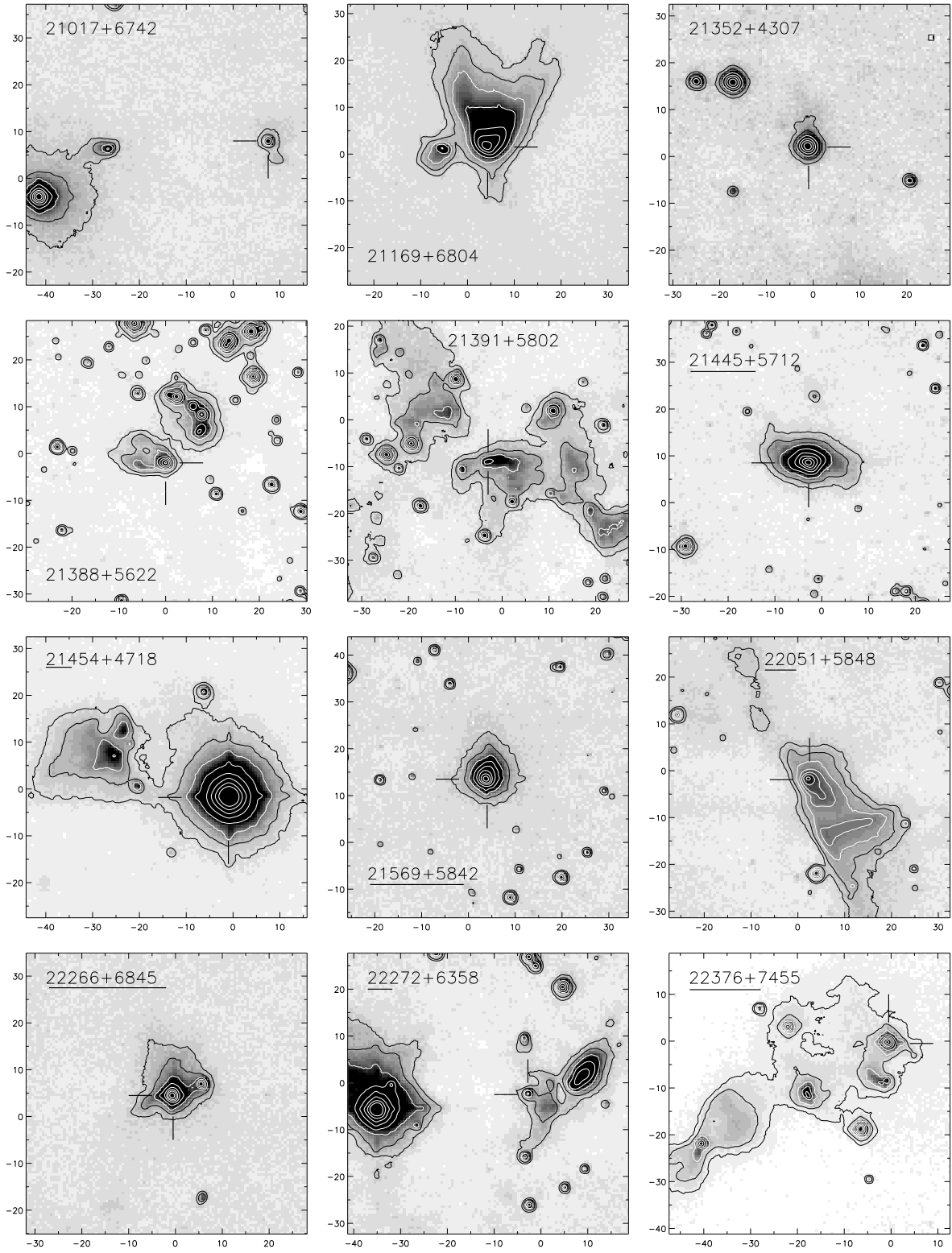


Fig. 2.—

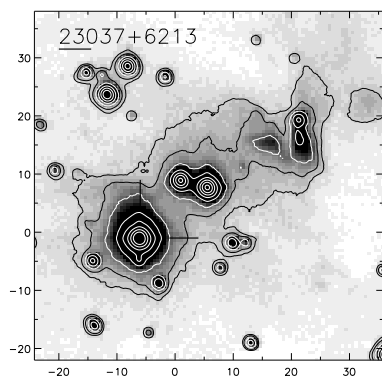


Fig. 2.—

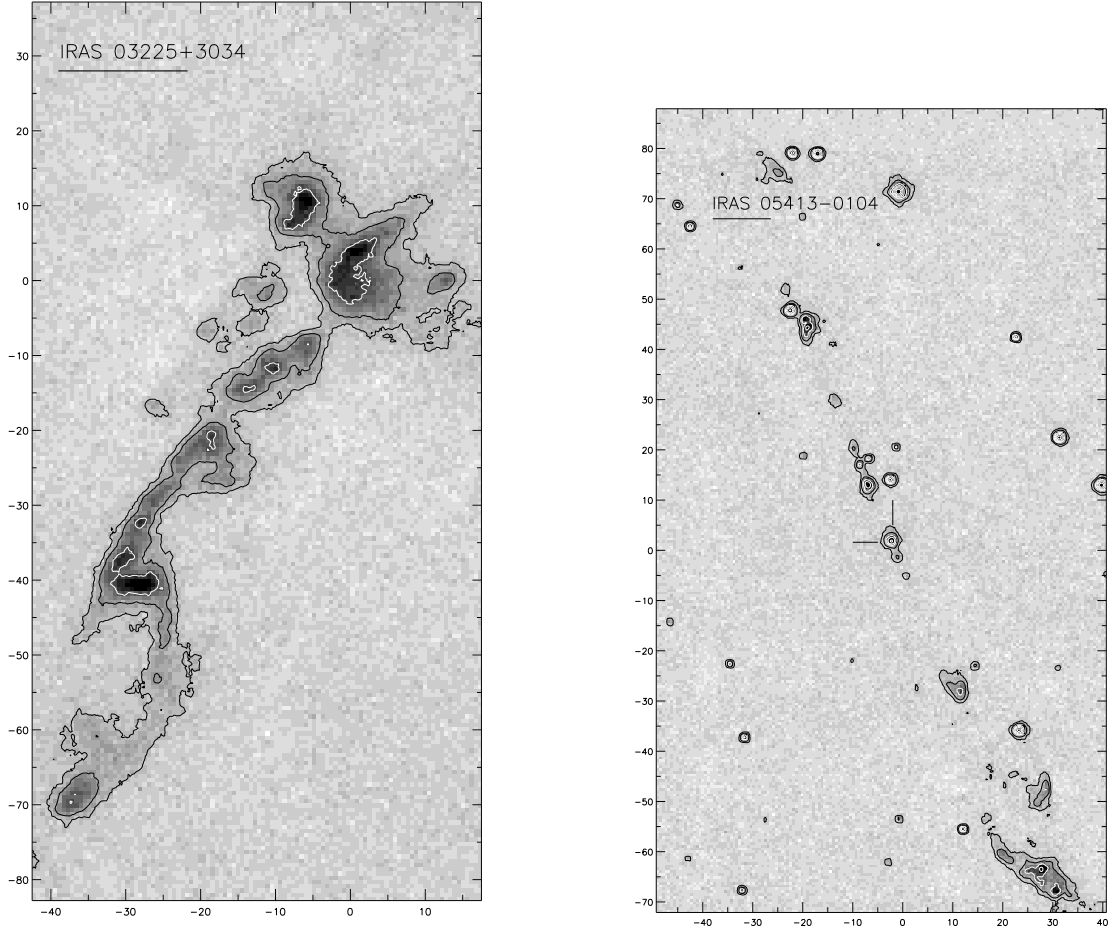


Fig. 3.— Left: IRAS 03225+3034, a Class 0 $7''_3$ binary detected at 3.6 cm at the VLA by Reipurth et al. (2002). Right: HH 212. Most of the K-band flux is from shocked H_2 emission.

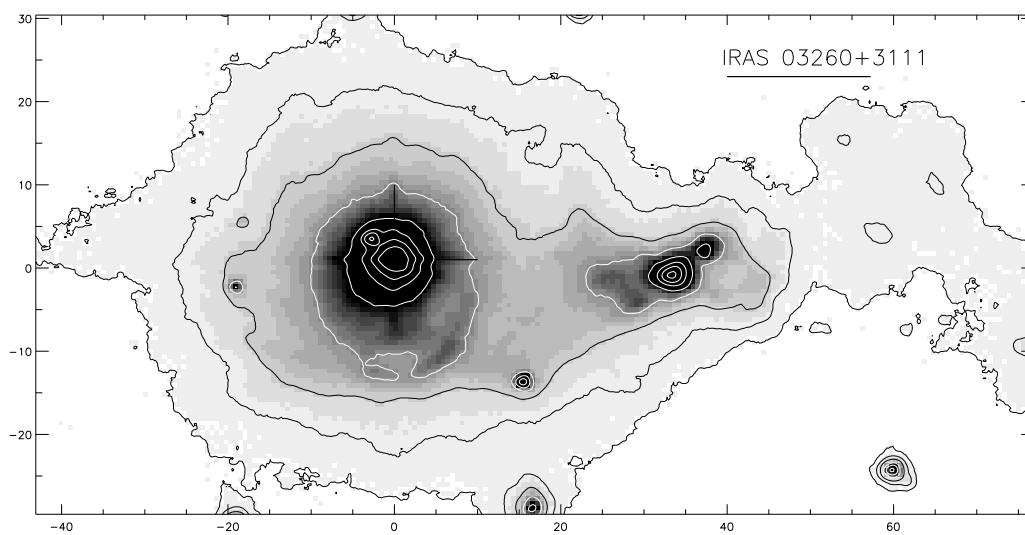


Fig. 4.— IRAS 03260+3111

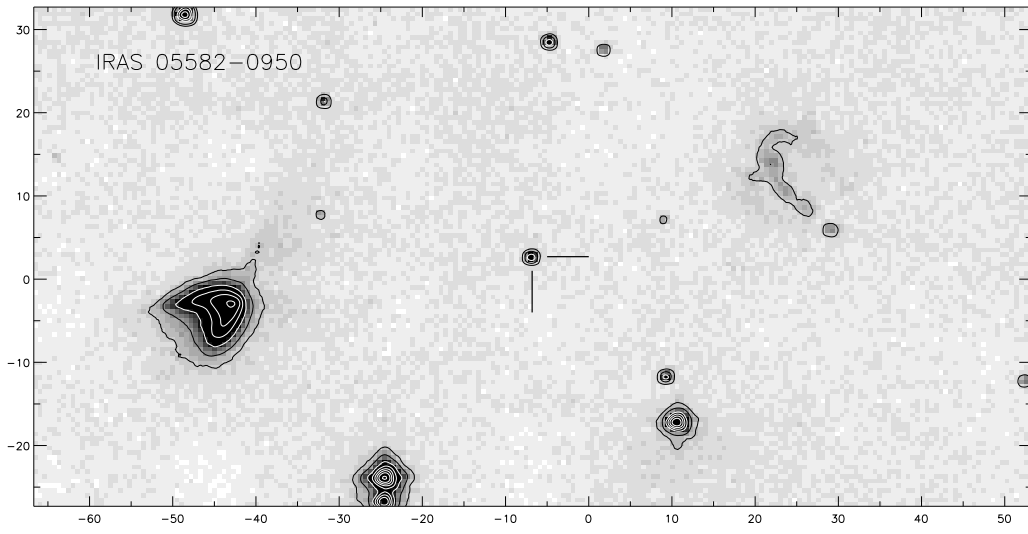


Fig. 5.— IRAS 05582-0950

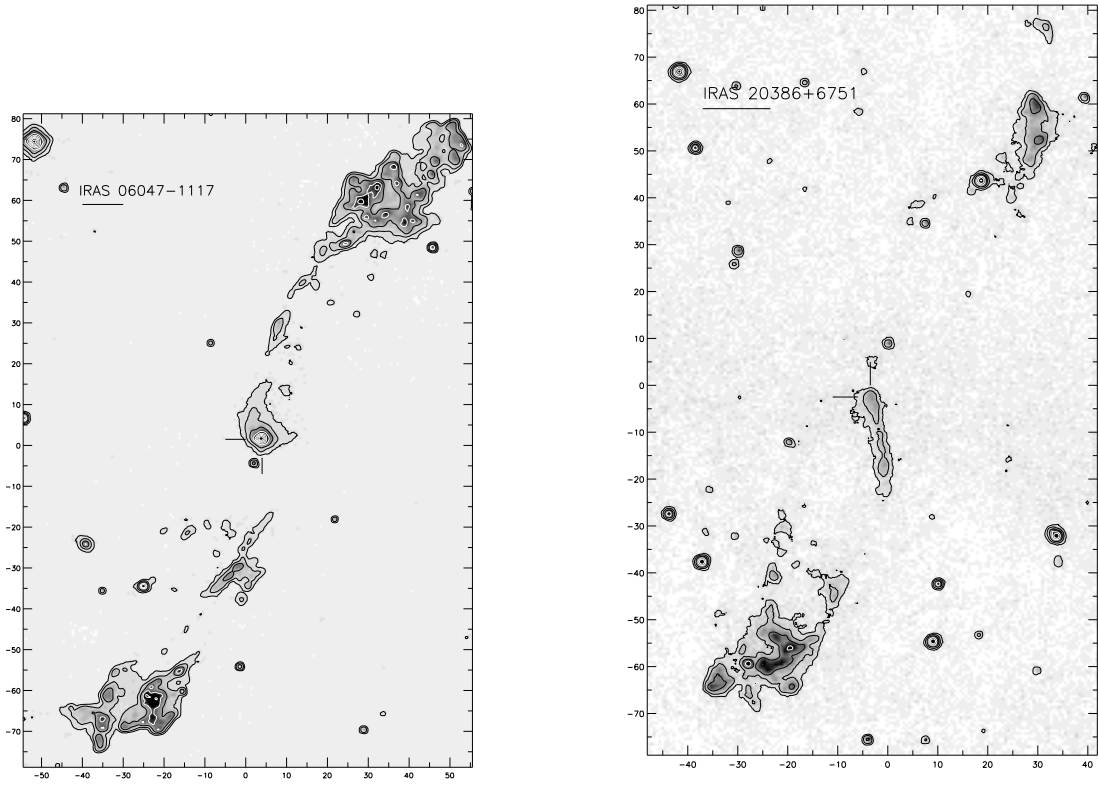


Fig. 6.— Left: IRAS 06047-1117, a large recently discovered outflow. Right: IRAS 20386+6751.

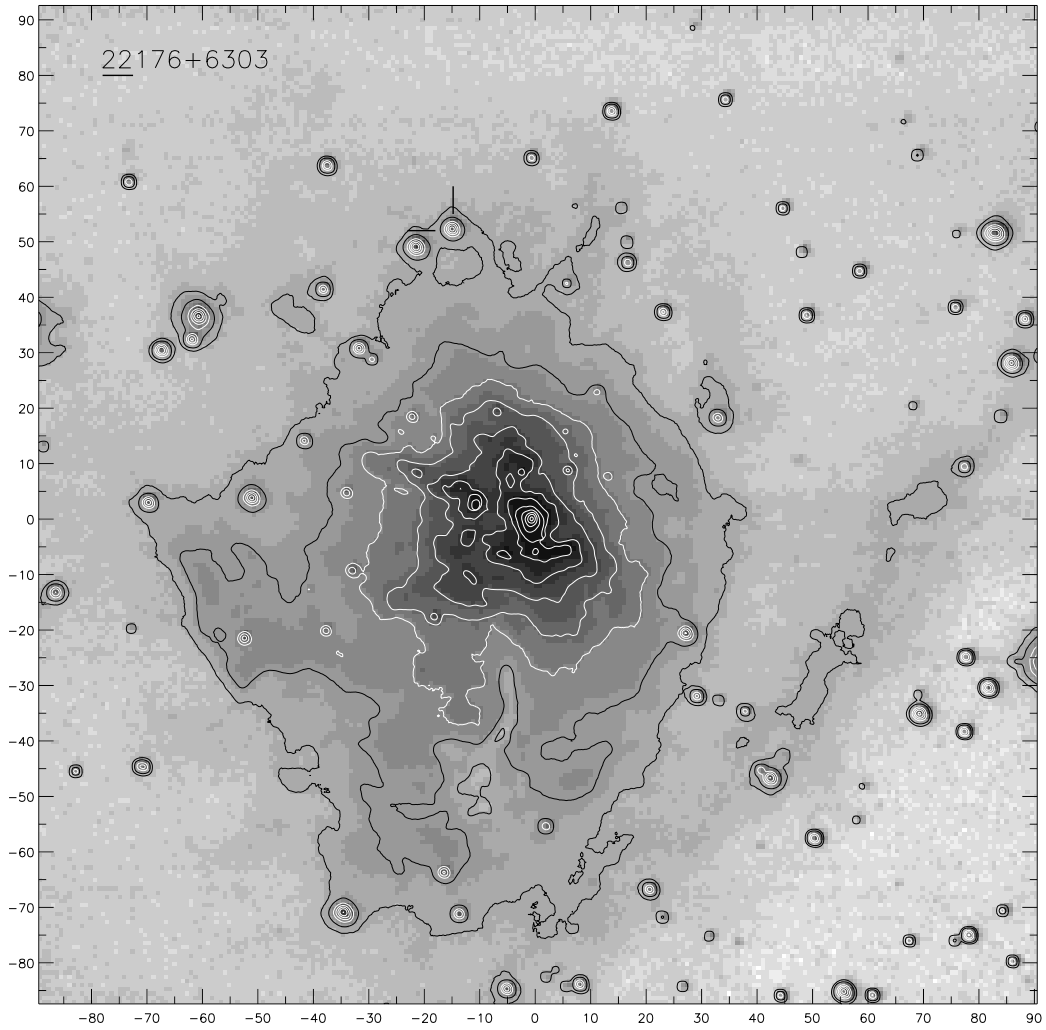


Fig. 7.— IRAS 22176+6303.

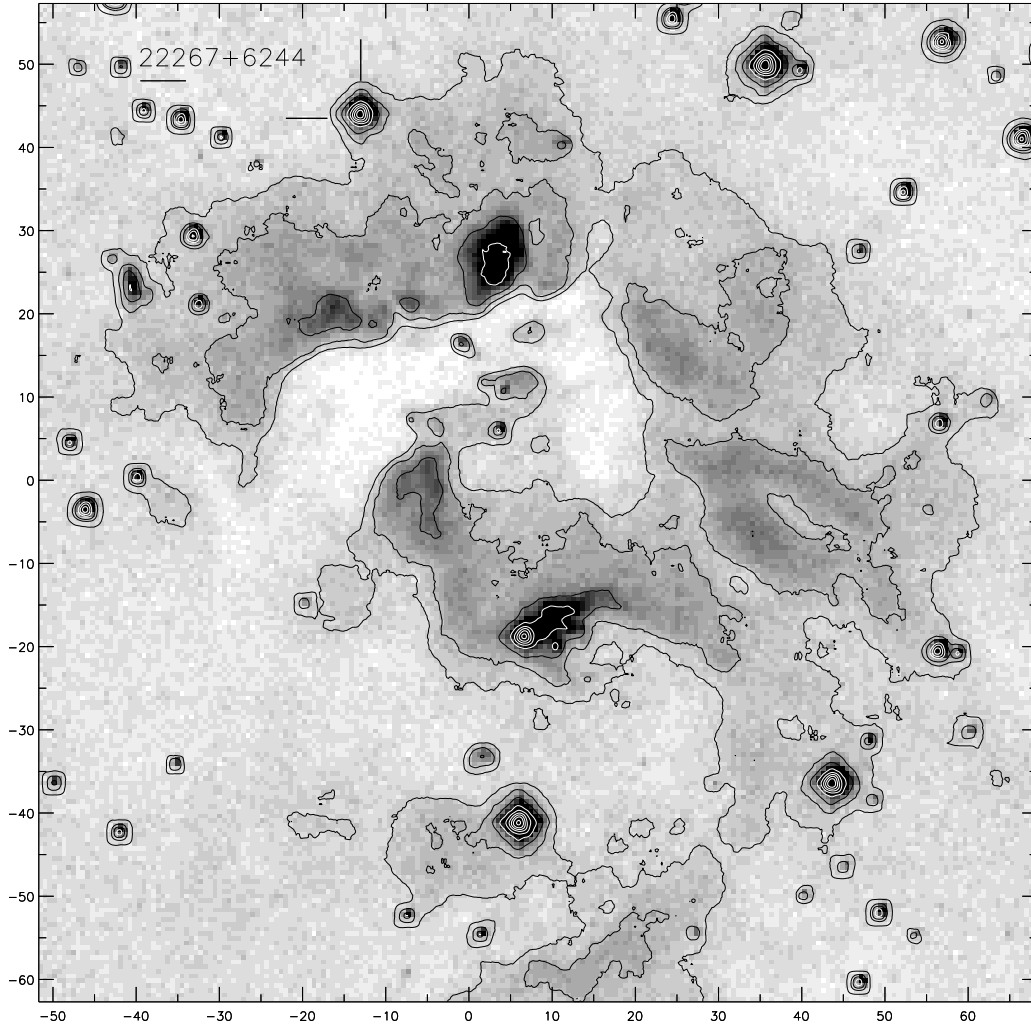


Fig. 8.— IRAS 22267+6244.

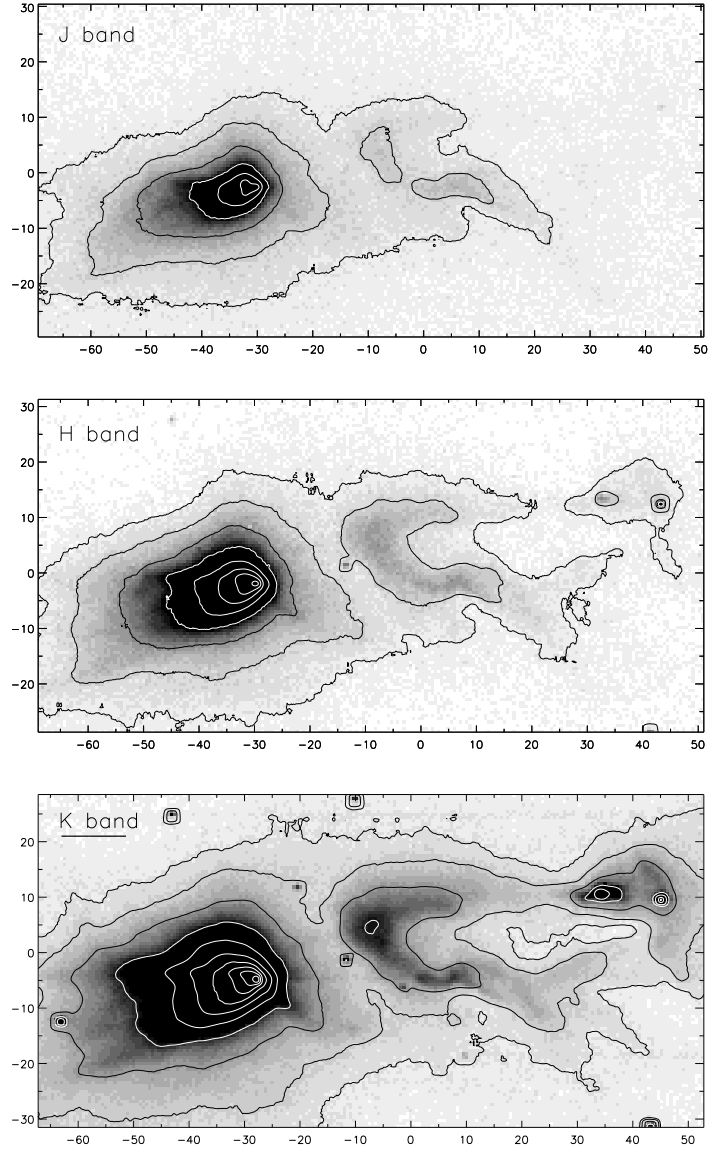


Fig. 9.— J, H, and K contour plots of IRAS 05450+0019. The outer most contours are $J = 21$, $H = 20$, and $K = 20$ magnitudes per square arcsecond, and the contours are at 1 magnitude intervals. As in the other plots, (0,0) is at the IRAS coordinate. This appears to be a purely reflection nebula, with no significant excess seen when observed with the H_2 S(1) filter at $2.12 \mu\text{m}$ or the [FeII] filter at $1.64 \mu\text{m}$. The coordinate given in Table 2 is for the K-band peak.

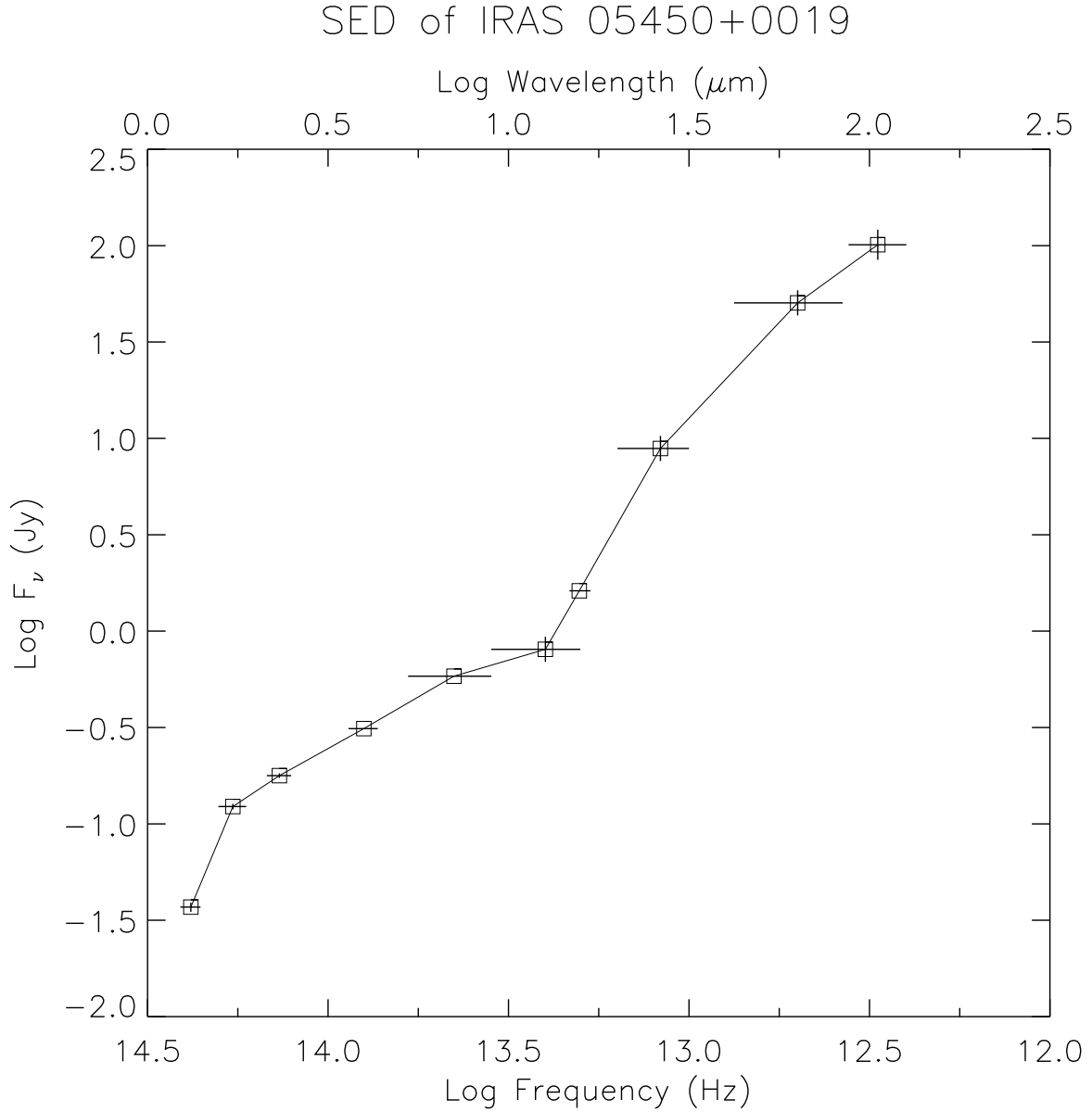


Fig. 10.— SED for IRAS 05450+0019, which combines IRAS (12 μm , 25 μm , 60 μm , and 100 μm), ISO (6.7 μm and 14.3 μm), IRTF (3.8 μm), and 2MASS (1.2 μm , 1.6 μm , 2.2 μm) data. An SED that rises from near-IR through 100 μm is characteristic of Class I sources. The J, H, K, L', 6.7 μm and 14.3 μm flux error bars are smaller than the plot symbol size. The horizontal error bars represent the filter bandpasses.

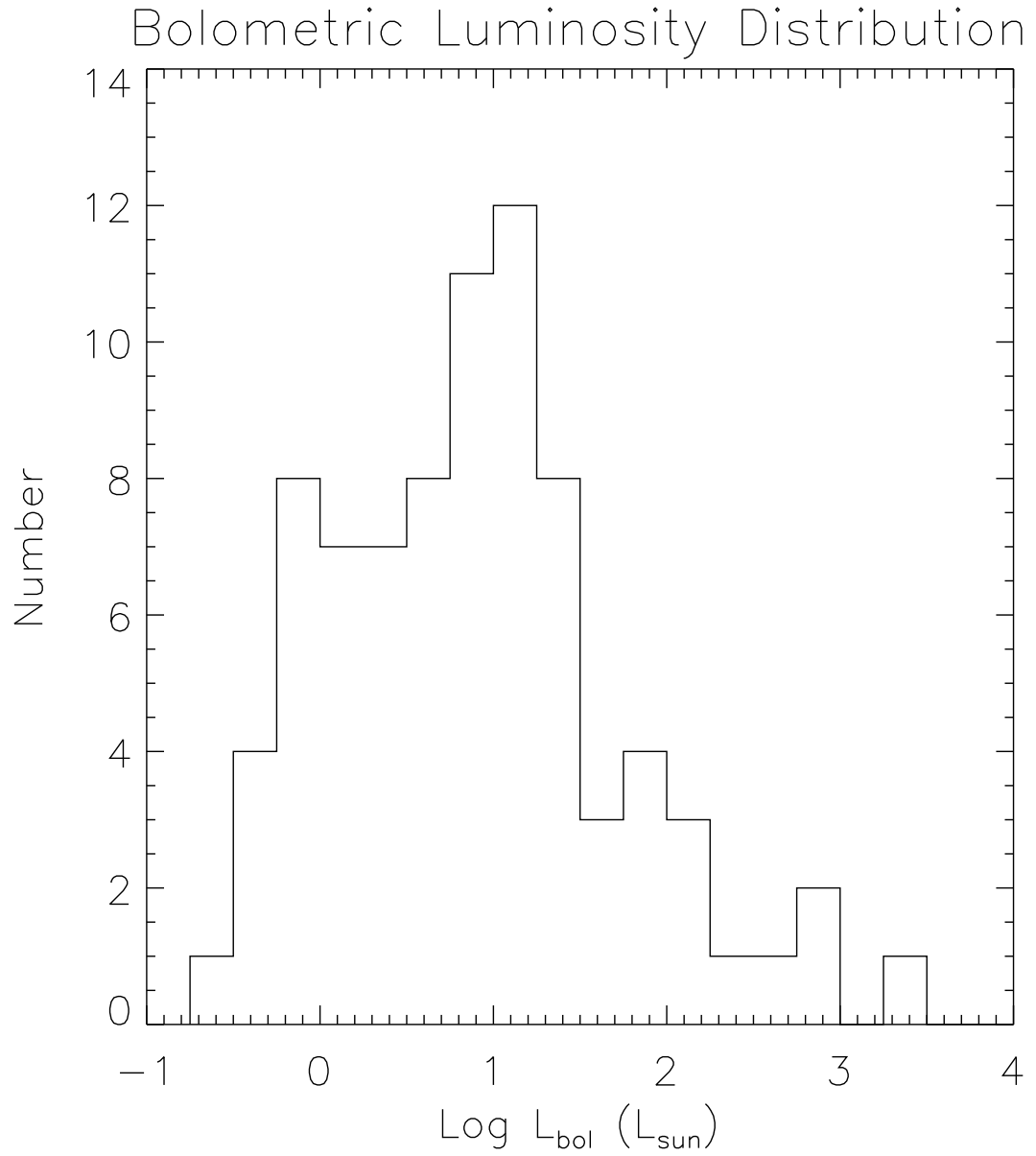


Fig. 11.— The bolometric luminosity distribution for our sample of nebulae, with a median value of $5.8 L_{\odot}$.

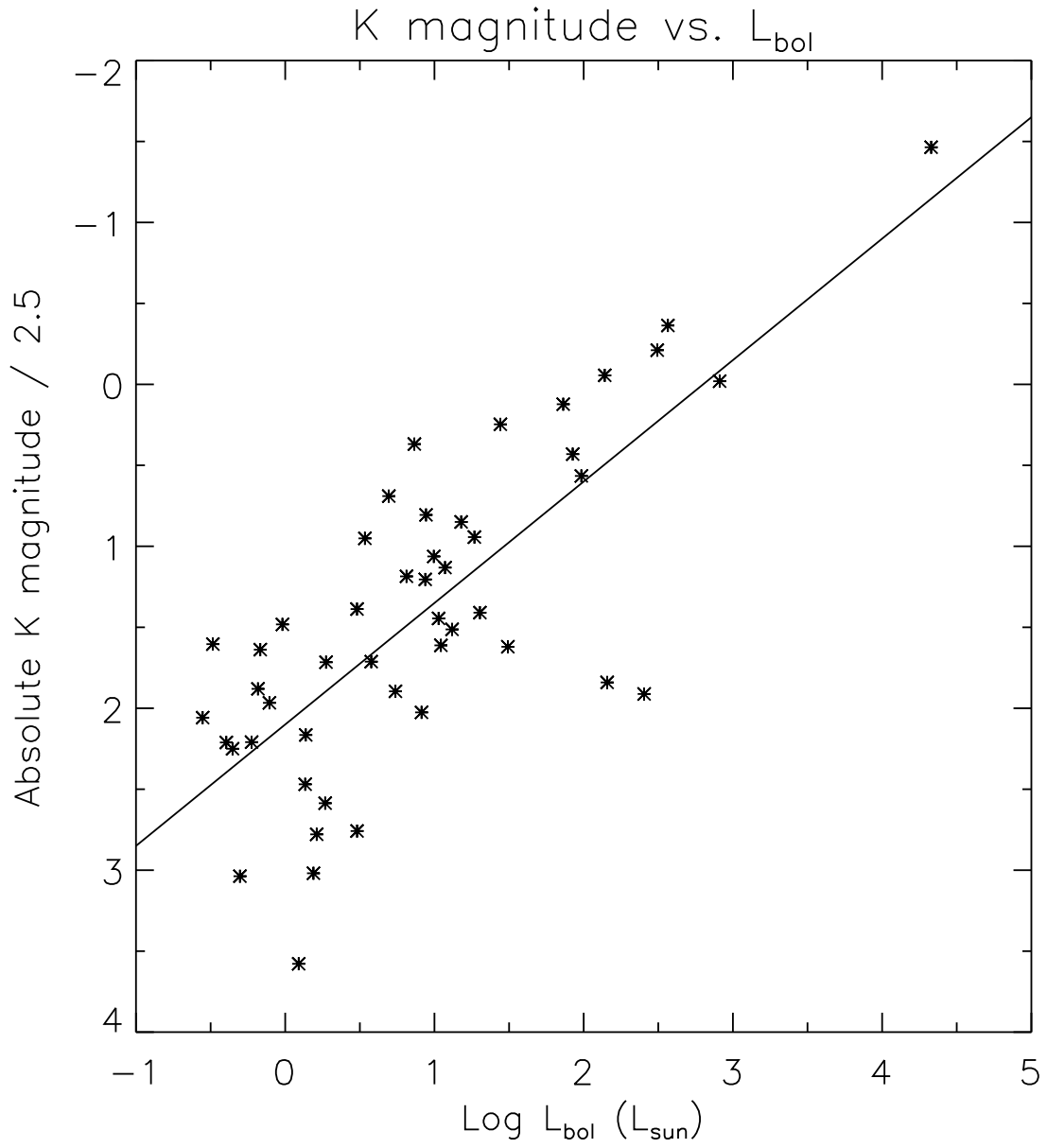


Fig. 12.— K-band absolute magnitude (divided by 2.5) vs. bolometric luminosity. The slope of the regression line is 0.75, with the data points having a standard deviation from the regression line of 1.63 magnitudes (a factor of 4.5).

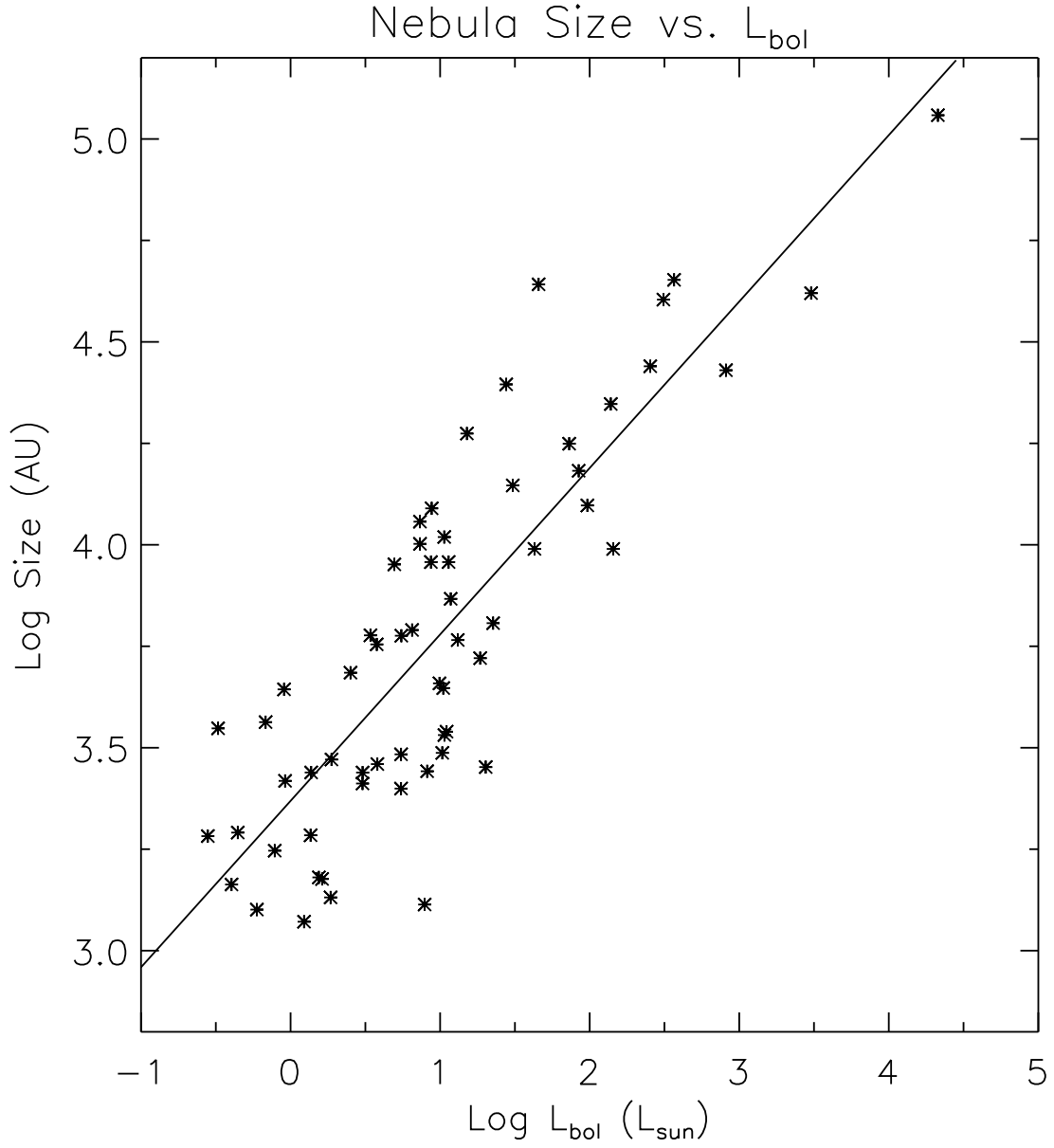


Fig. 13.— Nebula size vs. bolometric luminosity. The slope of the regression line is 0.41, with the data points having a standard deviation from the regression line of 0.25 (a factor of 1.8).

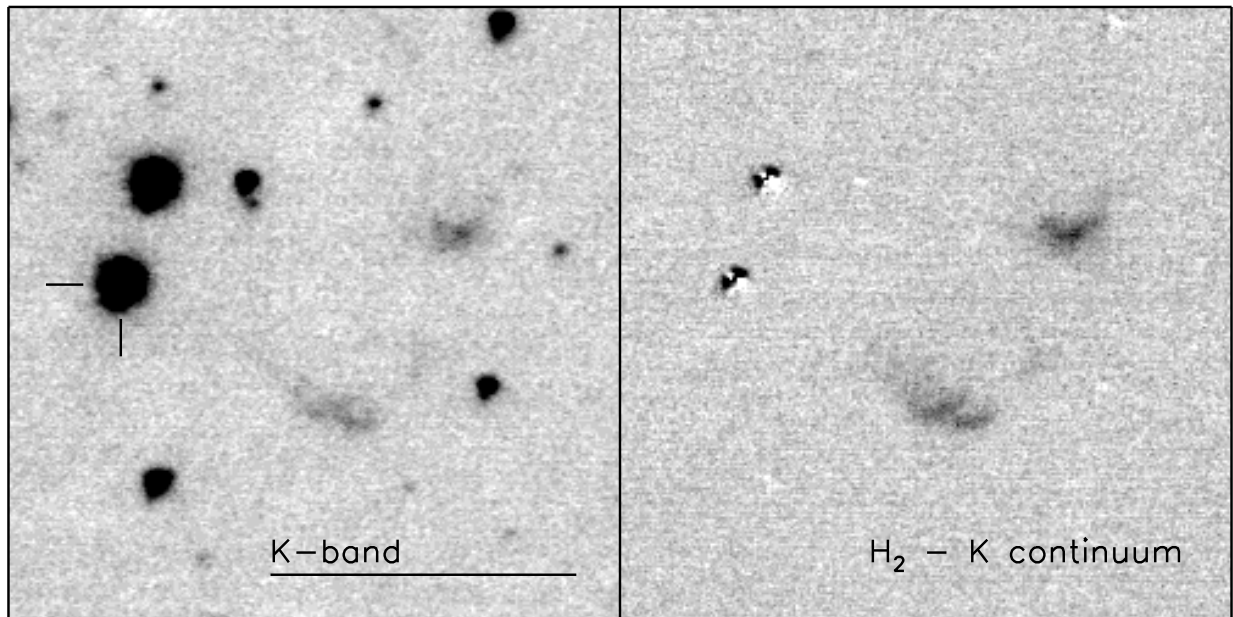


Fig. 14.— K-band and H₂ images of IRAS 00182+6223

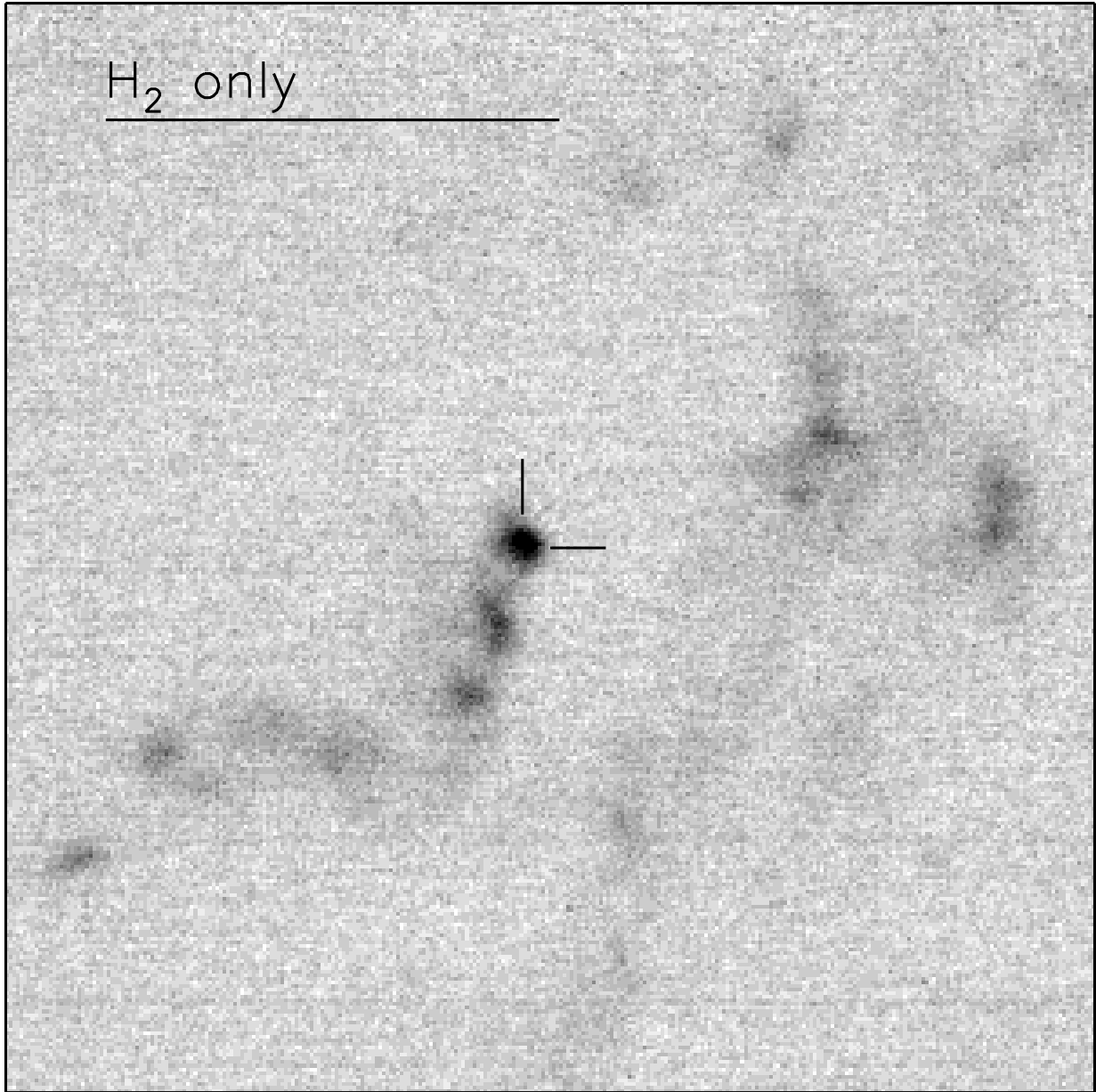


Fig. 15.— H₂ image of IRAS 03220+3035. This field is $\sim 1.5'$ to the NE of the IRAS source coordinates, which are 03 25 09.43 +30 46 21.7. Since no K continuum flux was detected, the K-band image is not presented.

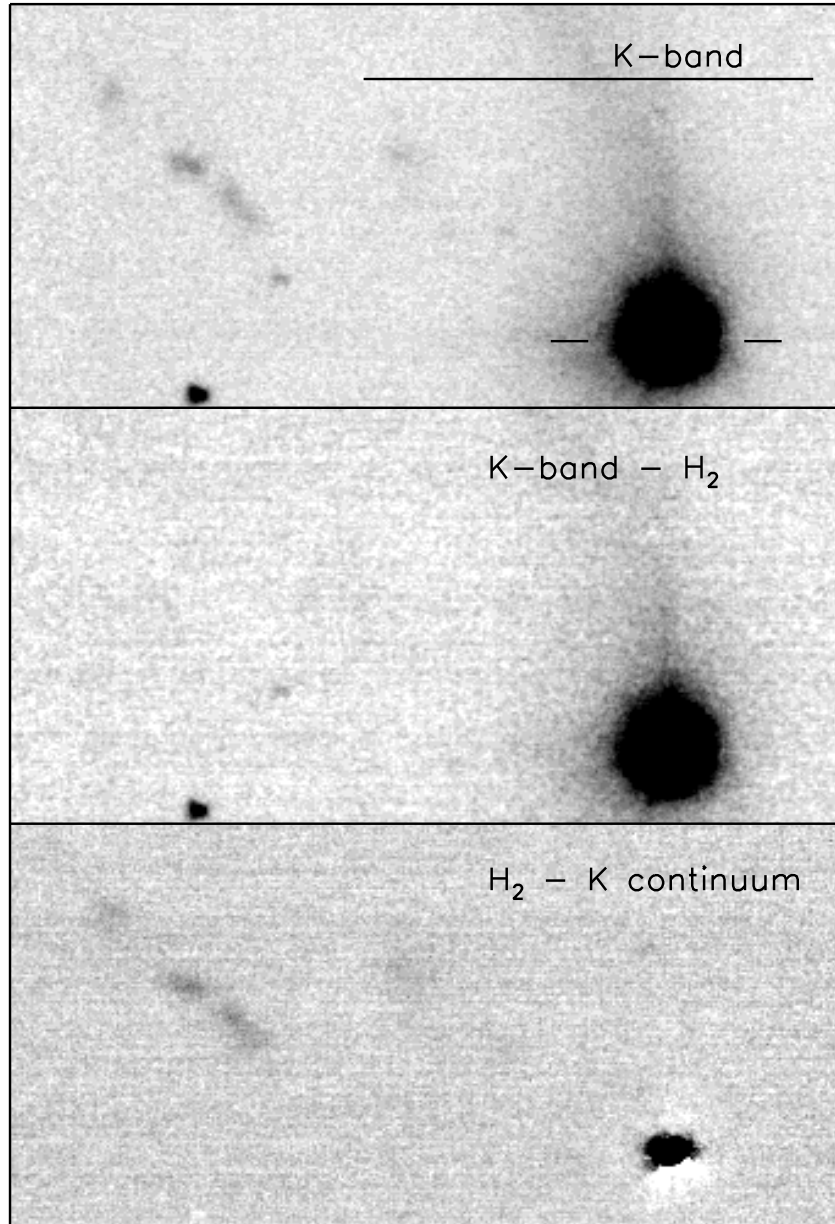


Fig. 16.— K-band, K continuum, and H₂ images of IRAS 03445+3242

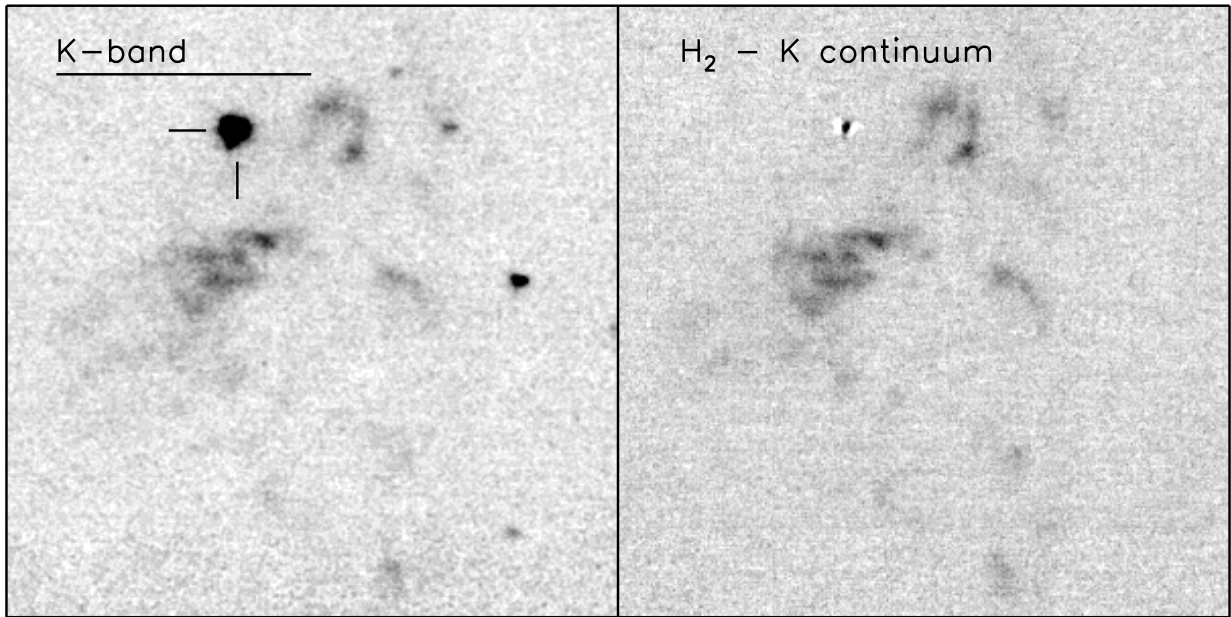


Fig. 17.— K-band and H₂ images of IRAS 04327+5432. This field is $\sim 1'$ to the NNW of the IRAS source coordinates.

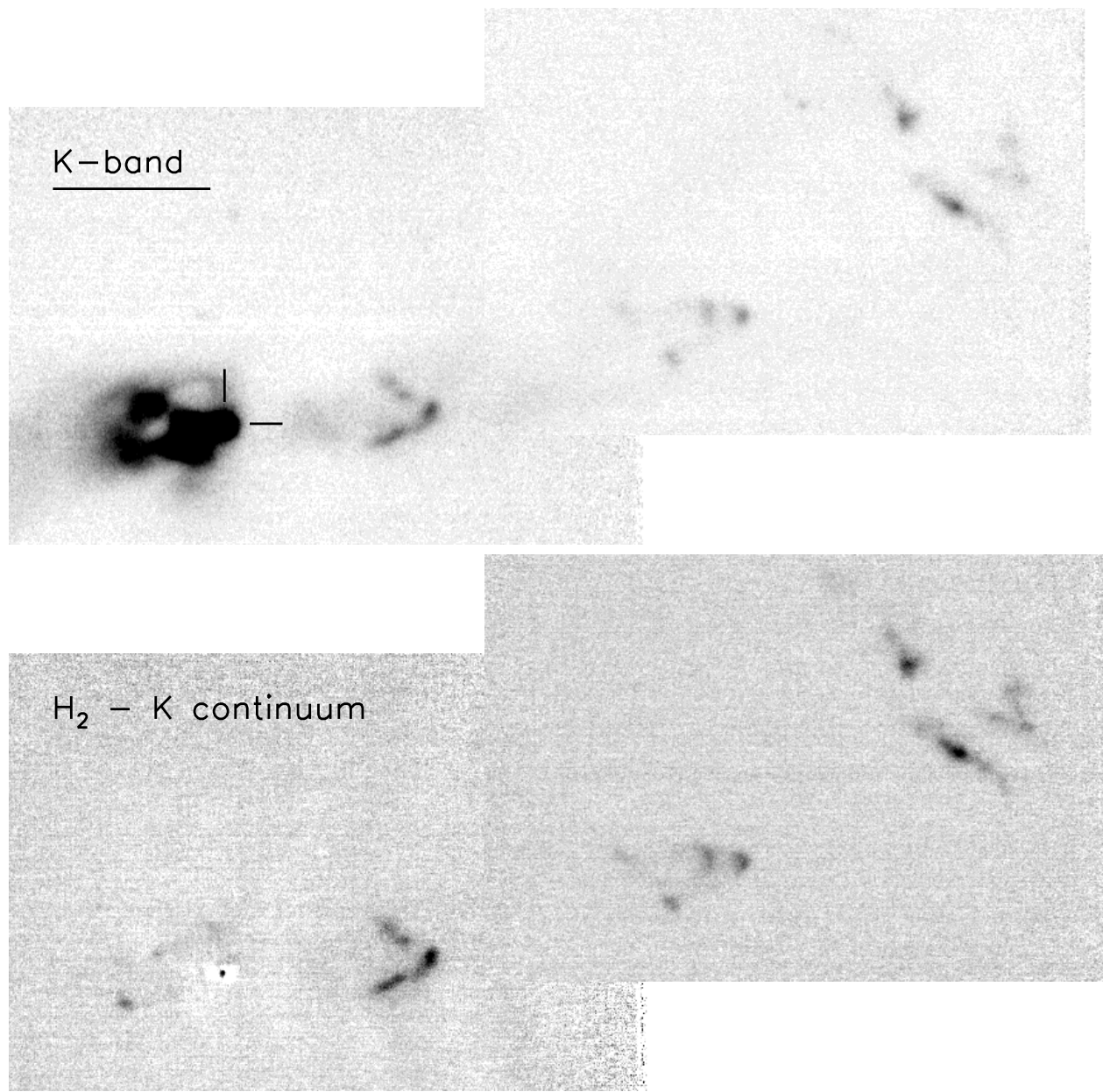


Fig. 18.— K-band and H₂ images of IRAS 05155+0707

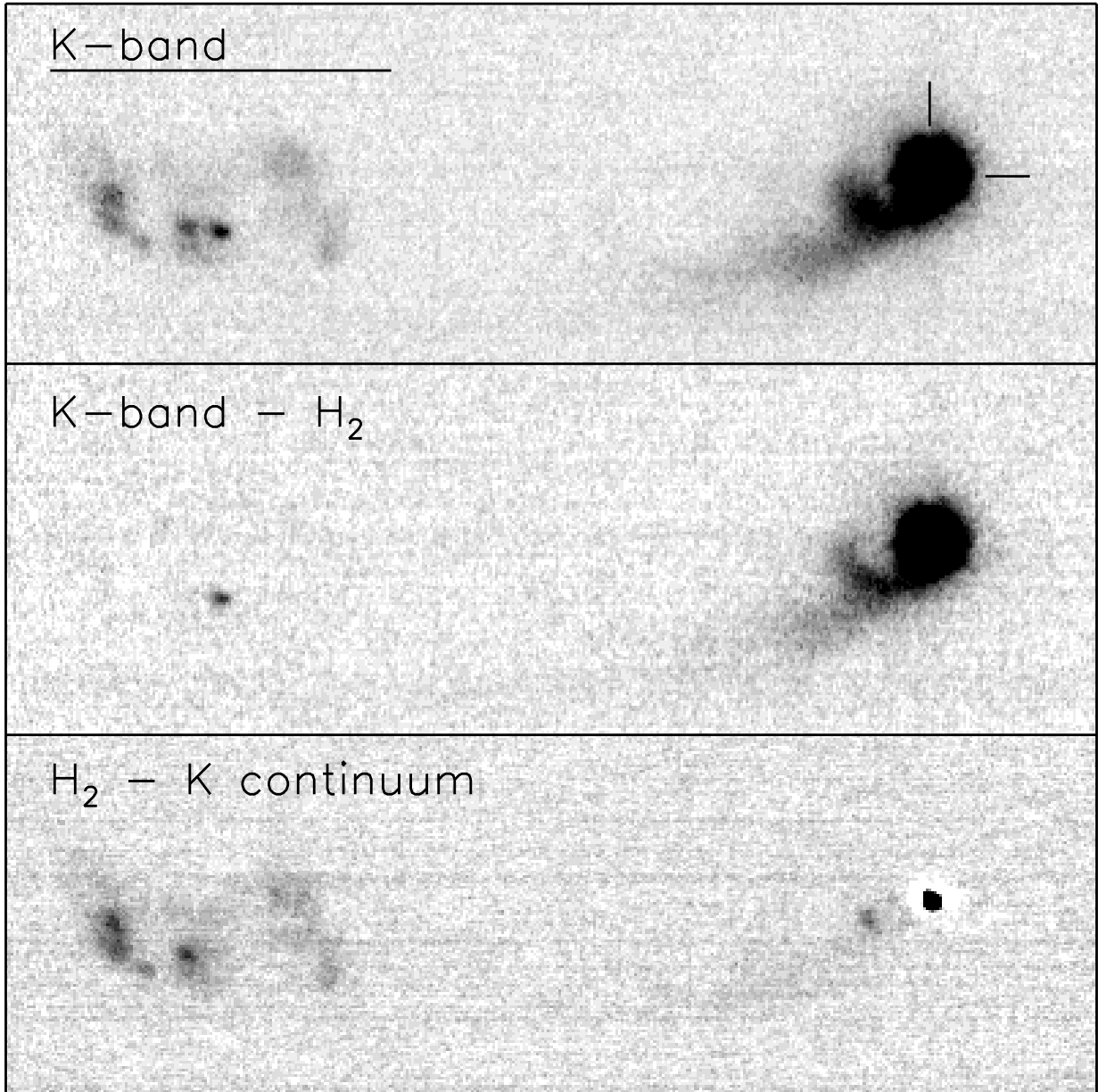


Fig. 19.— K-band, K continuum, and H₂ images of IRAS 05403-0818

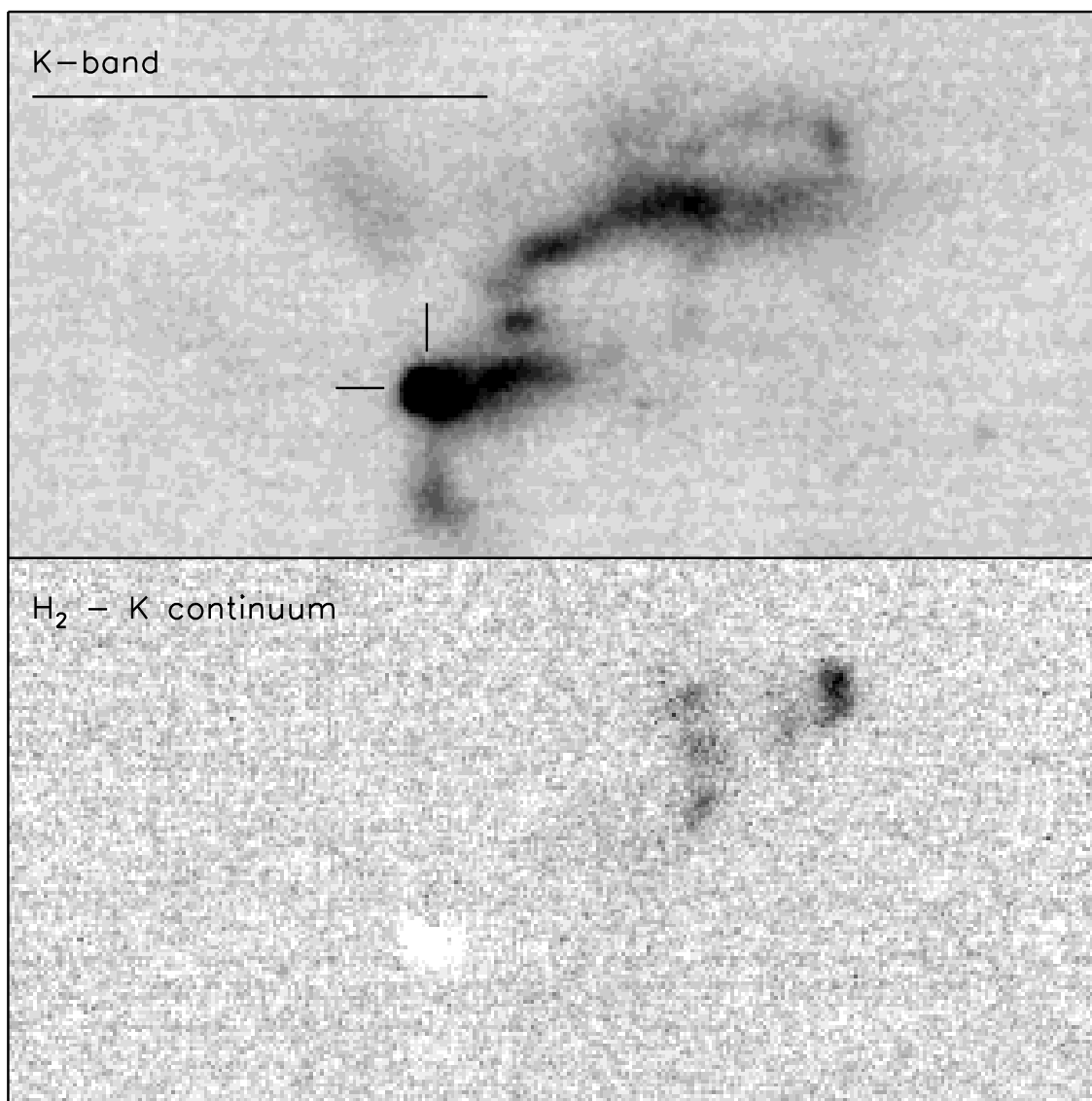


Fig. 20.— K-band, and H₂ images of IRAS 18264-0143

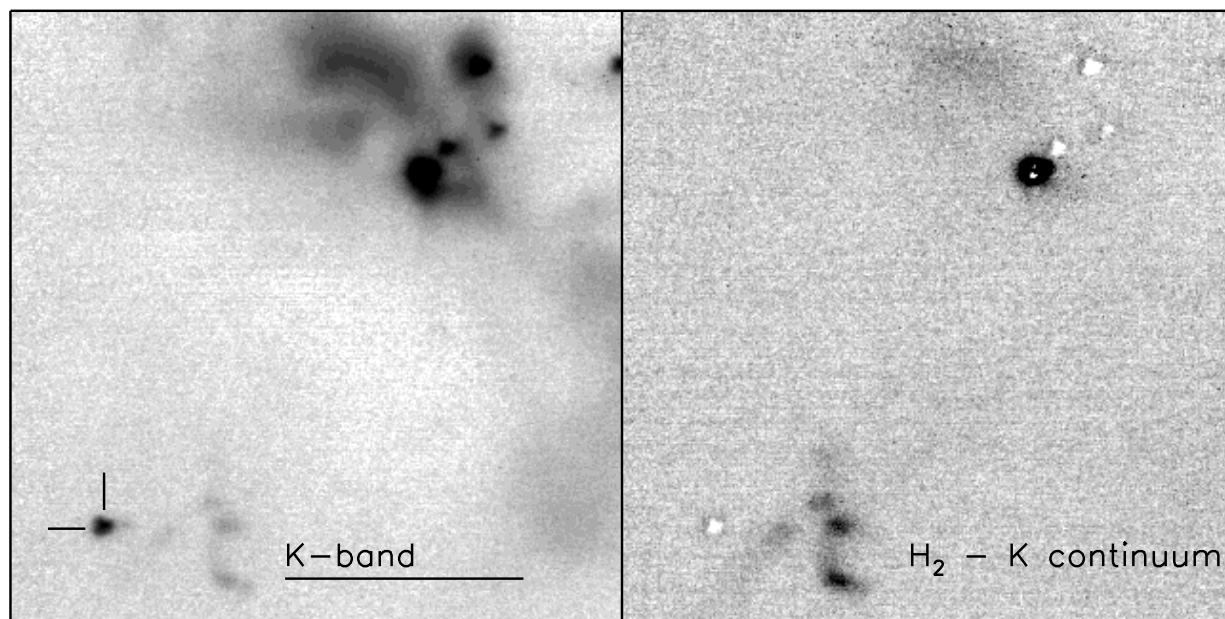


Fig. 21.— K-band, and H₂ images of IRAS 18270–0153. The stars and nebulae seen in the northern part of the field are to the east of the IRAS source coordinates

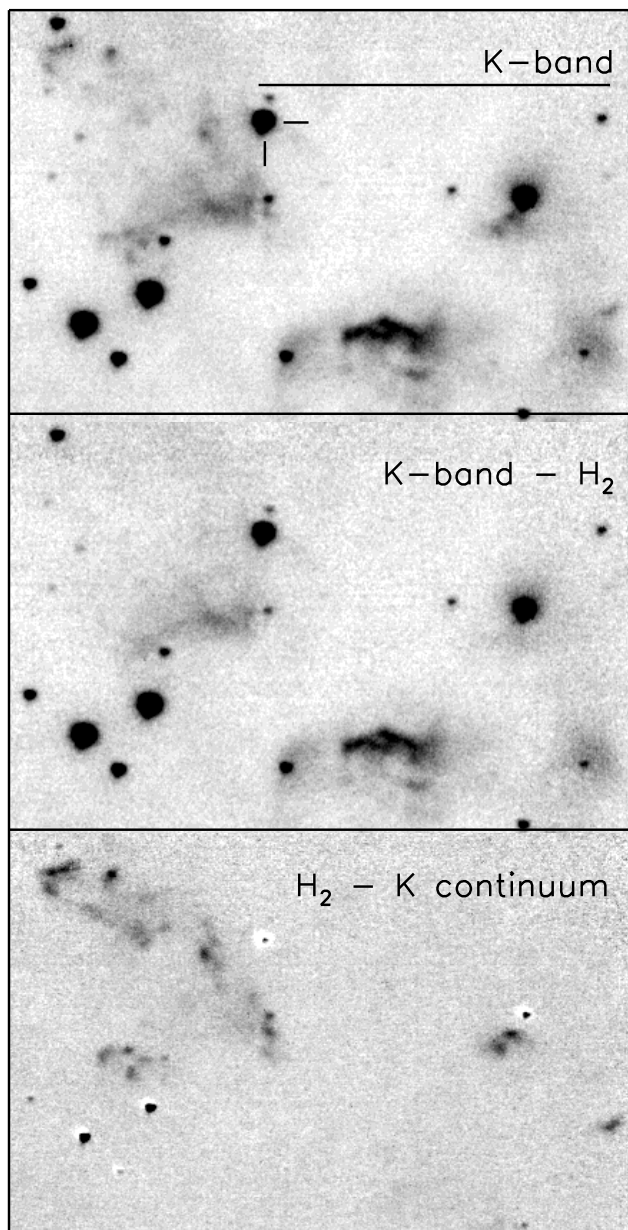


Fig. 22.— K-band, and H₂ images of IRAS 21391+5802

Table 1. Observation Notes.

IRAS	α (J2000)	δ (J2000)	t(s) ^a	Date (UT)	FWHM(") ^b	Contour ^c	S/N ^d
00182+6223	00 20 58.1	+62 40 18	540	2003 Jul 20	0.80	19	2.13
00465+5028	00 49 25.0	+50 44 45	540	2003 Jul 18	0.98	19	2.83
01166+6635	01 20 03.7	+66 51 32	540	2003 Jul 17	0.93	19	2.15
02086+7600	02 13 42.0	+76 15 02	540	2003 Sep 07	0.72	19	2.15
03225+3034	03 25 36.0	+30 45 19	540	2003 Jul 18	—	19	1.04
03245+3002	03 27 39.0	+30 12 59	300	2003 Jan 10	0.57	19	1.83
03260+3111	03 29 10.4	+31 21 59	540	2003 Sep 06	0.83	19	2.55
03271+3013	03 30 14.9	+30 23 48	1620	2003 Sep 09	0.75	19	4.71
03301+3057	03 33 16.3	+31 07 51	300	2003 Jan 10	0.68	19	1.22
03331+6256	03 37 28.5	+63 06 29	540	2003 Jul 20	0.69	19	2.21
03445+3242	03 47 41.3	+32 51 42	1740	2003 Sep 10	0.65	20	2.57
03507+3801	03 54 06.3	+38 10 43	1620	2003 Sep 10	0.68	20	2.32
04016+2610	04 04 42.9	+26 18 56	540	2003 Jul 18	1.23	19	2.95
04067+3954	04 10 08.4	+40 02 25	300	2003 Jan 10	0.62	19	1.41
04073+3800	04 10 41.2	+38 07 54	300	2003 Jan 09	0.55	19	1.51
04169+2702	04 19 58.0	+27 09 56	300	2003 Jan 10	0.65	19	1.76
04189+2650	04 22 00.6	+26 57 28	540	2003 Jul 20	0.87	19	2.23
04191+1523	04 21 59.0	+15 30 17	300	2003 Jan 10	0.78	19	1.76
04223+3700	04 25 38.9	+37 07 06	1620	2003 Sep 09	0.71	19	4.97
04239+2436	04 26 55.3	+24 43 34	300	2003 Jan 10	0.74	18	3.87
04248+2612	04 27 57.2	+26 19 17	300	2003 Jan 10	0.62	19	1.80
04275+3531	04 30 48.2	+35 37 51	2160	2003 Sep 09	0.73	20	2.28
04287+1801	04 31 35.8	+18 08 08	660	2003 Jul 20	—	20	1.02
04302+2247	04 33 16.8	+22 53 21	540	2003 Sep 07	0.70	19	2.56
04325+2402	04 35 33.1	+24 08 15	540	2003 Sep 06	0.70	19	1.66
04327+5432	04 36 44.2	+54 39 01	540	2003 Aug 09	1.15	19	2.38
04365+2535	04 39 34.8	+25 41 43	300	2003 Jan 10	0.60	19	1.47
04381+2540	04 41 11.6	+25 46 32	1620	2003 Sep 08	0.70	20	1.66
04530+5126	04 56 56.8	+51 30 50	540	2003 Aug 10	0.75	19	2.27
04591–0856	05 01 30.2	–08 52 14	300	2003 Jan 10	0.71	19	1.51
05155+0707	05 18 17.1	+07 11 01	540	2003 Aug 09	0.86	19	2.35
05302–0537	05 32 41.7	–05 35 48	540	2003 Aug 10	0.76	19	1.65
05311–0631	05 32 41.7	–05 35 48	300	2003 Jan 09	0.68	19	1.43
05327–0457	05 35 14.4	–04 55 45	300	2003 Jan 09	0.78	19	1.79
05378–0750	05 40 16.7	–07 48 33	540	2003 Sep 07	0.78	20	1.00
05379–0758	05 40 20.5	–07 56 32	540	2003 Sep 07	0.62	20	1.48
05384–0808	05 40 48.8	–08 06 51	300	2003 Jan 09	0.76	19	1.88
05391–0841	05 41 29.8	–08 40 14	540	2003 Sep 07	0.78	19	2.41
05399–0121	05 42 27.7	–01 20 02	1380	2003 Sep 10	0.75	20	1.38
05403–0818	05 42 47.3	–08 17 06	1080	2003 Sep 08	0.87	20	1.38
05404–0948	05 42 47.7	–09 47 24	540	2003 Aug 10	0.73	19	2.02
05405–0117	05 43 02.6	–01 16 23	1620	2003 Sep 08	0.77	19	4.28
05413–0104	05 43 51.5	–01 02 52	540	2003 Sep 06	0.65	20	0.90
05417+0907	05 44 29.8	+09 08 54	540	2003 Aug 09	0.83	19	2.23
05450+0019	05 47 34.6	+00 20 08	660	2003 Jan 10	0.67	20	1.52
05510–1018	05 53 22.8	–10 17 38	540	2003 Aug 09	1.12	19	1.85

Table 1—Continued

IRAS	α (J2000)	δ (J2000)	t(s) ^a	Date (UT)	FWHM(") ^b	Contour ^c	S/N ^d
05513–1024	05 53 42.5	–10 24 01	540	2003 Sep 06	0.73	19	2.77
05548–0935	05 57 13.0	–09 35 10	540	2003 Aug 14	1.16	19	1.99
05564–1329	05 58 47.5	–13 29 16	540	2003 Aug 10	0.79	19	2.00
05581–1026	06 00 28.5	–10 26 34	1620	2003 Sep 09	0.66	20	1.21
05582–0950	06 00 35.9	–09 50 35	540	2003 Sep 08	0.74	19	2.74
05596–0903	06 02 01.7	–09 03 06	540	2003 Sep 06	0.70	19	2.37
05598–0906	06 02 16.3	–09 06 32	540	2003 Aug 10	0.74	19	1.69
06027–0714	06 05 08.2	–07 14 42	300	2003 Jan 10	0.78	19	1.68
06033–0710	06 05 48.2	–07 10 30	540	2003 Sep 06	0.68	20	1.02
06047–1117	06 07 08.7	–11 17 51	1620	2003 Sep 10	0.76	21	
06057–0923	06 08 05.1	–09 23 52	540	2003 Sep 06	0.72	19	2.56
06249–0953	06 27 17.4	–09 55 27	300	2003 Jan 09	0.80	19	1.60
06368+0938	06 39 35.7	+09 35 35	1380	2003 Sep 10	0.70	20	1.63
06381+1039	06 40 58.0	+10 36 49	1380	2003 Sep 09	0.71	20	1.79
06382+1017	06 41 03.3	+10 15 01	540	2003 Sep 10	0.71	20	0.96
06393+0913	06 42 06.9	+09 10 24	1140	2003 Sep 08	0.69	20	1.64
07180–2356	07 20 06.7	–24 02 21	300	2003 Jan 08	1.10	19	1.28
15398–3359	15 43 02.2	–34 09 06	540	2003 May 15	1.56	19	2.08
16288–2450E	16 31 56.0	–24 56 28	540	2003 May 14	1.13	19	2.70
16288–2450W	16 31 56.0	–24 56 28	540	2003 May 14	1.13	19	2.70
16295–4452	16 33 08.6	–44 58 23	540	2003 May 16	1.24	18	2.11
16316–1540	16 34 29.1	–15 47 00	540	2003 May 14	1.10	19	2.59
16442–0930	16 46 57.4	–09 35 19	540	2003 May 14	1.21	19	2.08
17364–1946	17 39 23.5	–19 47 51	540	2003 May 16	1.01	19	1.74
17441–0433	17 46 50.8	–04 34 34	540	2003 May 15	0.93	19	0.97
18148–0440	18 17 29.8	–04 39 38	540	2003 May 14	1.10	20	1.01
18264–0143	18 29 05.7	–01 41 57	540	2003 May 14	1.20	19	2.82
18270–0153	18 29 37.0	–01 51 02	540	2003 May 15	1.17	19	2.51
18274–0212	18 30 01.4	–02 10 26	540	2003 May 16	0.84	18	2.17
18278–0212	18 30 28.0	–02 10 48	540	2003 May 16	0.82	18	2.69
18331–0035	18 35 42.1	–00 33 18	540	2003 May 14	1.33	19	2.53
18341–0113	18 36 45.7	–01 10 30	540	2003 May 14	1.24	19	3.13
18383+0059	18 40 51.7	+01 02 09	540	2003 May 15	1.17	19	3.02
18595–3712	19 02 59.5	–37 07 33	540	2003 May 14	1.24	20	0.83
19266+0932	19 29 01.1	+09 38 46	540	2003 May 14	1.29	19	3.03
19411+2306	19 43 18.1	+23 13 59	540	2003 May 16	0.74	19	2.32
20353+6742	20 35 46.5	+67 52 59	1800	2003 Sep 06	0.58	20	1.55
20361+5733	20 37 20.8	+57 44 13	2160	2003 Sep 06	0.68	21	0.89
20377+5658	20 38 57.4	+57 09 34	540	2003 May 15	1.04	19	2.68
20386+6751	20 39 06.6	+68 02 13	540	2003 Aug 09	0.81	20	0.92
20453+6746	20 45 54.2	+67 57 39	540	2003 May 15	1.02	19	2.50
20568+5217	20 58 21.4	+52 29 27	840	2003 May 15	1.03	19	2.65
20582+7724	20 57 13.2	+77 35 46	540	2003 May 15	1.18	19	2.41
21004+7811	20 59 14.3	+78 23 01	300	2003 Sep 06	0.63	19	1.28
21007+4951	21 02 22.9	+50 03 06	540	2003 Jul 20	0.78	19	2.12
21017+6742	21 02 22.6	+67 54 13	540	2003 Jul 18	1.00	19	2.38

Table 1—Continued

IRAS	α (J2000)	δ (J2000)	t(s) ^a	Date (UT)	FWHM('') ^b	Contour ^c	S/N ^d
21169+6804	21 17 39.4	+68 17 32	540	2003 May 15	1.24	19	2.52
21352+4307	21 37 11.3	+43 20 36	540	2003 Jul 17	1.28	19	2.61
21388+5622	21 40 29.0	+56 35 58	540	2003 Jul 18	0.91	19	2.38
21391+5802	21 40 42.4	+58 16 10	540	2003 Jul 18	0.97	19	2.15
21445+5712	21 46 06.8	+57 26 23	540	2003 May 15	0.81	19	2.48
21454+4718	21 47 21.8	+47 32 09	540	2003 Jul 17	1.37	19	2.72
21569+5842	21 58 36.4	+58 57 09	540	2003 Jul 20	0.78	19	2.38
22051+5848	22 06 50.7	+59 02 46	540	2003 May 15	0.81	19	2.92
22176+6303	22 19 18.2	+63 18 46	540	2004 Aug 05	0.90	18	5.43
22266+6845	22 28 02.9	+69 01 13	540	2003 Aug 10	0.74	19	2.22
22267+6244	22 28 29.4	+62 59 44	540	2003 Sep 09	0.71	20	0.99
22272+6358A	22 28 52.3	+64 13 43	540	2003 May 15	0.99	19	2.79
22376+7455	22 38 47.2	+75 11 29	540	2003 Sep 07	0.66	19	2.32
23037+6213	23 05 48.9	+62 30 02	540	2003 Jul 17	1.19	19	2.50

Note. — Coordinates are from IRAS

^at = On source integration time

^bMedian seeing = 0.78"

^cThis is the first (outer most) surface brightness contour, in units of K magnitudes per square arcsecond.

^dThis is the pixel value under the first surface brightness contour divided by the standard deviation of the pixel counts on the sky

Table 2. Source Characteristics

IRAS	Associations	D(pc) ^a	L_{bol}	α (J2000) ^b	δ (J2000) ^b	J ^c	H ^c	K_s ^c	α^d	Size(") ^e
00182+6223	L1280	4680(4)	366.93	00 20 56.79	+62 40 21.0	15.688	13.982	12.443	1.53	9.6
00465+5028	CB6, LBN 613	800(6)	8.7792	00 49 24.50	+50 44 43.6	13.822	12.297	11.531	1.01	15.4
01166+6635		249(4)	0.4437	01 20 03.93	+66 51 35.9	16.029	14.037	12.606	0.38	7.8
02086+7600	L1333	180(5)	0.7839	02 13 43.61	+76 15 06.0	13.715	12.254	11.193	0.88	9.8
03225+3034	L1448 IRS 3, RNO 14	290(1)	13.124			13.745	12.363	11.095	1.52	20.1
03245+3002	L1455 IRS 1, RNO 15 FIR	260(1)	7.8807	03 27 38.83	+30 13 25.0	1.91	5.0
03260+3111	L1450, SVS 3	290(1)	138.43	03 29 10.38	+31 21 59.2	9.368	7.987	7.173	0.59	76.6
03271+3013	in NGC 1333	290(2)	1.6255	03 30 15.16	+30 23 49.4	14.259	0.86	5.2
03301+3057	Barnard 1 IRS	290(2)	3.0314	03 33 16.68	+31 07 54.9	14.208	1.52	9.5
03331+6256		1560(4)		03 37 28.45	+63 06 31.2	14.590	0.45	3.9
03445+3242	L1471, HH 366 VLA 1, Barnard 5 IRS 1	280(1)	3.8062	03 47 41.60	+32 51 43.8	...	14.047	11.214	0.16	10.3
03507+3801	HH 462	350(1)	2.5178	03 54 06.19	+38 10 42.5	12.474	10.863	10.098	0.22	13.8
04016+2610	L1489 IRS, HH 360	140(1)	3.0280	04 04 43.05	+26 18 56.2	12.655	10.861	9.199	0.31	18.4
04067+3954	L1459	350(1)	15.105	04 10 08.40	+40 02 24.6	13.767	11.478	9.844	1.17	53.7
04073+3800	L1473, HH 463	350(1)	22.600	04 10 41.09	+38 07 54.0	15.339	13.552	10.500	0.07	18.3
04169+2702	L1495, near HH 391	140(1)	0.9190	04 19 58.45	+27 09 57.1	16.528	12.554	10.428	0.53	18.7
04189+2650	FS Tau B, HH 157, Haro 6-5B	140(3)	0.6454	04 22 00.70	+26 57 32.5	15.082	13.351	11.753	-0.04	21.8*
04191+1523	–	140(7)	0.4031	04 22 00.44	+15 30 21.2	16.592	12.354	11.259	0.97	10.4
04223+3700	L1478	350(1)	2.7410	04 25 39.80	+37 07 08.2	...	13.170	10.271	0.47	10.4*
04239+2436	L1524, HH 300 VLA 1	140(1)	1.1028	04 26 56.30	+24 43 35.3	14.323	11.530	9.764	0.09	8.5*
04248+2612	L1521D, HH 31 IRS2, Barnard 217	140(1)	0.3276	04 27 57.30	+26 19 18.4	11.619	10.270	9.741	0.52	25.2
04275+3531		350(1)	1.5456	04 30 48.52	+35 37 53.2	15.268	0.51	4.3
04287+1801	L1551 IRS 5B, HH 154,	140(1)	20.179	04 31 34.08	+18 08 04.9	12.230	10.550	9.255	0.76	20.2
04302+2247	HH 394, near L1536	140(1)	0.2797	04 33 16.50	+22 53 20.2	13.489	11.772	10.876	1.34	13.7
04325+2402	L1535 IRS, Barnard 18I	140(1)	0.6805	04 35 35.39	+24 08 19.4	16.122	11.504	9.826	1.71	26.1
04327+5432	L1400, HH 378	170(1)	1.8530	04 36 45.50	+54 39 04.5	16.437	13.974	12.618	0.84	8.0
04365+2535	TMC-1A, L1534	140(1)	1.8774	04 39 35.19	+25 41 44.7	16.389	12.062	10.020	0.68	21.1
04381+2540	TMC-1, L1534	140(1)	0.5949	04 41 12.68	+25 46 35.4	16.076	12.954	11.254	0.64	9.0
04530+5126	L1438, V347 Aur, RNO 33	none		04 56 57.02	+51 30 50.9	9.990	8.825	8.062	0.05	19.3*
04591–0856	HHL 17, IC 2118	210(8)	0.9043	05 01 29.64	–08 52 16.9	11.359	10.341	9.933	0.62	21.0
05155+0707	HH 114	460(17)	11.773	05 18 17.30	+07 10 59.9	...	12.567	10.214	1.55	24.5
05302–0537	Haro 4-145	470(2)	42.749	05 32 41.65	–05 35 46.1	...	15.116	11.389	0.38	20.8
05311–0631	L1641, HH 83 VLA 1	470(3)	7.3329	05 33 32.52	–06 29 44.2	13.358	11.487	9.749	0.23	21.4
05327–0457	Ced 55e	450(9)	920.15	05 35 13.10	–04 55 52.5	13.166	10.886	9.360	1.76	22.0*
05378–0750	L1641	480(1)	8.1978	05 40 14.95	–07 48 48.5	...	15.392	13.470	0.25	5.8
05379–0758	L1641	480(1)	6.3836	05 40 20.55	–07 56 39.9	12.851	10.678	9.399	0.19	9.3*
05384–0808	L1641 S4, S85	480(1)	10.809	05 40 50.59	–08 05 48.7	13.134	11.349	10.276	1.03	28.3*
05391–0841	L1641	480(1)	3.5872	05 41 30.05	–08 40 09.2	...	14.729	11.855	0.77	5.80*
05399–0121	L1630, HH 92,	430(1)	10.686	05 42 27.64	–01 19 57.0	1.53	7.9
05403–0818	L1641 S2	480(1)	9.8998	05 42 47.07	–08 17 06.9	15.671	13.155	11.063	0.40	9.5
05404–0948	L1647	480(1)	49.781	05 42 47.67	–09 47 22.5	10.818	9.810	9.232	0.76	21.4*

Table 2—Continued

IRAS	Associations	D(pc) ^a	L_{bol}	α (J2000) ^b	δ (J2000) ^b	J ^c	H ^c	K_s ^c	α^d	Size(") ^e
05405–0117	L1630	430(1)	4.3714	05 43 03.06	–01 16 29.2	15.981	13.592	12.068	0.71	10.7*
05413–0104	L1630, HH 212	430(1)	10.500	05 43 51.50	–01 02 58.5	2.91	10.3
05417+0907	L1594, HH 175, Barnard 35A	465(1)	18.380	05 44 30.01	+09 08 57.1	...	15.913	12.400	1.68	17.8*
05450+0019	L1630	430(1)	27.648	05 47 36.55	+00 20 06.3	11.406	9.604	8.784	1.26	57.8
05510–1018	–	none		05 53 23.71	–10 17 27.6	16.267	15.085	12.787	0.93	11.0
05513–1024	–	none		05 53 42.55	–10 24 00.7	9.803	7.635	5.956	0.18	41.7*
05548–0935	–	none		05 57 13.23	–09 35 10.9	14.573	13.357	12.544	0.72	10.0*
05564–1329	–	none		05 58 46.91	–13 29 18.8	14.021	12.061	10.762	0.38	12.8*
05581–1026	–	none		06 00 28.64	–10 26 31.9	17.464	...	14.701	0.47	4.1
05582–0950	RNO 60	none		06 00 36.26	–09 51 11.9	14.031	12.202	11.218	1.26	12.0
05596–0903	–	none		06 02 02.47	–09 03 13.3	1.11	5.4
05598–0906	HHL 34,GGD 10	none		06 02 16.20	–09 06 29.0	14.553	11.876	9.813	0.43	29.2*
06027–0714		830(1)	8.6831	06 05 07.90	–07 14 42.6	16.226	13.473	12.607	1.08	10.9
06033–0710		830(1)	10.333	06 05 48.61	–07 10 31.2	1.28	3.7
06047–1117	–	500(10)	4.9455	06 07 08.50	–11 17 51.0	14.119	12.222	10.220	0.64	17.9
06057–0923	–	none		06 08 05.29	–09 23 47.3	0.97	5.8
06249–0953	L1652	830(1)	6.4991	06 27 17.34	–09 55 27.4	15.034	13.652	12.559	1.04	7.4
06368+0938	L1613	790(11)	6.5302	06 39 32.09	+09 35 41.5	0.93	
06381+1039		960(4)	143.60	06 40 58.15	+10 36 52.1	14.513	1.93	10.2
06382+1017	HH 124, NGC 2264, L1610/1613	800(3)	84.413	06 41 02.64	+10 15 02.1	13.362	12.218	10.592	1.00	19.0
06393+0913		950(4)	28.887	06 42 08.13	+09 10 30.0	15.243	12.048	10.593	1.42	6.78*
07180-2356	L1660, HH 72 IRS	1500(17)	185.95	07 20 08.36	–24 02 23.0	...	14.176	11.648	0.81	6.94*
15398–3359	HH 185, Lupus 1, Barnard 228	170(3)	1.3606	15 43 01.32	–34 09 15.3	15.963	13.992	12.326	1.59	11.3
16288-2450(E)	L1689 IRS 5, ρ Oph S	160(1)		16 32 02.22	–24 56 16.8	...	13.813	10.726	0.70	15.6
16288-2450(W)	ρ Oph S	160(1)	5.479	16 31 52.98	–24 56 24.6	11.783	9.391	7.557	0.70	19.0
16295–4452	–	600(12)	30.602	16 33 07.73	–44 58 24.7	...	15.086	12.270	0.79	23.3
16316–1540	L43, RNO 91	160(1)	11.398	16 34 29.29	–15 47 01.9	10.994	9.635	8.464	0.84	27.5
16442–0930	L260	160(1)	0.6570	16 46 58.27	–09 35 19.7	14.316	12.339	10.721	0.22	10.5*
17364–1946	L219	none		17 39 23.25	–19 47 54.7	13.757	0.96	11.2
17441–0433	L425	none		17 46 50.89	–04 34 33.7	16.700	15.270	13.325	0.50	10.8
18148–0440	L483 FIR	225(1)	11.050	18 17 29.56	–04 39 35.7	16.188	12.640	10.790	1.36	15.4
18264–0143		none		18 29 05.31	–01 41 56.9	13.968	1.39	13.3
18270–0153		none		18 29 36.69	–01 50 59.1	16.356	12.956	10.772	0.49	24.5
						13.700	11.797	10.711		
18274–0212		none		18 30 01.36	–02 10 25.6	...	15.145	11.489	0.12	6.64*
18278–0212		none		18 30 27.28	–02 11 00.2	14.550	1.62	14.7
18331–0035	L588, HH 109, HH 108 IRAS	310(3)	3.7700	18 35 42.00	–00 33 22.1	16.347	13.911	11.738	2.02	18.3
18341–0113	L564	none		18 36 46.33	–01 10 29.5	14.849	11.974	10.229	0.91	19.5
18383+0059	–	none		18 40 51.87	+01 02 12.9	14.892	11.748	9.602	0.50	15.3*
18595–3712	ISO-CrA 182	129(13)	1.2313	19 02 58.70	–37 07 34.1	...	15.881	14.498	1.83	9.1
19266+0932	HH 221, Parsamian 21	300(3)	3.4202	19 29 00.86	+09 38 42.9	11.205	10.485	9.763	0.37	19.9

Table 2—Continued

IRAS	Associations	D(pc) ^a	L_{bol}	α (J2000) ^b	δ (J2000) ^b	J ^c	H ^c	K _s ^c	α^d	Size(") ^e
19411+2306	–	2100(14)	3026.1	19 43 17.94	+23 14 01.6	13.946	11.548	9.596	1.11	19.9
20353+6742	L1152, HH 376	370(1)	1.3738	20 35 46.33	+67 53 02.0	15.263	14.230	13.254	1.41	7.4
20361+5733	L1041	none		20 37 20.36	+57 44 14.8	1.91	2.5
20377+5658	L1036	440(1)	4.7624	20 38 57.48	+57 09 37.6	13.925	11.226	9.507	0.32	17.6*
20386+6751	L1157 IRS, HH 375 VLA 1	370(1)	5.5027	20 39 06.28	+68 02 13.8	2.23	16.1
20453+6746	PV Cep, HH 215, L1158	500(3)	63.697	20 45 53.94	+67 57 38.7	12.453	9.497	7.291	-0.32	25.2*
20568+5217	L1002, HH 381 IRS	1270(4)	45.55	20 58 21.09	+52 29 27.7	11.544	9.813	8.305	0.62	34.5
20582+7724	L1228, HH 199	175(1)	1.2112	20 57 12.94	+77 35 43.7	13.024	10.608	9.171	0.31	16.0*
21004+7811	HHL 66, HH 198, RNO 129	300(3)	13.538	20 59 14.03	+78 23 04.1	9.437	7.530	6.319	0.20	25.5*
21007+4951	L988	700(1)	31.059	21 02 23.85	+50 03 06.8	16.368	14.818	13.276	0.69	10.1*
21017+6742	L1172	288(15)	0.4974	21 02 21.27	+67 54 20.1	14.890	0.66	20.1
21169+6804	L1177, CB 230	450(6)	7.3301	21 17 38.69	+68 17 33.4	11.562	9.898	9.188	1.75	25.3
21352+4307	Barnard 158	600(6)	11.721	21 37 11.39	+43 20 38.4	...	15.877	12.915	0.17	7.6*
21388+5622	HH 588	750(16)	96.504	21 40 28.98	+56 35 55.7	12.801	11.620	10.789	0.59	16.7
21391+5802	L1121, IC 1396N	750(16)	254.17	21 40 42.80	+58 16 01.1	...	15.642	14.155	2.15	36.7
21445+5712		360(4)	18.527	21 46 07.12	+57 26 31.8	13.950	11.965	10.139	0.54	14.6
21454+4718	L1013B/1031B, V1735 Cyg	900(1)	106.66	21 47 20.66	+47 32 03.6	9.889	8.087	7.040	0.70	33.0*
21569+5842	L1143	250(4)	0.9577	21 58 35.90	+58 57 22.8	15.457	12.936	10.695	0.08	12.5*
22051+5848	L1165, HH 354 IRS	750(3)	72.956	22 06 50.37	+59 02 45.9	11.370	10.248	9.682	1.15	23.7
22176+6303	L1240, RAFGL 2884, S 140 IRS1-3	910(1)	21313.	22 19 20.39	+63 19 38.5	12.304	9.298	6.135	0.87	125.7
22266+6845	L1221, HH 363	200(1)	1.8195	22 28 02.99	+69 01 16.7	16.575	13.544	11.465	0.53	14.3*
22267+6244		900(1)	311.24	22 28 31.29	+63 00 28.2	15.826	11.799	9.244	1.45	44.7
22272+6358A	L1206	950(1)	815.52	22 28 52.60	+64 13 41.0	16.690	12.197	9.840	1.76	28.3
22376+7455	L1251B 3, HH 189	330(1)	10.659	22 38 42.49	+75 11 45.6	13.977	12.073	11.206	1.09	31.7
23037+6213	Cep C		188.79	23 05 48.07	+62 30 09.9	16.162	14.644	10.611		
									1.23	34.3*

^aThe estimated distance to each source in parsecs. The citation for the distances estimate is designated by the number in the parentheses, and are as follows: 1) Hilton, J., & Lahulla, J. 1995; 2) Educated guess based on proximity to nearby objects; 3) Reipurth, A General Catalog of HH Objects, 1999 (<http://casa.colorado.edu/~hrcat/>); 4) Wouterloot, J., & Brand, J. 1989; 5) Obayashi et al. 1998; 6) Launhardt & Henning 1997; 7) André et al. 1999; 8) Kun et al. 2001; 9) Mookerjea et al. 2000; 10) Yun et al. 2001; 11) Sagar et al. 1983; 12) Moreira et al. 2000; 13) Marraco & Rydgren 1981; 14) Guetter, H. 1992; 15) Straizys et al. 1992; 16) Battinelli & Capuzzo-Dolcetta 1991; 17) Reipurth & Aspin 1997; none = Searched for and could not find a distance estimate

^b2MASS coordinate for selected object in field

^cMagnitudes from the 2MASS extended source catalog, in the 2MASS photometric system.

^dThe spectral index of the source

^eThe square root of the area within the K=19 magnitudes per square arcsecond surface brightness contour. * denotes sources where the stellar image dominates the measured size.

Note. — RNO designates objects in "Red and Nebulous Objects in Dark Clouds: a Survey". Cohen, M. 1980

Table 3. Nebulae observed in H₂

IRAS	α (J2000) ^a	δ (J2000) ^a
00182+6223	00 21 01.47	+62 39 39.1
03220+3035	03 25 14.34	+30 46 55.6
03445+3242	03 47 41.60	+32 51 43.8
04327+5432	04 36 41.65	+54 40 00.4
05155+0707	05 18 17.30	+07 10 59.9
05403–0818	05 42 47.07	–08 17 06.9
18264–0143	18 29 05.31	–01 41 56.9
18270–0153	18 29 40.26	–01 51 27.8
21391+5802	21 40 43.65	+58 16 19.1

^aThe RA and declination of the star or nebula marked in each figure.